Application of a pre-targeting drug delivery system for precise treatment of breast and ovarian cancer

Inaugural Dissertation
submitted to the
Faculty of Medicine
in partial fulfillment of the requirements
for the PhD-Degree
of the Faculties of Veterinary Medicine and Medicine
of the Justus Liebig University Giessen

by
Chaoyu Zhang
of
Ningbo, China

Giessen 2023

From the Department of Gynecology and Obstetrics
Director / Chairman: Prof. Dr. med. Ivo Meinhold Heerlein
of the Faculty of Medicine of the Justus Liebig University Giessen

First Supervisor and First Reviewer: Prof. Dr. med. Ivo Meinhold Heerlein
Second Supervisor and Vice-Chair: Prof. Dr. rer. nat. Sandra B. Hake
Second Reviewer: Prof. Dr. Twan Lammers
Chair: Prof. Dr. Christine Wrenzycki

Date of Doctoral Defense:
31.01.2024

Ehrenwörtliche Erklärung

„Ich erkläre: Ich habe die vorgelegte Dissertation selbständig, ohne unerlaubte fremde Hilfe und nur mit den Hilfen angefertigt, die ich in der Dissertation angegeben habe. Alle Textstellen, die wörtlich oder sinngemäß aus veröffentlichten oder nicht veröffentlichten Schriften entnommen sind, und alle Angaben, die auf mündlichen Auskünften beruhen, sind als solche kenntlich gemacht. Bei den von mir durchgeführten und in der Dissertation erwähnten Untersuchungen habe ich die Grundsätze guter wissenschaftlicher Praxis, wie sie in der „Satzung der JustusLiebig-Universität Gießen zur Sicherung guter wissenschaftlicher Praxis“ niedergelegt sind, eingehalten.“

_____ _____

Ort/Datum Unterschrift

Contents

1. Introduction

1.1 Cancer therapy

Cancer has existed for thousands of years and now is one of the leading causes of death worldwide. With the countless efforts paid and remarkable progresses achieved by scientists and physicians, we have witnessed the transition of some types of cancer from incurable disease to chronic disease. Surgery, chemotherapy and radiotherapy used to be the mainstream for cancer treatment, either alone or in combination. Although surgical excision aims at removal of all the solid tumor from body, it is still a pipe dream under current technology. Study has reported that the growth of minimal residual disease is changed after tumor excision due to multiple causes: 1) unexpected or inevitable spread during the operation; 2) generation of immunosuppressive environment during recovery period; 3) increased angiogenesis and cell viability [1]. Chemotherapy and radiotherapy have opened a window of opportunity to reduce minimal residual disease to improve the cure rate, and the neoadjuvant chemotherapy or radiotherapy implemented before surgery allows inoperable cancer to be operable [2]. However, these traditional therapies still confront obstacles such as tumor recurrence, drug resistance and side effect. The conventional chemotherapy is more prime to kill fast-dividing cells so as to achieve anti-tumor efficacy, as tumor cells are usually actively cycling cells [3]. Therefore, healthy cells undergoing fast division such as hair follicle cells, skin cells, cells in gastrointestinal tract and bone marrow can also be attacked, causing hair loss, skin changes, nausea and vomiting, as well as myelosuppression [4, 5]. Meanwhile, dormant cancer cells which are related with recurrence and metastasis can escape from death [3]. Recently, the emergence of targeted therapy which distinguishes and eliminates cancer cells by biomarkers rather than cell cycles has increased the specificity of cancer treatment and might be a promising approach to treat cancer.

1.2 Targeted therapy

Targeted therapy is an old but renewed field for antineoplastic therapy. Paul Ehrlich first proposed the concept of “magic bullets” in 1890s, indicating that a drug could be specific for a target presented in infected cells or tumor cells while be safe to normal cells [6]. Even Paul Ehrlich’s triumphs are mainly remained in infectious diseases, the “magic bullets” concept is deemed the birth of targeted therapy. However, the targeted therapy just reached its prime time in the last two decades, benefiting from the groundbreaking researches in tumor-associated genes and growing knowledge of molecular mechanism of carcinogenesis [7].

Targeted therapy falls into two broad categories: small molecules and macromolecules. The main category of small molecules now are signal transduction inhibitors including multikinase inhibitors (e.g., sorafenib, sunitinib and vandetanib) and selective inhibitors (e.g., erlotinib, gefitinib and vemurafenib) [8]. These drugs usually function by blocking the active site of targets, and thus the inhibition is limited by the difficult-to-drug targets, multidomain scaffolding proteins which contain several active domains, accumulation of proteins and conformational changes of protein induced by nonsynonymous mutations [9]. In comparison to macromolecules, small molecules are easier to penetrate cell membrane and blood brain barrier by virtue of the small size, but the off-target effect is more commonly observed due to high systemic drug concentration and competitive nature [9, 10]. Monoclonal antibody (mAb) is a prototypical example of macromolecules and is one of the hottest science fields due to its attractive property of binding antigen specifically. The birth of mAb can be dated back to 1975 when Georges J. F. Köhler and César Milstein initially described a method using a fused cell line of mouse myeloma and spleen cells from an immunized donor to produce predefined specific antibodies by continuous cultivation [11]. The mechanisms of mAbs and their derivatives mainly focus on directly killing tumor cells, inhibiting immune checkpoints, modifying tumor microenvironment and delivering cytotoxic agents [12, 13]. The mAbs have revolutionized not only biomedical science but also the medical treatment in clinical setting, especially cancer treatment. Since muromonab-

CD3 was firstly approved by U.S. Food and Drug Administration (FDA) in 1986, there have been over one hundred antibodies approved to date [14]. Considering the large size of the mAb which impedes its' accumulation and penetration in tumor site, targeted therapy based on antibody has been recently developed by generating antibody fragments such as single-chain variable fragment (scFv), antigen-binding fragment and nanobody to achieve better tissue distribution [15]. Nevertheless, even the generation of new mAbs and antibody fragments is increasing robustly, most antibodies target the antigens presented on cell surface and not all of them exhibit enough cytotoxicity so can be translated to clinical use. Researchers have fused antibodies with protein transduction domain to target intracellular antigen [16], and also used antibodies as vehicle to deliver highly potent agents to the tumor site which termed antibody drug conjugate (ADC) [17]. All these novel approaches provide new armaments for research and clinical treatment, among which the ADC has achieved groundbreaking success in clinical outcomes by expanding the therapeutic window of antibodies and cytotoxic agents.

1.3 ADC

The ADC has emerged as a promising class of targeted therapy for cancer treatment. Up to date, a total of thirteen ADCs have been approved worldwide, including 12 approved by FDA and one in China (**Table 1.1**). A typical ADC compromises a highly specific mAb targeting tumor-associated antigen expressed on the cell surface with minimal expression on non-malignant cells, a stable and flexible linker that can survive during blood circulation and release cytotoxic agents effectively at target sites, and a potent cytotoxic payload which is usually a small molecule (**Figure 1.1a**).

The most classical mechanism of ADC is started with the ADC accumulation. The ADCs are transported by blood circulation to the tumor site and then penetrate the vessels (**Figure 1.1b**) [18]. As demonstrated in **figure 1.1c**, once antibody recognizes the antigen on the cell surface, the ADC-antigen complex will be internalized through endocytosis, followed by degradation in lysosome. The released drugs can cause cell

death by either inhibiting microtubule polymerization or damaging DNA [19, 20]. Apparently, the combination of mAb and cytotoxic payload achieves the targeted delivery of cytotoxic agent to tumor by integrating the high antigen specificity and potent antitumor activity in a single molecule. To produce an ideal ADC, apart from the three key components should be taken into consideration, the antigen selection and conjugation method also play a vital role.

Table 1.1 Currently approved ADCs

ADC	Target	mAb subtype	Linker	Payload	DAR	Disease indication (first approved)	First approval (country, year)
Tisotumab vedotin (Tivdak®)	TF	IgG1	Cleavable	MMAE	4 (mean)	recurrent or metastatic cervical cancer with disease progression on or after chemotherapy	US, 2021
Sacituzumab govitecan (Trodelvy®)	Trop-2	IgG1	Cleavable	SN38	7-8	Unresectable locally advanced or metastatic TNBC with two or more prior systemic therapies, at least one of them for metastatic disease; Locally advanced or metastatic UC with prior platinum-containing chemotherapy and either PD-1 or PDL1 inhibitor	US, 2020
Polatuzumab vedotin (Polivy®)	CD79b	IgG1	Cleavable	MMAE	3.5 (mean)	DLBCL not otherwise specified or HGBL and who have an International Prognostic Index score of 2 or greater; Relapsed/refractory DLBCL, not otherwise specified, after at least two therapies	US, 2019
Mirvetuximab soravtansine (Elahere®)	FRα	IgG1	Cleavable	DM4	3.4 (mean)	FOLR1-positive, platinum-resistant epithelial ovarian, fallopian tube, or primary peritoneal cancer with one to three prior systemic treatment regimens	US, 2022
Loncastuximab tesirine (Zynlonta®)	CD19	IgG1/kappa	Cleavable	SG3199	2.3 (mean)	B-cell lymphoma after two or more lines of systemic therapy	US, 2021
Inotuzumab ozogamicin (Besponsa®)	CD22	IgG4	Cleavable	Calicheamicin	2-6	Relapsed or refractory B-cell precursor ALL	US, 2017
Gemtuzumab ozogamicin (Mylotarg®)	CD33	IgG4	Cleavable	Calicheamicin	0-6	CD33-positive AML	US, 2000

Continued table 1.1 Currently approved ADCs

ADC	Target	mAb subtype	Linker	Payload	DAR	Disease indication (first approved)	First approval (country, year)
Enfortumab vedotin (Padcev®)	Nectin4	IgG1	Cleavable	MMAE	3.8 (mean)	Locally advanced or metastatic urothelial cancer after PD-1 or PD-L1 inhibitor and a platinum-containing chemotherapy; Locally advanced or metastatic setting.	US, 2019
Disitamab vedotin (Aidixi®) [18]	Her2	IgG1	Cleavable	MMAE	4 (mean)	locally advanced or metastatic gastric cancer after at least two systemic chemotherapy	China, 2021
Brentuximab vedotin (Adcetris®)	CD30	IgG1	Cleavable	MMAE	4 (mean)	Hodgkin lymphoma after ASCT or two multi-agent chemotherapy; Systemic anaplastic large cell lymphoma after at least one multi-agent chemotherapy regimen	US, 2011
Belantamab mafodotin (Blenrep®)	BCMA	IgG1	Non-cleavable	MMAF	4 (mean)	relapsed or refractory multiple myeloma with four prior therapies	US, 2020
Ado-trastuzumab emtansine (Kadcyla®)	Her2	IgG1	Non-cleavable	DM1	3.5 (mean)	Her2-positive, metastatic breast cancer after trastuzumab and a taxane treatment, separately or in combination; Locally advanced or metastatic Her2-positive gastric or gastroesophageal junction adenocarcinoma after trastuzumab-based regimen	US, 2013
trastuzumab deruxtecan (Enhertu®)	Her2	IgG1	Cleavable	DXd	~ 8	unresectable or metastatic Her2-positive breast cancer after two or more anti-Her2-based regimens	US, 2019

The information is collected from prescribing information approved by FDA, except Disitamab vedotin (Aidixi®).

ADC: antibody drug conjugate; DAR: drug-to-antibody ratio; TF: tissue factor; Trop2: Trophoblast cell-surface antigen 2; FRα: folate receptor alpha; Nectin4: nectin cell adhesion molecule 4; Her2: human epidermal growth factor receptor 2; BCMA: B-cell maturation antigen; MMAE: Monomethyl auristatin E; MMAF: Monomethyl auristatin F; TNBC: triple-negative breast cancer; UC: urothelial cancer; DLBCL: diffuse large B-cell lymphoma; HGBL: high-grade

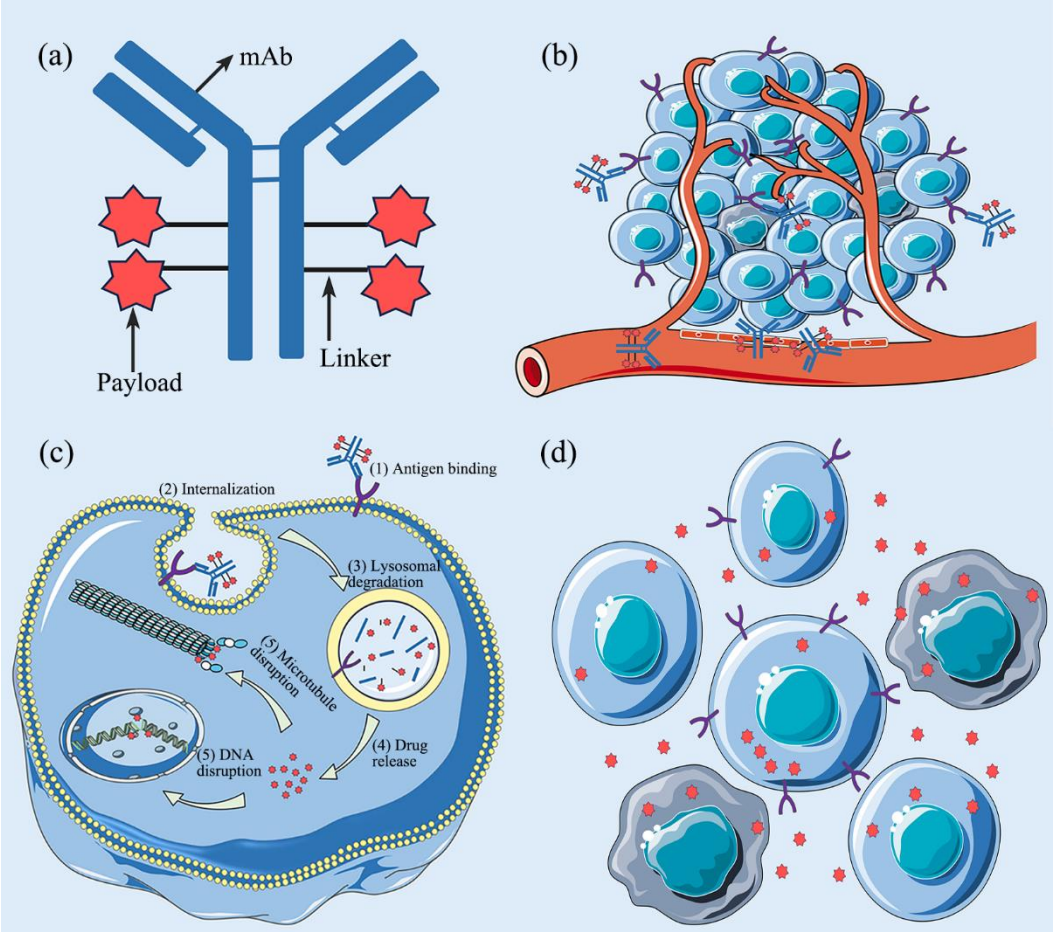

Figure 1.1. Structure and mechanism of ADC. (a) A general structure of an ADC. (b) ADCs are transported to the tumor site. (c) The process of ADC to cause cell death. (d) The bystander effect triggered by diffused cytotoxic drugs.

1.3.1 Target antigen selection

The initial step to design an ADC is selecting an appropriate target antigen which is a guiding light during the drug delivery. First, an ideal target must have high expression on the target tumor cell surface and have restricted expression on normal cells to reduce the on-target, off-tumor toxicity [21]. For example, human epidermal growth factor receptor 2 (Her2) which is one of the most commonly used antigens in approved ADCs for breast cancer treatment is 100-fold higher expressed in Her2 positive cancer cells (2×10^6 receptors per cell) compared to other cells (2×10^4 receptors per cell) [22]. Second, shedding of the target antigen should be low to avoid loss of ADCs during circulation and side effects [23]. Last, as canonical mechanism of ADC is to be internalized into cells through receptor-mediated endocytosis and then release effector

payload intracellularly to kill cancer cells, the target antigen should possess internalization property and should not be downregulated after treatment [22] [24]. In some cases, non-internalized ADCs are able to accumulate in tumor environment, and the released drug in the extracellular space can also diffuse to surrounding cells even without targeting antigen expression [25].

1.3.2 Antibody

Antibodies, also known as immunoglobulins (Ig), are produced by B lymphocytes, presenting on the surface of the B cells or being secreted into extracellular space to bind target antigens [26]. There are five major classes of Ig (IgA, IgD, IgE, IgG and IgM), and all of them share a basic Y-shaped structure, consisting of two heavy chains and two light chains. Furthermore, each chain is composed of constant regions and variable regions to carry out different functions: each heavy chain contains one variable heavy region (VH) and three constant heavy regions (CH1, CH2, CH3), and each light chain contains one variable light region (VL) and constant light region (CL). The fragment antigen-binding region (Fab) in charge of binding property is made up of the entire light chain and part of heavy chain (VH and CH1), while the fragment crystallizable region (Fc region) which includes CH2 and CH3 regions of the two heavy chains is mainly responsible for interaction with cell surface receptor named Fc receptors and activation of immune system [27].

As the ADC needs to deliver the chemotherapeutic drug to target site, the vehicle should possess: 1) target specificity, target binding affinity and low cross-reactivity to ensure accurate and efficient delivery; 2) good retention in blood circulation, which means not too long to cause undesirable uptake and not too short to lose effectiveness; 3) low immunogenicity to minimize adaptive immune responses such as anti-drug antibodies generated to against ADCs [28-30]. The majority of ADCs are built on full-length antibodies IgG scaffold, especially IgG1. The IgG has four subclasses (IgG1, IgG2, IgG3 and IgG4), among which IgG3 shows shorter serum half-life (7-21 days) compared to other three subtypes (around 21 days) and therefore not commonly used

in ADCs [31]. The molecular weight of a intact IgG is around 150 kDa, which hampers it to penetrate the vessel membrane or tissue, and thus the low accumulation in target sites, especially deep tumor site, might affect the efficacy of the ADCs. To overcome this problem, many studies have reported some small-size antibody moieties such as scFv and Fab [32]. Although these small antibody fragments have not been widely used in clinical treatment, they bring the hope for the development of ADC.

1.3.3 Linker

Since the antibody and payload are responsible for the targeting and cytotoxicity, the linker moiety plays as a connector to tether payload to antibody, a stabilizer to favor the stability of ADC during the circulation in bloodstream and avoid premature release, and an effector to liberate payload rapidly once the ADC is internalized [21, 33]. In addition, due to the hydrophobic property of most payloads, a hydrophilic linker is preferred to protect ADC from aggregation to reduce immunogenicity and hepatotoxicity [33, 34]. Currently, the linkers can be classified into cleavable and non-cleavable linkers, and the majority of linkers used in approved ADCs are cleavable linkers (**Table 1.1**).

The cleavable linkers break down and then liberate payloads when physiological environment changed after internalization, such as acidic conditions in lysosomes and endosomes (e.g., gemtuzumab ozogamicin and inotuzumab ozogamicin), reducing environment with high concentration of glutathione (e.g., gemtuzumab ozogamicin and mirvetuximab soravtansine), and proteolysis conducted by lysosomal enzymes (e.g., Brentuximab vedotin, Polatuzumab vedotin and Enfortumab vedotin) [33, 35-37]. The function of cleavable linker is not restricted in internalized ADCs. Recent studies have reported the use of disulfide linkers or dipeptide-containing linkers to generate non-internalizing ADCs. Once the cleavage started by reductants which are released by dying cancer cells or extracellularly overexpressed lysosomal enzymes, the chain-reaction will be triggered as more reductants and enzymes will be released by dead cells [35, 38, 39]. Of note, the bystander killing can be achieved in some cases by cleavable linker but not by non-cleavable linker, for the reason that some small cytotoxic agent is

able to penetrate the cell membrane after drug release and diffuse to neighbor to cause cell death of untargeted cell (**Figure 1.1d**) [40]. Considering the heterogeneous antigen expression of tumor, the bystander effect can increase the efficiency of ADC [40, 41]. Compared to cleavable linkers, non-cleavable linkers rely on the degradation of antibodies within the cells, so the efficacy might be reduced as the charged amino acids remained in released drug could affect its toxicity and diminish its membrane permeability to kill proximal cells [36]. However, non-cleavable linker exhibits better plasma stability over cleavable linker, and the cytotoxicity of metabolites can also be retained if suitable payloads are chosen [36, 42].

1.3.4 Payload

Payload is the warhead of the target therapy, playing most important role in the cancer-killing by ADC. To maximize the efficacy of ADC, high stability is required to keep ADC stable during systemic circulation to protect healthy cells [43]. Furthermore, payload should be high potent owing to the low fraction of administered ADC (0.003–0.08%) can reach the tumor site [31, 43, 44]. The first-generation ADCs, which aims to improve the efficacy of traditional chemotherapeutics such as methotrexate and doxorubicin shows lower cytotoxicity in contrast to its parent agents [45]. Accordingly, high potent small-molecule drugs are explored to further develop ADC. The payloads now are generally classified into microtubule-disrupting agent and DNA damaging agents [28].

Auristatins and maytansinoids are two main classes of microtubule-disrupting agents. Auristatins including monomethyl auristatin E (MMAE) and monomethyl auristatin F (MMAF) are the most used toxic compounds in approved ADCs, accounting for six out of thirteen of the current ADCs (**Table 1.1**). The agents are derived from a natural product named dolastatins 10, arresting cells in metaphase by binding to vinca alkaloid binding site on tubulin and inhibiting tubulin polymerization [46, 47]. Maytansinoid is isolated from maytansine which is isolated from plant *Maytenus ouatus* [48, 49], binding to maytansine site of microtubule to destabilize microtubule structure [47, 50].

Compared to conventional tubulin inhibitors such as paclitaxel and vinblastine, maytansinoids show 100- to 1000-fold more toxic at subnanomolar half maximal inhibitory concentration (IC_{50}) values [50].

DNA damaging agents, for example calicheamicin, pyrrolobenzodiazepine analogs and duocarmycin, also have been utilized in ADCs. Gemtuzumab ozogamicin and inotuzumab ozogamicin are coupled with calicheamicin to treat hematological malignancy [51, 52]. The calicheamicin are able to recognize minor groove in DNA and induce site-specific double-strand DNA breaks [53]. The SG3199, a pyrrolobenzodiazepine dimer, is recently successfully conjugated to a CD19-targeting antibody to treat the diffuse large B-cell lymphoma [54, 55]. The pyrrolobenzodiazepine is a DNA minor groove cross-linking agents and is reported to be capable to eliminate slowly dividing tumor cells and maintain cytotoxicity in cell lines with multidrug resistant proteins [55].

Apart from these two mainstream of payloads, more and more cytotoxic agents have been identified such as deruxtecan (DXd, used in trastuzumab deruxtecan, approved) and α-amanitin (used in HDP-101, in clinical trial) which belong to topoisomerase I inhibitor and RNA polymerase II inhibitor, respectively [50, 56, 57].

1.3.5 Conjugation method

In addition to the careful selection of antibody, linker and payload, the conjugation methods are also essential to design an ideal ADC. Non-specific conjugation methods usually use the side chains of lysine or cysteine which naturally exist in the antibody to react with linker-drug complex. Nevertheless, this random conjugation results in heterogeneous products for the reason that a IgG scaffold contains about 16 cysteine pairs and 80 lysine residues in which up to eight reactive cysteine thiol groups after reduction of the four inter-chain disulfide bonds and around 10-20 lysine residues are chemically accessible to be used for conjugation [33, 36]. The heterogeneous mixture could be either antibody conjugated with different number of payloads or payloads tethered to different sites of the antibody, leading to inconsistent pharmacokinetics [58].

The first marketed ADC Mylotarg® utilizes the lysine-coupling approach but is temporarily withdrawn due to safety concerns which may be partly related to its heterogeneity [59-61]. Even so, taking the advantage of the facile reactivity by nature residues, the followed two marketed ADCs still use the lysine (Kadcyla®) and cysteine (Adcetris®) to conjugate drugs: Kadcyla® is generated by a two-step conjugation methods that the lysine is first reacted with an amine- and thiol-reactive N-hydroxysuccinimide ester through amine-reactive group and then the product reacts with payloads through thiol-reactive group, leading to hundreds of different products; Adcetris using reduced cysteines decreases the conjugation sites but still provide up to eight thiol-reactive sites [62].

Recent researches are paying more attention to developing site-specific conjugation methods to produce homogeneous products and uniform the pharmacokinetics, including non-natural amino acids incorporation, free cysteine insertion without disruption of disulfide bonds, enzymatic conjugation and so on [63]. One of the most promising methods is enzymatic conjugation. Benefiting from the high specificity of enzyme to substrate, enzyme-mediated conjugation generally produces homogeneous ADC with highly controlled drug-antibody ratio (DAR) [33, 63]. The O^6-alkylguanine-DNA alkyltransferase, which is also known as SNAP-tag, is a modified mutant of human DNA repair enzyme. The enzyme is able to irreversibly transfer an alkyl group to a cysteine residue, allowing specific reaction with O^6-benzylguanine (BG) derivatives and forming stable thioether bond [64, 65]. Previous studies have demonstrated the utilization of SNAP-tag technology for antibody modification to carry fluorescent dyes or drugs, protein immobilization, protein-protein interaction determination, and protein property study [66-68].

To date, the thirteen approved ADCs are all using chemical conjugation, among which nine (Tivdak®, Trodelvy®, Polivy®, Zynlonta®, Padcev®, Adcetris®, Blenrep®, Enhertu® and Aidixi®) are conjugated through cysteine residues and four (Elahere®, Besponsa®, Mylotarg® and Kadcyla®) used lysine residues. Even though the enzymatic conjugation methods have not been widely used in ADC design, the increasing studies portend a

bright future for novel approach [69-71].

1.3.6 Approved ADCs for breast and ovarian cancer

1.3.6.1 Approved ADCs for breast cancer

Female breast cancer is the leading cause of cancer incidence and fifth leading cause of cancer mortality worldwide with 2.3 million new cases and 685,000 deaths in 2020 [72]. Genomic studies have classified breast cancer into luminal, basal-like, *Her2* positive and normal-like subtypes based on the expression of *estrogen receptor* (*ER*), *progesterone receptor* (*PgR*) and *Her2*.[73, 74]. The *ER* status subclassifies the breast cancer into *ER-high* and *ER-low* subtypes. The former is termed luminal subtype which accounts for approximately 75% of breast cancer as it is associated with high expression of luminal cell related genes, while the later further falls into basal-like, Her2-positive and normal breast-like subtypes [75]. Triple negative breast cancer (TNBC) is a special type of breast cancer which is characterized by immunohistochemistry with the absence or low expression of ER, PgR and Her2 [76]. The TNBC and basal-like breast cancer are diagnosed by different methods but are often used interchangeably in most studies and are considered to be synonymous as they have almost 80% overlap of biological and pathological features [77, 78]. At time of writing this thesis, there are three ADCs have been approved for breast cancer, among which two target to Her2-positive breast cancer and one is used for TNBC. Here, these breast cancer related ADCs are briefly introduced.

Ado-trastuzumab emtansine (Kadcyla®) The ado-trastuzumab emtansine (T-DM1) is made up of a mAb trastuzumab conjugated with an average of 3.5 emtansine molecules via a non-cleavable linker [79]. Kadcyla® is the first approved ADC for patients with Her2-positive, metastatic breast cancer and have received trastuzumab or taxane previously. The phase 3 trial which supports the indication and usage has revealed that the application of T-DM1 notably improves the clinical outcome compared to lapatinib plus capecitabine treatment, resulting in prolonged progression-free survival (PFS) (9.6

months *vs.* 6.4 months), extended median overall survival (OS) (30.9 months *vs.* 25.1 months), higher objective response rate (ORR) (43.6% *vs.* 30.8%) and fewer adverse events of grade 3 or over [80]. Apart from benefiting the advanced breast cancer, the T-DM1 is then extended to early breast cancer. Patients who have residual invasive disease after receiving neoadjuvant therapy are treated with T-DM1. In comparison to patients treated with trastuzumab, T-DM1 significantly reduces the risk of recurrence by 50%, but more adverse events are observed [81].

Trastuzumab deruxtecan (Enhertu®) The trastuzumab deruxtecan (T-DXd) is approved for the treatment of patients with advanced breast cancer who have previously treated with at least two anti-Her2-based regimens. The T-DXd also uses trastuzumab as a backbone, but it is conjugated with about 8 molecules of deruxtecan (a topoisomerase inhibitor) and connected by a tetrapeptide-based cleavable linker. A phase 2 clinical trial, in which patients with Her2-positive advance breast cancer received T-DXd after prior treatment with T-DM1, shows that 6% patients have a complete response and the median PFS is 16.4 months [82]. Interestingly, a phase 3 trial uncovers that T-DXd can also prolong medium PFS (9.9 months) and OS (23.4 months) in patients with Her2-low advanced breast cancer, while physician's choice of chemotherapy group exhibites 5.1 months and 16.8 months, respectively [83]. As a second approved Her2-based ADC, T-DXd is supposed to have better efficacy than T-DM1. A recent study has proved the scenario that T-DXd can reduce risk of disease progression or death more effectively, as the patients treated with T-DXd have three-time longer medium PFS than with T-DM1 (28.8 months *vs.* 6.8 months), increased OS rate (77.4% *vs.* 66.9%) and higher ORR (79% *vs.* 39%) [84, 85].

Sacituzumab govitecan (Trodelvy®) TNBC is a refractory cancer compared to other breast cancer subtypes due to the absence of hormone receptors and Her2. A growing body of literature indicate that trophoblastic cell-surface antigen-2 (Trop-2) which is highly related with disease progression and poor survival is overexpressed in many epithelial cancers including breast cancer, especially TNBC [86-89]. The approval of sacituzumab govitecan (SG) as a second-line treatment for advanced or metastatic

breast cancer brings the hope for TNBC treatment. The SG consists of a humanized monoclonal antibody hRS7 targeting Trop-2, a hydrolysable cleavable linker and on average 7-8 molecules of topoisomerase inhibitor SN-38 [90]. The Patients received SG have better clinical outcomes by assessing medium PFS, medium OS and ORR (5.6 months *vs.* 1.7 months, 12.1 months *vs.* 6.7 months, 35% *vs.* 5%, respectively), compared to patients treated with single-agent chemotherapy [91]. As the Trop-2 is also highly expressed in other breast cancer subtypes whilst not as high as in TNBC, SG is also evaluated in hormone receptor-positive but Her2-low metastatic breast cancer. Satisfactorily, the results demonstrate a 34% reduction in risk of disease progression or death, providing a new treatment option for patients who are resistant to hormone therapy [92].

1.3.6.2 Approved ADCs for ovarian cancer

Ovarian cancer is one of the most common and the deadliest gynecologic malignancies. According to the most recent global statistics in 2020, approximately 313,959 new cases of ovarian cancer and 207,252 deaths occurred in the US [72]. There are around two-thirds of epithelial ovarian cancers diagnosed at advanced stages (stage III-IV) due to the limited screening methods, insidious symptoms and aggressive biological behaviors [93]. Although cytoreductive surgery and chemotherapy are still the main regimens to date, several targeted therapies have developed but still remain some limitations: 1) the poly adenosine diphosphate-ribose polymerase inhibitors have already widely used as maintenance treatment and have achieved satisfactory results, but the sensitivity depends on the *BRCA* mutation; 2) bevacizumab is approved for patients with advanced newly diagnosed ovarian cancer, but it still remains controversial in practical implementation as front-line maintenance treatment [94, 95]. In addition, the immune check inhibitors, which have made a triumph of many types of cancers, have failed in ovarian cancer, and the more trials are still in progress [94, 96]. Even so, a latest approved ADC named mirvetuximab soravtansine (MIRV, Elahere®) provides a new option for patients with folate receptor alpha (FRα)-positive and

platinum-resistant epithelial ovarian cancer, who have been treated with one to three chemotherapy regimens [97]. FRα is confirmed to be overexpressed in epithelial ovarian cancer, thus the MIRV contains a FRα-directed mAb attached with an average of 3.4 molecules of microtubule inhibitor DM4 via a cleavable linker [97-99]. Patients received the MIRV treatment do not achieved prolonged PFS but exhibit improved ORR (24% *vs.* 10%), cancer antigen-125 response rate (53% *vs.* 25%) as well as fewer adverse events of grade 3 or over (25.1% *vs.* 44.0%), compared to patients received chemotherapy [100]. Although the MIRV is the only approved ADC for ovarian cancer to date, there are many ongoing clinical trials of ADCs. One of the most promising ADC is MORAb-202 (clinical trials, NCT04300556, NCT05613088 and NCT03386942) which also targets FRα. A phase 1 study (clinical trial, NCT03386942) has confirmed the antitumor activity of MORAb-202, but the efficacy still needs to be awaited [101]. Aside from targeting FRα, ADCs targeting other tumor associated antigens such as tissue factor (tisotumab vedotin; clinical trial, NCT03657043), sodium-dependent phosphate transport protein (upifitamab rilsodotin; clinical trials, NCT05329545 and NCT04907968), Her2 (T-DXd; clinical trial, NCT04482309), Trop2 (SKB264; clinical trial, NCT04152499) and cadherin-6 (HKT288; clinical trial, NCT02947152) are also undergoing clinical trial.

1.4 Coiled coils

Coiled coils are commonly found in nature proteins to mediate biological process. The basic leucine-zipper (bZip) superfamily of transcription factors is a case in point, which is involved in many core cellular processes. The bZip protein conformation comprises a C-terminal leucine zipper region which leads the protein-protein interaction between two monomers to form a coiled coil structure, and a N-terminal basic region for DNA binding (**Figure 1.2**) [102]. The coiled coil structure contains two or more twisted α-helices to form a left-handed supercoil, and each α-helix is encoded by a heptad repeat $(\mathbf{abcdefg})_n$, in which **a** and **d** residues are hydrophobic for stability, **e** and **g** residues are polar or charged for specificity, and the rest residues exposed to the solvent are usually

hydrophilic [103-105].

Given its simple structure and biological importance, coiled coil motifs have been studied in depth and now widely used in molecular engineering. Grigoryan *et al.* has computationally designed 48 synthetic coiled coils without strong self-association that interact with coiled coil domains from 20 bZip families [106]. Reinke *et al.* from the this research group has further determined the interaction between these synthetic coiled coils along with additional 7 coiled coils from human bZips, revealing 27 heterospecific coiled coils pairs including 23 synthetic coiled coils and 3 human bZips [107]. The study extremely expands the coiled-coil toolkit, and lays the foundation for molecular engineering. Cho *et al.* has established a controllable chimeric antigen receptor (CAR) T-cell therapy by engineering a synthetic coiled coil on the extracellular portion of CAR on T cell and fusing a cognate coiled coil to a scFv [108]. Compared to conventional CAR T therapy, the improved CAR system allows the modification of antibodies without engineering the T cells, and the system can be tuned by competitive coiled coils to reduce or block the binding to prevent cytokine release syndrome caused by over activation of T cells [108]. Moreover, coiled coils are also used for drug delivery by capsulizing drugs through self-assembly, and then disassemble to release drugs at specific environment [109]. However, this drug delivery system lacks specificity towards target sites. Considering the specificity of antibody mentioned above, combining the antibody with coiled coil might provide a new method for drug delivery.

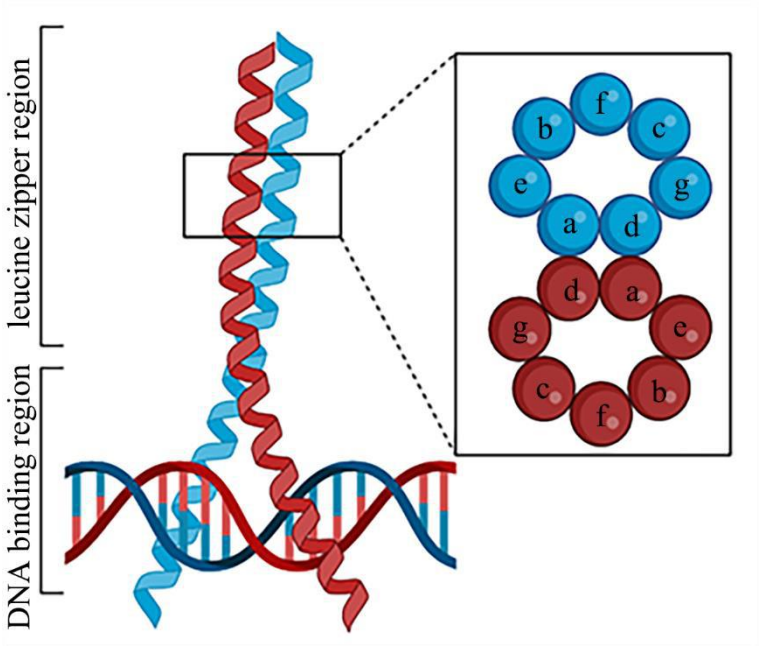

Figure 1.2 Structure of bZip. The bZip protein contains a leucine zipper region and a DNA binding region. The leucine zipper region contains heptad repeats by seven amino acids which are labeled by a-g. The figure was created with Biorender.com.

2. Aims

ADC has achieved great success in cancer treatment, especially in hematological malignancies, but in solid cancer, for example breast cancer and ovarian cancer, which this study is focusing on, still remains some limitations and has much room for improvement: 1) slow and low accumulation in target site; 2) adverse effects caused by off-target toxicity and long circulation time; 3) inconsistent pharmacokinetics due to the heterogeneous products; 4) limited specific antigens for targeting.

Therefore, this project contrives to establish a pre-targeting drug delivery system utilizing the specific interaction between a pair of coiled coil (hereinafter called Zip1 and Zip2) to improve the performance of ADC. In this system, scFv was enrolled instead of full-length antibody to reduce the size of the protein, Zip2 and Zip1 were genetically modified with antibody (scFv-Zip2) and SNAP-tag (Zip1-SNAP) respectively, and cytotoxic agent MMAE was conjugated with Zip1 (Zip1-MMAE) through SNAP-tag technology. To assess the drug delivery property and practicality of the system, functional assays were carried out in breast and ovarian cancer cell lines. In addition, this study also aims to find out more antigens as targets, and thus the epidermal growth factor receptor (EGFR), epithelial cell adhesion molecule (EpCAM), Her2 and Trop2 were tested as potential targets for breast and ovarian cancers.

The concept of this pre-targeting system might provide a novel approach for drug delivery. The improvement of the ADC design and the new targets assessed might be a potential solution to circumvent the aforementioned obstacles.

3. Materials and Methods

3.1 Materials

3.1.1 Chemicals and general consumables

All chemicals and consumables were purchased from Carl Roth, Greiner, Sigma, Corning, Eppendorf, Novolab and Sarstedt unless otherwise stated.

3.1.2 Buffers

Table 3.1 List of buffers

Buffer/Solution	Components	Concentration
4 × Ni-NTA binding buffer (pH 8.0)	NaH_2PO_4	200 mM
	NaCl	1200 mM
	Imidazole	40 mM
1× Ni-NTA binding buffer (pH 8.0)	NaH_2PO_4	50 mM
	NaCl	300 mM
	Imidazole	10 mM
Ni-NTA washing buffer (pH 8.0)	NaH_2PO_4	50 mM
	NaCl	300 mM
	Imidazole	40 mM
Ni-NTA elution buffer (pH 8.0)	NaH_2PO_4	50 mM
	NaCl	300 mM
	Imidazole	250 mM
Stripping buffer (pH 7.4)	NaH_2PO_4	20 mM
	NaCl	500 mM
	EDTA	50 mM
Regeneration buffer	$NiCl_2$	100 mM
5 × Protein Loading Buffer	Bromophenol blue	0.02% (v/v)
	Glycerol	30% (v/v)

	SDS	10% (v/v)
	Tris-HCl	250 mM
10% SDS-PAGE (separation gel)	Milli-Q water	40.8% (v/v)
	Acrylamide/Bisacrylamide (30%, 37.5:1)	32.9% (v/v)
	Tris-HCl (pH 8.8)	373 mM
	SDS	0.1% (w/v)
	TEMED	0.1% (v/v)
	APS	0.032% (w/v)
4% SDS-PAGE gel (stacking gel)	Milli-Q water	60.3% (v/v)
	Acrylamide/Bisacrylamide (30%, 37.5:1)	12.9% (v/v)
	Tris-HCl (0.5 M, pH 6.8)	125 mM
	SDS	0.1% (w/v)
	TEMED	0.1% (v/v)
	APS	0.1% (w/v)
SDS running buffer	Tris	25 mM
	Glycine	0.192 mM
	SDS	0.1% (w/v)
Coomassie brilliant blue gel staining solution	Brilliant blue R 250	1.21 mM
	Methanol	50% (v/v)
	Acetic acid	10% (v/v)
Coomassie brilliant blue gel destaining solution	Methanol	50% (v/v)
	Acetic acid	10% (v/v)
TAE buffer	Tris	40 mM
	Glacial acetic acid	5.71% (v/v)
	EDTA	1 mM
10 × PBS (pH 7.4)	Na_2HPO_4	76.8 mM
	$NaH_2PO_4 \cdot H_2O$	23.2 mM

	NaCl	1.54 M
TBS	Tris	200 mM
	NaCl	1500 mM
TBST (pH 7.6)	Tris	200 mM
	NaCl	1500 mM
	Tween 20	0.1% (v/v)
LB medium (pH 7.0)	LB-Medium (Luria/Miller)	25 g
	Milli-Q water	1000 ml
LB medium supplemented with ampicillin	LB medium	-
	Ampicillin	0.27 mM
LB-Ampicillin agar supplemented with ampicillin	LB medium	-
	Agar agar	0.015% (w/v)
	Ampicillin	0.27 mM
Annexin binding buffer (pH 8.0)	HEPES	10 mM
	NaCl	140 mM
	$CaCl_2$	2.5 mM

3.1.3 Kit

Table 3.2 List of kits

Kit name	Supplier
NucleoSpin® Plasmid	Macherey-Nagel
NucleoSpin® Gel and PCR Clean-up Kit	Macherey-Nagel
Quick Ligation™ Kit	New England Biolabs
Cell Proliferation (XTT) Kit II	Roche

3.1.4 Antibodies

Table 3.3 List of antibodies

Name	Supplier

EGFR Monoclonal Antibody (H11)	Thermo Fisher Scientific
Trop2 (EGP-1) Monoclonal Antibody (MR54)	Thermo Fisher Scientific
CD326 (EpCAM) Monoclonal Antibody (1B7)	Thermo Fisher Scientific
ErbB2 (HER-2) Monoclonal Antibody (3B5)	Thermo Fisher Scientific
Goat anti-Mouse IgG (H+L) Highly Cross-Adsorbed Secondary Antibody, Alexa Fluor™ Plus 647	Thermo Fisher Scientific

3.1.5 Columns

Table 3.4 List of columns

Name	Application	Supplier
Ni-NTA superflow cartridge	Protein purification	Qiagen
HiTrap Desalting column	Buffer exchange	Cytiva
Eurospher II 100-5 C18 column	HPLC	Knauer
40K MWCO Zeba ™ Spin Desalting Columns	Size exclusion	Thermo Fisher Scientific
7K MWCO Zeba ™ Spin Desalting Columns	Size exclusion	Thermo Fisher Scientific

3.1.6 Equipment

Table 3.5 List of equipment

Name	Manufacture
ÄKTA start system	GE Healthcare Bio-Sciences AB
Balances	Kern & Sohn
BD FACSCanto TM II Flow Cytometer	BD Biosciences
Centrifuge Megafuge™ 16	Thermo Fisher Scientific
Centrifuge 5427 R	Eppendorf
ChemiDoc XRS+ System	BIORAD
CytoFLEX Flow Cytometers	Beckman Coulter

DMi8 S Live-cell microscope	Leica Microsystems
ECLIPSE Ts2 inverted microscope	Nikon
Eppendorf ThermoMixer® F2.0	Eppendorf
Fisherbrand™ Multi-Platform Shaker	Fisher Scientific
Incubator IN75	Memmert
Incubation shaker Multitron Standard	Infors
Infinite® Mplex microplate reader	Tecan
Incubator Model CB 170	BINDER
NanoDrop™ One/OneC	Thermo Fisher Scientific
Odyssey DLx Imager	LI-COR Biosciences
PEQLAB PCR Thermal Cycler (PEQLAB PEQSTAR)	PEQLAB Biotechnology
Schott CG 840 pH Meter	Schott
Trans-Blot® Turbo™ Transfer System	BIORAD
Vortex RS-VA 10	Phoenix Instrument
Water bath WB 7	Memmert

3.1.7 Software for data analysis

Table 3.6 List of software

Name	Producer	Application
Adobe Photoshop 2021	Adobe	Image editing
FlowJo 10.7.1	Becton, Dickinson & Company	Image and Data analysis
GraphPad Prism 9.0.0	GraphPad Software	Data analysis
ImageJ	National Institutes of Health	Image analysis
Image Studio Lite Ver 5.2	LI-COR Biosciences	Image analysis
Image Lab software	Bio-Rad	Image analysis
PowerPoint 2019	Microsoft	Image editing

3.1.8 Cell lines

Breast cancer cell lines MDA-MB-468 (ACC 738), MDA-MB-231 (ACC 732), MDA-MB-453 (ACC 65), Hs578T (ACC 781), MCF-7 (ACC 115), SKBR3 (ACC 736) and BT474 (ACC 64) were purchased from the Leibniz Institute DSMZ-German Collection of Microorganisms and Cell Cultures. Ovarian cancer cell lines SKOV3 (HTB-77), OVCAR3 (HTB-161), A2780 (93112519) and human embryonic kidney cell line HEK293T (CRL-11268) were purchased from American Type Culture Collection. Hey was kindly provided by Dr. Karen Bräutigam (Department of Gynecology and Obstetrics, University Hospital Schleswig-Holstein, Campus Lübeck) as a gift.

3.1.9 Medium

RPMI-1640 (Biowest) and DMEM (Thermo Fisher Scientifc) medium were supplemented with 10% (v/v) fetal bovine serum (FBS) (Thermo Fisher Scientifc) and 1% (v/v) penicillin and streptomycin (Thermo Fisher Scientifc) as complete culture medium. Additional 0.1% (v/v) zeocin (InvivoGen) was added to RPMI 1640 complete culture medium to keep selecting transfected cells during the protein expression.

3.1.10 Designing the scFv genes

The VH and VL of Herceptin, Erbitux, Sacituzumab (hereinafter called Sacit) amino acid sequences were determined from their full length mAbs from Global Substance Registration System. The amino acid sequences were reverse translated and the VH and VL were connected by a glycine-serine linker and have a 5´SfiI and 3´XbaI restriction site sequences. The designed scFv genes synthesis by GenScript and subcloned into default pUC57 vector. The constructs of scFv-425-SNAP and scFv-EpCAM-SNAP have been generated as described [110, 111].

3.1.11 Enzymes

All restriction enzymes were purchased from New England Biolabs. Ultra-DNA

polymerase was purchased from Jena Bioscience. In-Fusion® Snap Assembly Master Mix was purchased from TaKaRa.

3.2 Methods

3.2.1 Molecular cloning

3.2.1.1 Preparation of chemically competent *E. Coli*

DH5α *E. Coli* cells were plated on LB agar plate and incubated at 37°C overnight. Single colonies were inoculated into 2 ml LB liquid medium and incubated at 37°C overnight with vigorous shaking (250 rpm). 1 ml of the overnight *E. Coli* culture was transferred into 100 ml of LB liquid medium and incubated at 37°C with vigorous shaking (250 rpm) for 1.5-2 h until the OD600 reached 0.25-0.3. *E. Coli* culture was chilled on ice for 15 min, and then centrifuged at 3300 g for 10 min at 4°C. Cells were resuspended in 35 ml of ice-cold 0.1 M $CaCl_2$ and incubated on ice for 30 min. The centrifugation step was repeated. Cell pellets were then resuspended with 6 ml of ice-cold 0.1 M $CaCl_2$ and 15% glycerin. For long-term storage, aliquots of 100 µl of the cell suspension was prepared in sterile 1.5 ml tubes and frozen in liquid nitrogen, and then stored in -80°C directly.

3.2.1.2 Bacterial transformation

Chemically competent DH5α *E. Coli* cells (100 µl) were thaw on ice and gently mixed with 5-10 µl of ligation reaction or 10 pg-100 ng of plasmid DNA. Cells were incubated on ice for 30 min, followed by heat shock at 42°C for 45 s, and then chilled on ice for 5 min. Cells were mixed with 800 µl of LB medium and incubated at 37°C with shaking for 1 h. After centrifugation at 5000 rpm for 2 min, 800 µl of supernatant was discarded, the cells were resuspended and plated on LB agar plate containing 100 µg/ml ampicillin. Cells were incubated at 37°C overnight.

3.2.1.3 Bacterial inoculation

Single colony observed in LB agar plate was inoculated using a sterile pipette tip into 2 ml of LB medium supplemented with 100 µg/ml ampicillin. Cells were incubated with 220 rpm shaking at 37°C overnight.

3.2.1.4 Extraction of plasmid DNA from *E. Coli* and bacterial preservation

Plasmid DNA was extracted from 1.5 ml of DH5α *E. Coli* LB culture after overnight incubation using NucleoSpin plasmid kit according to manufacturer's instructions. The rest 0.5 ml of bacterial culture were mixed with 500 µl of 50% (v/v) glycerol and divided into 250 µl aliquots. The glycerol stocks were stored at -80°C.

3.2.1.5 Digestion of DNA by restriction enzyme

The digestion reaction was prepared as **table 3.7**. The digestion could be either single-temperature double digest or multi-temperature double digest depending on the restriction enzymes used. The reaction was incubated at 37°C for 1 h in single-temperature double digest, and incubated at 37°C for 1 h followed by at 50°C for 1 h in multi-temperature double digest. The restriction enzymes used, and optimal temperature were listed in **table 3.8**.

Table 3.7 Digestion reaction

Components	Volume (µl)	Final concentration
DNA	variable	1 µg
Restriction enzyme	variable	5 U
10 × CutSmart® buffer	2.5 µl	1 ×
Ultrapure water	To 25 µl	-

Table 3.8 List of restriction enzymes

Restriction enzyme	Optimal temperature
SfiI	50°C
XbaI	37°C

BlpI	37°C

3.2.1.6 Polymerase chain reaction

Polymerase chain reaction (PCR) was used to amplify the DNA sequence of fragments and vectors for further usage. The reaction was set up as **table 3.9**, and the program was run as **table 3.10**.

Table 3.9 PCR reaction

Components	Volume	Final concentration
DNA template	1 µl	1 ng
5 × DNA buffer	10 µl	1 ×
Forward primer	1 µl	0.2 µM
Reverse primer	1 µl	0.2 µM
dNTP mix*	1-3 µl	0.2-0.6 µM
Ultra-DNA polymerase	0.5 µl	0.02 units
PCR grade water	Fill up to 50 µl	-

*1 µl of dNTP mix was used for fragment amplification, and 3 µl was used for vector amplification.

Table 3.10 PCR cycling condition

Steps	Temperature	Time	Cycle
Initial denaturation	98°C	3 min	1 ×
Denaturation	98°C	1 min	
Annealing	60°C	1 min	35 ×
Elongation	68°C	1 min/kb	
Final elongation	68°C	10 min	1 ×

3.2.1.7 Agarose gel electrophoresis

Agarose gel electrophoresis was used to separate DNA fragments from PCR or digestion reaction. DNA samples were mixed with 6 × purple gel loading dye (New England Biolabs) and run in 1% (w/v) agarose gel supplemented with 1 × SYBR Safe DNA Gel Stain (Invitrogen) along with 2-Log DNA ladder (New England Biolabs) at

100 V for 30 min. Gel was visualized under UV light using ChemiDoc XRS+ System.

3.2.1.8 Extraction of plasmid DNA from agarose gel

DNA fragment of interest was extracted from agarose gel using NucleoSpin® Gel and PCR Clean-up Kit according to manufacturer's instructions.

3.2.1.9 Ligation

All ligation reactions were performed using Quick Ligation™ Kit following manufacturer's protocol unless specifically stated otherwise. The reaction using Quick Ligation™ Kit was set up as showed in **table 3.11**.

Table 3.11 Ligation reaction of Quick Ligation™ Kit

Components	Volume	Final concentration
Ligase	1 µl	1 µg
2 × Reaction buffer	10 µl	1 ×
Vector DNA	variable	50 ng
Insert DNA*	variable	variable
Nuclease-free water	Fill up to 20 µl	-

*The reaction used a molar ratio of 1:3 vector to insert. Formula: required mass insert (g) = desired insert/vector molar ratio × mass of vector (g) × ratio of insert to vector lengths.

The Annexin V-SNAP was generated by In-Fusion Snap Assembly cloning kit using protocol from manufacturer. The reaction was prepared as showed in **table 3.12**.

Table 3.12 Ligation reaction of In-Fusion Snap Assembly cloning kit

Components	Volume	Final concentration
5 × In-Fusion Snap Assembly Master Mix	2 µl	1 ×
Vector DNA	variable	50 ng
Insert DNA*	variable	variable
Nuclease-free water	Fill up to 10 µl	-

*The reaction used a molar ratio of 1:3 vector to insert. Formula: required mass insert (g) = desired insert/vector molar ratio × mass of vector (g) × ratio of insert to vector lengths.

3.2.1.10 DNA sequencing

All generated plasmids were sent to Eurofins Genomics for sequencing to confirm the correct insertion. The primer used for sequencing were listed below.

Table 3.13 Primers for sequencing

Primer	Sequence	Purpose
IgK-For	ACACACTCCTGCTATGGG	General primer to confirm insertion of Erbitux, EpCAM, Herceptin, Sacit, Zip1 and Annexin V.
Zip2-Rev	CCCTCCTCTAGACTGTTC GTGAGACGCC	To confirm the insertion of Zip2.

3.2.1.11 Establish of expression constructs

The pSecTag2-based pMS eukaryotic expression vector was previously used to establish the pMS-scFv-425-SNAP construct as described [65]. Briefly, scFv-425 PCR product and pMS vector were digested and ligated by SfiI and XbaI restriction enzymes. The pMS-scFv-425 and SNAP-tag PCR product were digested by XbaI and BlpI and then ligated to generate pMS-scFv-425-SNAP. To generate other scFv-SNAP constructs, scFv-425 DNA was replaced by scFv-Erbitux, scFv-Herceptin or scFv-Sacit via SfiI and XbaI digestion and ligation.

Zip1 PCR product amplified by Zip1-SfiI-For and Zip1-XbaI-Rev and pMS-scFv-SNAP were digested and ligated by SfiI and XbaI to generate pMS-Zip1-SNAP. Zip2 PCR product amplified by Zip2-XbaI-For and Zip2-BlpI-Rev, while pMS-scFv-425-SNAP plasmids were digested and ligated by XbaI and BlpI to generate pMS-scFv-Zip2.

The pMS- Annexin V-SNAP was generated for apoptosis assay as described [112]. Vector pMS-SNAP was amplified from pMS-scFv-425-SNAP by Vector-Annexin V-for and Vector-Annexin V-Rev using ultra DNA polymerase. Fragment Annexin V was amplified from pJ128 by Frag-Annexin V-For and Frag-Annexin V-Rev using ultra

DNA polymerase. pJ128 was a gift from Jonathan Tait (Addgene plasmid # 19962; http://n2t.net/addgene:19962; RRID: Addgene_19962).

Fragments and vectors were ligated by In-Fusion Snap Assembly cloning kit following manufacturer's protocol.

The primers used were listed below.

Table 3.14 Primers for generating expression constructs

Primer	Sequence	Purpose
scFv-425-For	TAAGCAGGCCCAGCCGGCC ATGGCCGAGGTGCAACTGC	Amplify scFv-425
scFv-425-Rev	TATACCTCTAGAGTCCCCGA GCCGAACGTG	Amplify scFv-425
SNAP-For	TAAGCATCTAGAATGGACA AAGACTGCGAAATG	Amplify SNAP-tag
SNAP-Rev	TATACCGCTGAGCCAGCCC AGGCTTGCCCAGTC	Amplify SNAP-tag
Zip1-SfiI-For	CGGGTCGGCCCAGCCGGCC AATCTCGTAGCCCAAC	Amplify Zip1
Zip1-XbaI-Rev	TTCGTGTCTAGACTCCTCAA TCTTTTTCCG	Amplify Zip1
Zip2-XbaI-For	CAGCCGTCTAGAGCGCGGA ACGCGTATCTAAG	Amplify Zip2
Zip2-BlpI-Rev	ACCCTCGCTCAGCCTGTTC GTGAGACGCC	Amplify Zip2
Vector-Annexin V-for	TCTAGAATGGACAAAGACT GCGAAATGA	Amplify pMS-SNAP
Vector-Annexin V-Rev	GTCACCAGTGGAACCTGGA AC	Amplify pMS-SNAP
Frag-Annexin V-For	GGTTCCACTGGTGACATGG CGGGTGGTTGTGG	Amplify Annexin V

Frag-Annexin V-Rev	TTTGTCCATTCTAGAGTCAT CTTCTCCAGAGAGCAGC	Amplify Annexin V

3.2.2 Protein production

3.2.2.1 Cell culture

Breast cancer cell lines (MDA-MB-468, MDA-MB-231, MDA-MB-453, Hs578T, MCF-7, SKBR3 and BT474) were cultured in DMEM complete culture medium. The human embryonic kidney cell line HEK293T and ovarian cancer cell lines (SKOV3, OVCAR3, OVCAR4, Hey and A2780) were cultured in RPMI 1640 complete culture medium. Transfected HEK293T cells for protein expression were cultured in RPMI 1640 complete culture medium supplemented with 0.1% zeocin for selection. Cells were passaged every 3-5 days when cells reached about 80% confluency. Cells were incubated at 37°C in a humidified atmosphere containing 5% CO_2.

3.2.2.2 Transfection of HEK293T cells with recombinant DNA

HEK293T cells were transfected with recombinant DNA by Roti® Fect (Carl Roth) using the manufacturer's instructions. Cells were seeded at the concentration of 400,000/well in 2 ml medium in a 6-well dish. Generally, 2 µg of plasmid was mixed with serum-free RPMI 1640 medium without antibiotics to reach the volume of 100 µl, and 10 µl of transfection reagent was mixed with 90 µl of serum-free RPMI 1640 medium without antibiotics. The two solutions were mixed gently and then incubated at room temperature for 20 min. The medium in the well was removed. After being rinsed gently by DPBS, well was refilled by 1.5 ml fresh antibiotic-free RPMI 1640 medium with serum. The nucleic acid-lipid complex (200 µl) was added dropwise to the cells. Cells were incubated at incubator (37°C, 5% CO_2) overnight. The medium was replaced after 24 h with RPMI 1640 complete medium supplemented with 0.1% (v/v) zeocin to select successfully transfected cells.

3.2.2.3 Expression of recombinant proteins

The successfully transfected cells were cultured in RPMI 1640 complete medium supplemented with 0.1% (v/v) zeocin to keep selection during the protein expression. Cells were grown in triple-layer flasks containing 150-200 ml culture medium. Culture medium was replaced and collected every 5-7 days for totally three times. Collect culture supernatant (450-600 ml) was stored at 4°C up to 2 weeks.

3.2.2.4 Protein enrichment

All SNAP- and Zip2-fusion proteins were enriched by an Ni-NTA superflow cartridge using the C-terminal 6 × His-tag. The culture supernatant was centrifuged at 5000 rpm for 10 min at 4°C and then filtered through 0.45 μm Corning® Vacuum Filter to get cell-free culture supernatant. The pH and buffer composition of the culture supernatant were adjusted by mixing with 4 × Ni-NTA binding buffer in a 1:4 ratio. The culture supernatant was run through Ni-NTA superflow cartridge at a 0.5 – 1 ml/min flow rate after equilibrating the cartridge with 10 column volumes of 4 × Ni-NTA binding buffer. Ni-NTA washing buffer was applied to get rid of non-specifically bound proteins until the UV absorbance value reached the baseline. SNAP- and Zip-fusion proteins were eluted by Ni-NTA elution buffer. Cartridge was washed by NaOH (0.5 M) to remove residual proteins from the resin, followed by stripping buffer to strip the nickel ions from the column. The column was then recharged by $NiCl_2$ solution and could be used for next purification. All the eluted fractions were collected during purification. After incubation with SNAP-Surface® Alexa Fluor® 488 for 20 min at room temperature in the dark, fractions were run in 10% SDS gel to confirm the activity of SNAP-tag and the presence of proteins followed by Coomassie brilliant blue staining.

3.2.2.5 Buffer exchange of purified proteins

For long-term storage of purified proteins and further experiments, the protein in elution fraction from 3.2.2.4 was exchanged to PBS by using HiTrap Desalting column. The

column was washed with 5-column volumes of water, followed by 5-column volumes of PBS. Sample was applied to column at 1-2 ml/min flow rate. The elution fraction was collected when the UV absorbance started to increase until the value reached baseline. The column was washed with 5-column volumes of water, and then with 5-column volumes of 20% ethanol and stored at room temperature. Proteins were stored at -20°C.

3.2.2.6 Protein electrophoresis

Sodium dodecyl-sulfate polyacrylamide gel electrophoresis (SDS-PAGE) is a commonly used methods for protein separation and analysis. Protein samples were mixed with 5 × Protein Loading Buffer and run in 10% SDS gel along with blue prestained protein standard broad range (New England Biolabs) at 160 V for 60 min. Gel was visualized using ChemiDoc XRS+ System or Odyssey DLx Imager.

3.2.2.7 Protein concentration quantitation

The protein concentration was determined by Image Lab software (BioRad) using bovine serum albumin (BSA) standards. Serially diluted BSA was prepared by mixing BSA (New England Biolabs, 20 mg/ml) with PBS to set 4 concentrations (0.2, 0.1, 0.05, 0.025 µg/µl). Protein samples and 10 µl of standard BSA solutions were run in 10% SDS gel. The standard curve and protein concentration were generated and calculated by Image Lab software.

3.2.3 Protein labeling

3.2.3.1 Synthesis of benzylguanine-modified cytotoxic drug

Amino-PEG4-Val-Cit-PAB-MMAE and BG-GLA-NHS were dissolved to 10 mM in DMSO. Amino-PEG4-Val-Cit-PAB-MMAE and BG-GLA-NHS was incubated at a 1:2 molar ratio in PBS at room temperature for 4 h. BG-GLA-PEG4-Val-Cit-PAB-MMAE (hereinafter called BG-MMAE) was analyzed and purified by high-performance liquid

chromatography (HPLC) via a Eurospher II 100-5 C18 column (8 × 250 mm, 5 µm, 100 Å) at a flow rate of 4 ml/min. Separations were carried out using 40% acetonitrile, 60% water, and 0.1M ammonium acetate (4 ml/min/isocratic). The mass of BG-MMAE was confirmed using a Bruker MicroTOF LC mass spectrometer with an electrospray ion source. Accurate masses were derived from mass spectra in the range 0–2000 m/z. All HPLC and mass spectrometry analysis were done by the HPLC facility, Institute of Organic Chemistry, Justus-Liebig-University Giessen).

3.2.3.2 Conjugation of SNAP-tag fusion proteins with benzylguanine-modified agents

SNAP-Surface® Alexa Fluor® 488, SNAP-Surface® Alexa Fluor® 647 or BG-modified MMAE were conjugated to SNAP-tag fusion proteins by incubating at a 2:1 molar ratio at room temperature in dark for 2 h. The residual agents were removed by 40K MWCO Zeba ™ Spin Desalting Columns according to manufacturer's protocol.

3.2.3.3 Conjugation of Zip2-fusion protein with fluorescent dye

To investigate the colocalization of the pre-targeting antibody and Zip1-SNAP, these two probes were conjugated with different fluorescent dye. As the Zip1-SNAP was conjugated with SNAP-Surface® Alexa Fluor® 647, the scFv-Zip2 was conjugated with Alexa Fluor® 488 NHS-ester (succinimidyl ester) at a 1:3 molar ratio at room temperature in dark for 2 h. The succinimidyl ester is commonly used to label primary amine of protein as a random conjugation method. The residual agents were removed by 7K MWCO Zeba ™ Spin Desalting Columns according to manufacturer's protocol.

3.2.4 Functional assays

3.2.4.1 Far-western blotting

The interaction between scFv-Zip2 proteins and Zip1-SNAP was confirmed by far-western blotting in polyvinylidene difluoride (PVDF) membrane. The scFv-Zip2

proteins (1 µg) and scFv-Erbitux-SNAP (negative control) were separated in 10% SDS gel at 160 V for 60 min. Proteins were transferred into a PVDF membrane using a Trans-Blot Turbo System at 25 V, 1.3 A for 15 min. The membrane was incubated in blocking buffer (1% BSA in TBST) at room temperature for 1 h. Then the membrane was incubated with 3 µg of SNAP-Surface® Alexa Fluor® 488 labeled Zip1-SNAP in blocking buffer at room temperature in dark for 1 h. After three washing steps with TBST, membrane was visualized under UV light using ChemiDoc XRS+ System.

3.2.4.2 Flow cytometry

3.2.4.2.1 Antigen expression

The EGFR, EpCAM, Her2 and Trop2 expression was confirmed by flow cytometry. Here, 4×10^5 cells were collected and washed with 1 ml PBS twice, followed by incubation with anti-EGFR (EGFR monoclonal antibody, H11, 0.5 µg), anti-EpCAM (CD326 monoclonal antibody, 1B7, 0.125 µg) and anti-Trop2 (Trop2 monoclonal antibody, MR54, 1 µg) antibodies in 200 µl of PBS for 30 min on ice. Considering that the anti-Her2 (ErbB2 monoclonal antibody, 3B5) antibody targets intracellular domain of Her2, cells were fixed by 4% formaldehyde solution at room temperature for 10 min, and then permeabilized with 0.1% Triton X-100 in TBS at room temperature for 5 min. Cells were blocked by blocking buffer (10% FBS and 1% BSA in PBS) on ice for 30 min followed by incubation with anti-Her2 antibody. After two washing steps, cells were incubated with goat anti-mouse IgG (H+L) Highly Cross-Adsorbed Secondary Antibody conjugated with Alexa Fluor™ Plus 647 (0.25 µg) for 30 min on ice. After two washing steps, cells were resuspended in 200 µL of PBS and analyzed by CytoFLEX Flow Cytometers. Data was analyzed in FlowJo 10.7.1.

3.2.4.2.2 Binding property analysis

To confirm the cell-binding property of the pre-targeting complex and to compare the binding ability between pre-targeting complex and directly labeled scFv-SNAP, Zip1-

and scFv-SNAP fusion proteins were conjugated with SNAP-Surface® Alexa Fluor® 647 (scFv-647 and Zip1-647). Both breast (MDA-MB-468, MDA-MB-231, MDA-MB-453, Hs578T, MCF-7, SKBR3 and BT474) and ovarian (SKOV3, OVCAR3, OVCAR4, Hey and A2780) cancer cell lines were used in flow cytometry. Here, 4×10^5 cells were washed with 1 ml PBS twice, followed by incubation with 1 µg of scFv-647 or scFv-Zip2 in 200 µl of PBS for 30 min on ice. After two washing steps, cells treated with scFv-Zip2 were further incubated with 1 µg of Zip1-647 on ice for 30 min, and cells treated with directly labeled scFv-SNAP was treated with PBS. After two washing steps, cells were resuspended in 200 µL of PBS and analyzed by CytoFLEX Flow Cytometers or BD FACSCanto TM II Flow Cytometer. Data was analyzed in FlowJo 10.7.1.

3.2.4.2.3 Confirming the binding to different epitopes of EGFR

To confirm the recognition of 425 and Erbitux antibodies of different epitopes of EGFR, EGFR was blocked by either scFv-425-SNAP or scFv-Erbitux-SNAP and then incubated with fluorescence dye labeled scFv-Erbitux-SNAP or scFv-425-SNAP. Briefly, 4×10^5 cells were washed with 1 ml PBS twice and EGFR was blocked by 10 µg of scFv-425-SNAP or scFv-Erbitux-SNAP on ice for 30 min. After centrifugation at 500 rpm for 5 min, cells were incubated with 1 µg of SNAP-Surface® Alexa Fluor® 647 labeled same scFv-SNAP fusion proteins to confirm the blocking efficiency or the other scFv-SNAP fusion proteins to confirm the binding property to different epitopes of EGFR on ice for 30 min. After two washing steps, cells were resuspended in 200 µL of PBS and analyzed by CytoFLEX Flow Cytometers or BD FACSCanto TM II Flow Cytometer. Data was analyzed in FlowJo 10.7.1.

3.2.4.3 Fluorescence Microscopy

3.2.4.3.1 Binding and internalization properties of scFv-SNAP fusion proteins

To confirm the binding and internalization scFv-SNAP fusion proteins labeled with

SNAP-Surface® Alexa Fluor® 647 were used to validate internalization ability. Here, the cells were seeded in black 96-well plate with a clear bottom to a density of 40,000 cells/well and incubated overnight at 37°C. Cells were washed with PBS two times, and then incubated with 1 µg of each 647-labeled scFv at 37 °C for 3 h. After two washing steps, cells were incubated with Hoechst 33,342 fluorescent nuclear counterstain (1:500 in PBS) (Thermo Fisher Scientific) for 15 min at room temperature. Cells were washed with PBS twice and incubated in 100 µL of PBS. To determine the binding property, cells were incubated with antibodies for 1 h and all steps were carried out at 4°C. The internalization and binding were visualized with a DMi8 S Live-cell microscope using a 100 × oil objective.

3.2.4.3.2 Binding, internalization and co-localization of pre-targeting complex

Zip2-fusion scFvs were labeled with Alexa Fluor® 488 and Zip1-SNAP was labeled with SNAP-Surface® Alexa Fluor® 647 for better visualization of binding, internalization and co-localization. The procedure could refer to **3.2.4.3.1**, but cells were firstly incubated with scFv-Zip2-488 for 1 h followed by three-hour incubation at 37 °C with 1 µg of Zip1-647 for internalization assay, or incubated with scFv-Zip2-488 for 1 h followed by one-hour incubation at 4°C with 1 µg of Zip1-647 for binding assay. The images were merged by ImageJ to confirm the co-localization of the scFv-Zip2-488 and Zip1-647.

3.2.4.4 Cytotoxic Assay

The cytotoxicity of directly conjugated ADCs and pre-targeting ADCs were evaluated using a Cell Proliferation (XTT) Kit II. Cells were seeded in 96-well plates at a density of 5000 cells/well in 50 µL of culture medium and incubated at 37°C overnight, followed by incubation with serially diluted unconjugated antibodies (scFv-Herceptin-SNAP, scFv-Erbitux-SNAP, scFv-425-SNAP, scFv-αEpCAM-SNAP and scFv-Sacit-SNAP), directly conjugated antibodies (scFv-Erbitux-MMAE, scFv-425-MMAE, scFv-αEpCAM-MMAE and scFv-Sacit-MMAE) or MMAE (10, 20, 40, 80, 160, 320,

640 nM) at 37°C for 72 h. Due to our preliminary experiment (not shown), strong toxicity of scFv-Herceptin-MMAE, and the high amount of Her2 expressed by SKBR3 proved by previous studies [113, 114], the range of concentration was expanded in MDA-MB-468, MDA-MB-231, MDA-MB-453, Hs578T and BT474 cell lines (1.25, 2.5, 5, 10, 20, 40, 80, 160, 320, 640 nM), and reduced in SKBR3 (0.03125, 0.0625, 0.125, 0.25, 0.5, 1, 2, 4, 8, 16 nM). Cells incubated with PBS or zeocin were set as negative or toxic control.

For pre-targeting complex, cells were firstly treated with 640 nM of targeting molecules (scFv-Herceptin-Zip2, scFv-Erbitux-Zip2, scFv-425-Zip2, scFv-αEpCAM-Zip2 and scFv-Sacit-Zip2), and incubated at 37°C for 1 h, followed by treatment with serially diluted Zip1-MMAE (10, 20, 40, 80, 160, 320, 640 nM).

Cells were incubated at 37°C for 72 h. Viability was determined by incubating cells with a 50 µL XTT labeling mixture at 37°C for 4 h. The substrate conversion was monitored at a 450 nm absorbance wavelength and 650 nm reference wavelength using an Infinite® Mplex microplate reader. The experiment was repeated independently three times in triplicates.

3.2.4.5 Induction of Apoptosis

The induction of apoptosis was determined using Annexin V-SNAP conjugated with SNAP-Surface® Alexa Fluor® 647 (Annexin V-647) and propidium iodide (PI) [112]. Briefly, cells were seeded in 24-well plates at a density of 50,000 cells/well in triplicates, and then incubated with 640 nM of unconjugated antibodies (scFv-Herceptin-SNAP, scFv-Erbitux-SNAP, scFv-425-SNAP, scFv-αEpCAM-SNAP and scFv-Sacit-SNAP), directly conjugated antibodies (scFv-Herceptin-MMAE, scFv-Erbitux-MMAE, scFv-425-MMAE, scFv-αEpCAM-MMAE and scFv-Sacit-MMAE) or MMAE. SKBR3 was treated with 16 nM of scFv-Herceptin-MMAE.

For pre-targeting complex, cells were treated with 640 nM of targeted molecules (scFv-Herceptin-Zip2, scFv-Erbitux-Zip2, scFv-425-Zip2, scFv-αEpCAM-Zip2 and scFv-Sacit-Zip2), and incubated at 37°C for 1 h, followed by treatment with 640 nM of Zip1-

MMAE.

Cells treated with PBS or camptothecin (Merck KGaA) were used as negative or positive control, respectively. After incubation at 37C° for 48 h, floating cells was collected, and adherent cells were harvested by trypsinization and collected in 5ml round bottom polystyrene FACS tubes. Cells were washed by 1 ml of annexin binding buffer at 500 g for 5 min for twice, and then incubated with 0.5 µg of Annexin V-647 in 100 µl of Annexin binding buffer at room temperature for 30 min. After a washing step, cells were treated with 0.1 µg of propidium iodide (Thermo Fisher Scientific) in 100 µl of annexin binding buffer at room temperature for 10 min. The early and late apoptotic cells were detected on BD FACSCanto TM II Flow Cytometer. The experiment was repeated independently three times in triplicate.

4. Results

4.1 Design and construction of SNAP- and Zip2-fusion proteins

The sequences of scFv targeting EGFR, EpCAM, Her2 and Trop2 were derived from anti-EGFR human-mouse chimeric monoclonal antibody Erbitux (also known as cetuximab) [115], anti-EGFR murine IgG monoclonal antibody 425 [111, 116, 117], anti-EpCAM humanized scFv C54 [110, 118], anti-Her2 humanized monoclonal antibody Herceptin (also known as trastuzumab) [119] and anti-Trop2 humanized monoclonal antibody sacituzumab [90]. The open reading frames of SNAP- and Zip2-fusion protein DNA sequences (**Supplementary materials 9.1**) were inserted into the mammalian expression vector pMS (**Figure 4.1**). The cytomegalovirus enhancer and promoter were used to increase and initiate the downstream gene transcription. The murine immunoglobulin kappa chain leader was located upstream to the fusion proteins to allow the secretion of the fusion protein into culture medium. The VH and VL were connected by a glycine-serine linker consisting of three repeats of Gly–Gly–Gly–Gly–Ser to provide the structural flexibility. SNAP-tag or Zip2 was located downstream to the scFv or Zip1, followed by His-tag that would be used to facilitate protein enrichment in the C-terminus of protein. The pMS-scFv-425-SNAP construct was previously established as described [65]. To generate other SNAP-tag fusion proteins, scFv-425 was replaced by scFv-Erbitux, scFv-αEpCAM, scFv-Herceptin, scFv-Sacit and Zip1 using SfiI and XbaI restriction enzymes. Then, the SNAP-tag was replaced by Zip2 using XbaI and BlpI restriction enzymes. The presence of the inserted DNA and its sequence were confirmed by DNA sequencing (Sanger Sequencing services, Eurofins Genomics, Germany).

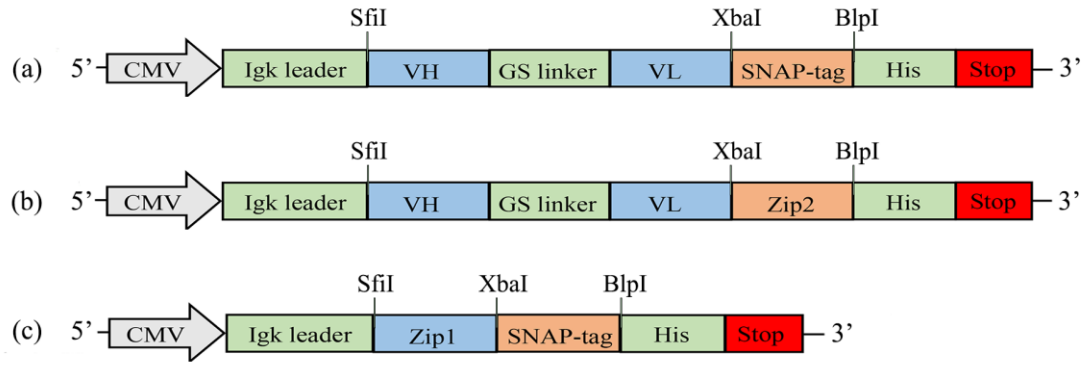

Figure 4.1. Schematic of scFv-SNAP, scFv-Zip2 and Zip1-SNAP construct design. CMV: cytomegalovirus enhancer and promoter; IgK leader: murine immunoglobulin kappa chain leader; VH: variable heavy chain; GS linker: glycine-serine linker; VL: variable light chain; His: polyhistidin tag; Stop: TGA stop codon.

4.2 Expression and enrichment of SNAP- and Zip2-fusion proteins

The expression of SNAP- and Zip2-fusion proteins were achieved using HEK293T cells, which was firstly confirmed by detecting the GFP signal in the transfected cells (data not shown). Protein in collected culture supernatant were enriched by immobilized metal affinity chromatography using an Ni-NTA superflow cartridge via the 6 × His-tag in C-terminal of the protein.

As the BG-modified molecules react solely with SNAP-fusion proteins, the success of the fusion protein enrichment was determined by incubating the collected protein fractions with SNAP-Surface® Alexa Fluor® 488 followed by protein separation in SDS gel. The presence of the SNAP-fusion proteins and the activity of SNAP-tag were confirmed by detecting the 488 fluorescence signal followed by determining the protein size by Coomassie blue staining. For the Zip2-fusion proteins, the success of the Zip2-fusion protein enrichment was confirmed by separating the collected protein fractions in SDS gel followed by Coomassie blue staining.

The scFv-Zip1-SNAP and scFv-Herceptin-Zip2 are shown as examples in **figure 4.2**. Proteins were eluted by Ni-NTA elution buffer with different concentrations of imidazole (10, 40 and 250 mM), especially with 250 mM of imidazole (highlighted with red box). The two lanes named 40 mM imidazole in figure 4.2 represent the earlier and later stage to better control the enrichment as the his-tagged proteins could also be

eluted at later stage with 40 mM of imidazole. The scFv-Zip1-SNAP (31.3 kDa) were detected by both UV-excited 488 fluorescence and Coomassie blue staining. Without visualization by fluorescence, the presence of scFv-Herceptin-Zip2 (40.5 kDa) was invisible due to the low amount in supernatant but was observed in eluate with 40 mM and 250 mM imidazole. Given the fact that the volume of protein eluted by 250 mM imidazole was only one-third of that eluted by 40 mM imidazole, the protein was mainly eluted with 250 mM imidazole, and the wastage was negligible. Meanwhile, proteins from culture medium were also removed stepwise, and almost only protein of interest was present at last. Other proteins were produced and validated in the same way (**Supplementary Figure 1**). This fast and high-expression system could yield SNAP-fusion proteins with up to 10 mg per liter of culture supernatant and Zip2-fusion proteins with up to 5 mg per liter of culture supernatant.

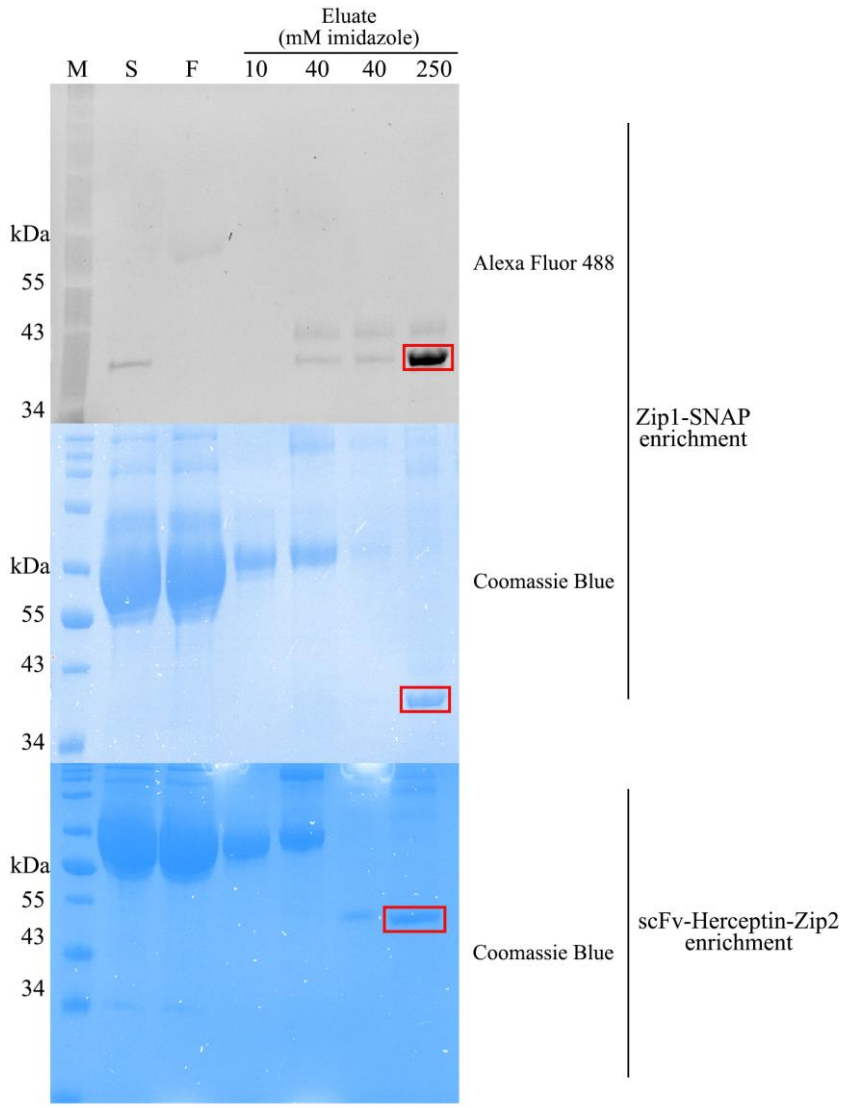

Figure 4.2. Zip1-SNAP and scFv-Herceptin-Zip2 are enriched. The His-tagged Zip1-SNAP and scFv-Herceptin-Zip2 were enriched by nickel purification and confirmed by SDS-PAGE. While the Zip1-SNAP was confirmed by SNAP-Surface® Alexa Fluor® 488 followed by Coomassie blue staining, the scFv-Herceptin was confirmed by Coomassie blue staining (highlighted with red box). The signal was visualized with ChemiDoc XRS+ System. M: Blue prestained protein standard broad range (11-250 kDa). S: cell-free culture supernatant; F: flowthrough.

4.3 Conjugation of SNAP-tag fusion proteins with BG-modified agents

Amino-PEG4-Val-Cit-PAB-MMAE (1370.7 Da) was modified with BG-GLA-NHS (481.5 Da) as described in **3.2.3.1**. The product BG-MMAE was purified and validated by HPLC (**Figure 4.3a-c**) and mass spectrometry analysis (**Figure 4.3d**). All HPLC and mass spectrometry analysis were done by the HPLC facility (Institute of Organic Chemistry, Justus-Liebig-University Giessen). The retention time of BG-GLA-NHS,

Amino-PEG4-Val-Cit-PAB-MMAE and BG-MMAE was 1.607, 6.547 and 8.073 min, respectively. The double and triple protonated products in mass spectrum analysis with total molecular weight 1852.787 Da indicated the successful generation of BG-MMAE. The conjugation efficiency of SNAP-tag fusion proteins was further explored. The SNAP-tag fusion proteins (scFv-425-SNAP, scFv-Erbitux-SNAP, scFv-αEpCAM-SNAP, scFv-Herceptin-SNAP, scFv-Sacit-SNAP and Zip1-SNAP) were conjugated with SNAP-Surface® Alexa Fluor® 647 (used as imaging agents) and BG-MMAE (used as therapeutic agents) (**Figure 4.4a**). The scFv-Herceptin-SNAP and Zip1-SNAP were showed as examples in **figure 4.4b**. The site-specific conjugation of BG-modified molecules to SNAP-tag fusion proteins was confirmed by post-incubation them with SNAP-Surface® Alexa Fluor® 488. While unconjugated proteins retained the full activity to couple SNAP-Surface® Alexa Fluor® 488, the specific coupling sites were blocked by SNAP-Surface® Alexa Fluor® 647 or BG-MMAE. SNAP-Surface® Alexa Fluor® 488 was observed under UV light using ChemiDoc XRS+ System, and the SNAP-Surface® Alexa Fluor® 647 signal was observed at 685 nm using an Odyssey DLx Imager. The presence of all proteins is shown in SDS gel stained with Coomassie brilliant blue. Our results demonstrated that BG-modified agents could be conjugated to SNAP-fusion proteins site-specifically and sufficiently within 2 h at room temperature. Other proteins were conjugated in the same way (**Supplementary Figure 2**).

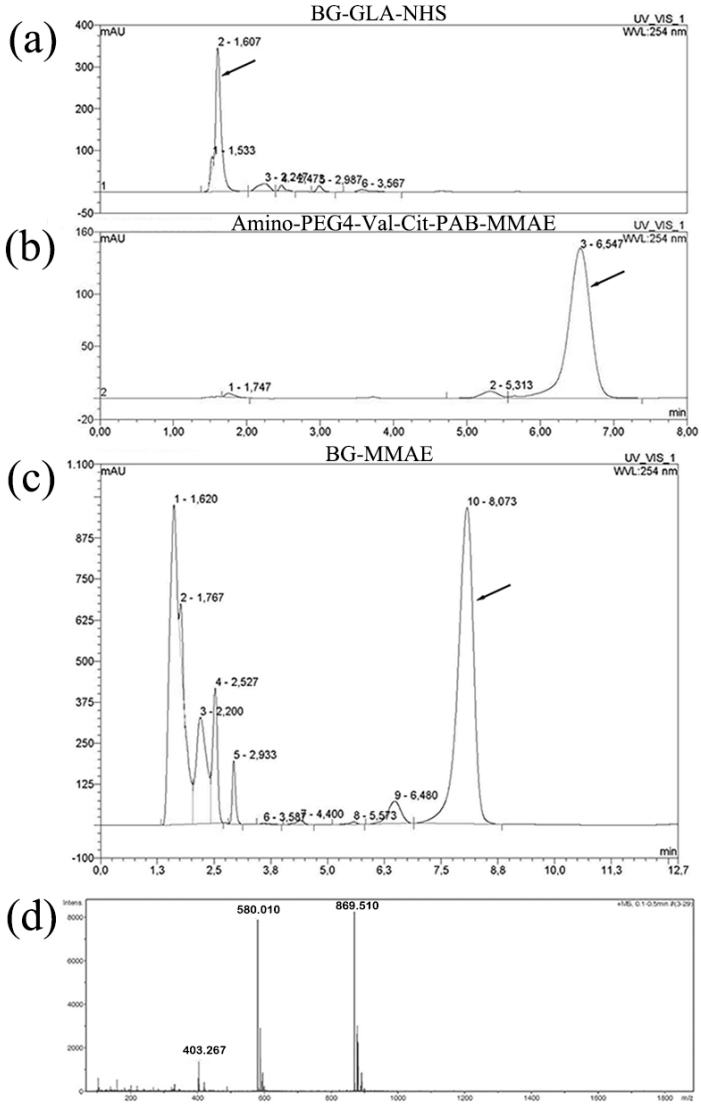

Figure 4.3.The BG-MMAE is purified and the size is validated. HPLC analysis of (a) BG-GLA-NHS, (b) Amino-PEG4-Val-Cit-PAB-MMAE and (c) the product BG-MMAE. The arrow indicates the retention times of 1.607, 6.547 and 8.073 min, respectively. (d) Mass spectra of protonated BG-MMAE with total molecular weight 1852.787 Da.

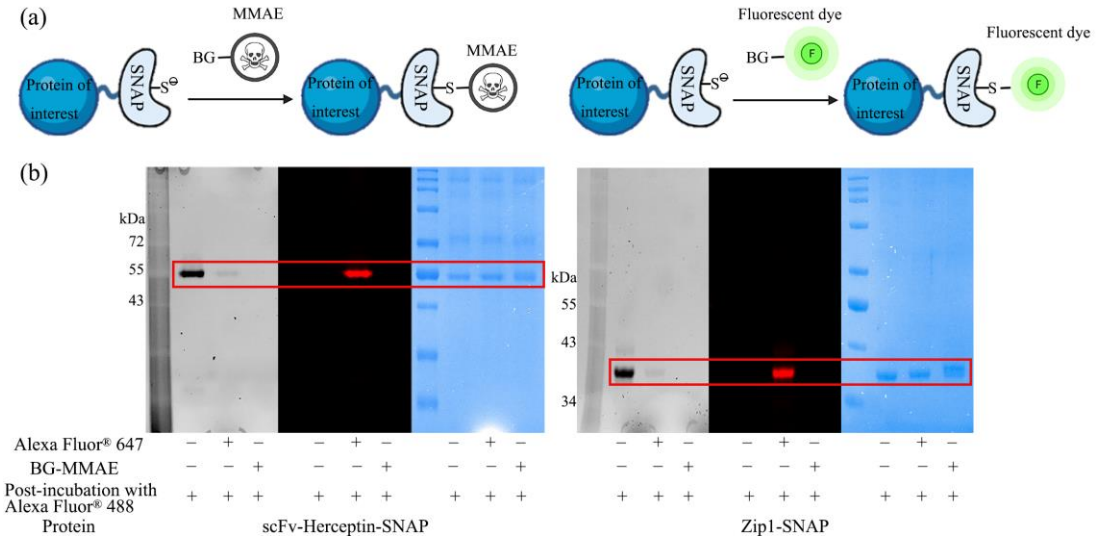

Figure 4.4. High conjugation efficiency between SNAP-fusion proteins and BG-modified agents. (a) Schematic diagram of scFv-SNAP fusion proteins conjugated with BG derivatives. (b) The conjugation of scFv-Herceptin-SNAP and Zip1-SNAP (highlighted with red box) were showed as examples. SNAP-fusion proteins were conjugated with either SNAP-Surface® Alexa Fluor® 647 or BG-MMAE followed by post-incubation with SNAP-Surface® Alexa Fluor® 488. The fluorescence was visualized and corresponding Coomassie blue staining was shown.

4.4 Specific binding property of Zip pair

The pre-targeting complex consists of two fusion proteins, the targeting protein (scFv-Zip2) that allows pre-targeting tumor cells and the vehicle protein (Zip1-SNAP), which could be conjugated either with cytotoxic agent or fluorescent dye as effector (**Figure 4.5a**).

The specific interaction between targeting protein and vehicle protein was confirmed by far-western blotting: scFv-Erbitux-Zip2, scFv-425-Zip2, scFv-αEpCAM-Zip2, scFv-Herceptin-Zip2 and scFv-Sacit-Zip2 were detected by Surface® Alexa Fluor® 488 conjugated Zip1-SNAP in PVDF membrane and visualized under UV light using ChemiDoc XRS+ System, while negative control scFv-Erbitux-SNAP was not detected (**Figure 4.5b**).

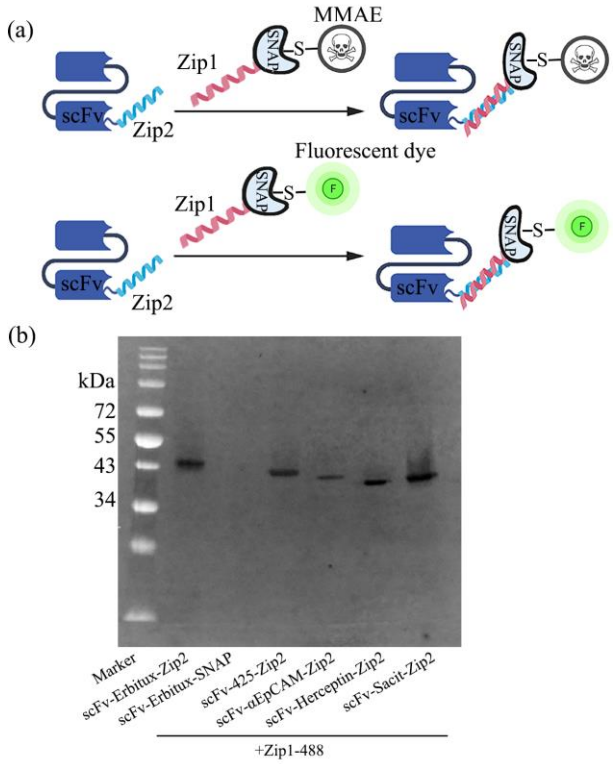

Figure 4.5. The Zip pair exhibits specific interaction. (a) Schematic diagram of the interaction between scFv-Zip2 and Zip1-SNAP. (b) The specific interaction of pre-targeting complex. The scFvs were detected by SNAP-Surface® Alexa Fluor® 488 conjugated Zip1-SNAP and visualized with ChemiDoc XRS+ System.

4.5 Functional assay in breast cancer

4.5.1 Different expression level of targets in breast cancer

The EGFR, EpCAM, Her2 and Trop2 expressions on cell surface were determined by flow cytometry using commercial EGFR, EpCAM, Her2 and Trop2-specific mAbs (listed in **3.1.4** and described in **3.2.4.2.1**). The results revealed that EGFR, EpCAM, Her2 and Trop2 were differently expressed on seven breast cancer cell lines (MDA-MB-468, MDA-MB-231, Hs578T, MDA-MB-453, MCF7, SKBR3 and BT474) (**Figure 4.6**, **Table 4.1**). MDA-MB-468, MDA-MB-231 and Hs578T expressed high level of EGFR, in which MDA-MB-468 ranked the highest. The SKBR3 and BT474 showed moderate expression of EGFR, while MDA-MB-453 and MCF7 expressed minimal level. The EpCAM was highly expressed on MDA-MB-453, MCF7, SKBR3 and BT474, moderate expressed on MDA-MB-468 and minimal expressed on MDA-

MB-231 and Hs578T. As the TNBC cell lines, MDA-MB-468, MDA-MB-231 and Hs578T exhibited lowest expression of Her2. The MCF7 have low-moderate expression of Her2, while MDA-MB-453, SKBR3 and BT474 showed high expression. The Hs578T was determined as the only cell line expressed minimal Trop2, and all other cell lines expressed high level of Trop2.

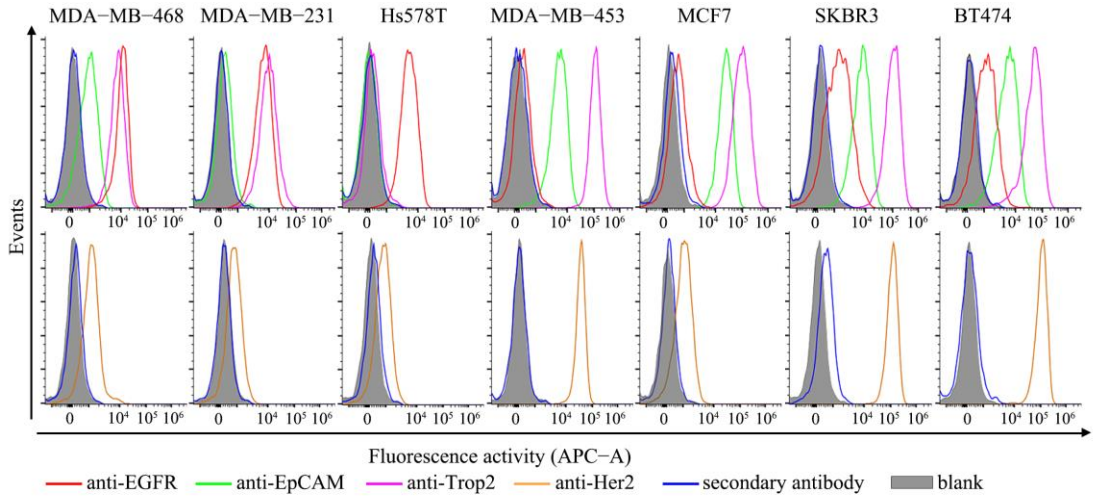

Figure 4.6. EGFR, EpCAM, Her2 and Trop2 are differently expressed in breast cancer cell lines. The EGFR, EpCAM, Her2 and Trop2 expression in breast cancer cell lines were determined by flow cytometry. The cells were treated with anti-EGFR (EGFR Monoclonal Antibody, H11), anti-EpCAM (CD326 monoclonal antibody, 1B7), anti-Her2 (ErbB2 monoclonal antibody, 3B5) and anti-Trop2 (Trop2 monoclonal antibody, MR54) antibodies, respectively, followed by incubation with the secondary antibody (Goat anti-Mouse IgG Highly Cross-Adsorbed Secondary Antibody, Alexa Fluor™ Plus 647).

Table 4.1 Expression profile of EGFR, EpCAM, Her2 and Trop2 in breast cancer cell lines

	MDA-MB-468	MDA-MB-231	Hs578T	MDA-MB-453	MCF7	SKBR3	BT474
EGFR	high	high	high	low	low	medium	medium
EpCAM	medium	low	low	high	high	high	high
Her2	low	low	low	high	low	high	high
Trop2	high	high	low	high	high	high	high

The expression levels of EGFR, EpCAM, Her2 and Trop2 were determined by flow cytometry.

4.5.2 The 425 and Erbitux bind to distinct epitopes on EGFR

The different binding epitopes of 425 and Erbitux antibodies on EGFR were confirmed by flow cytometry in breast cancer cell lines (**Figure 4.7**). The binding of scFv-425-647 and scFv-Erbitux-647 was observed on $EGFR^{high}$ (MDA-MB-468, MDA-MB-231

and Hs578T) and EGFR^{medium} (SKBR3 and BT474) cell lines but was limited on EGFR^{low} (MDA-MB-453 and MCF7) cell lines. After blocking 425 or Erbitux epitopes by its unconjugated scFv-425-SNAP or scFv-Erbitux-SNAP, the followed incubation with scFv-425-647 or scFv-Erbitux-647 indicated the successful block of binding regions. Meanwhile, the followed incubation with scFv-Erbitux-647 or scFv-425-647 showed that the binding of scFv-Erbitux-647 and scFv-425-647 was not affected by blocking the epitope and was still comparable with binding by antibodies on unblocked cells. The result revealed that the binding epitope of 425 and Erbitux antibodies did not overlapped, which expanded the application window of EGFR targeting therapy.

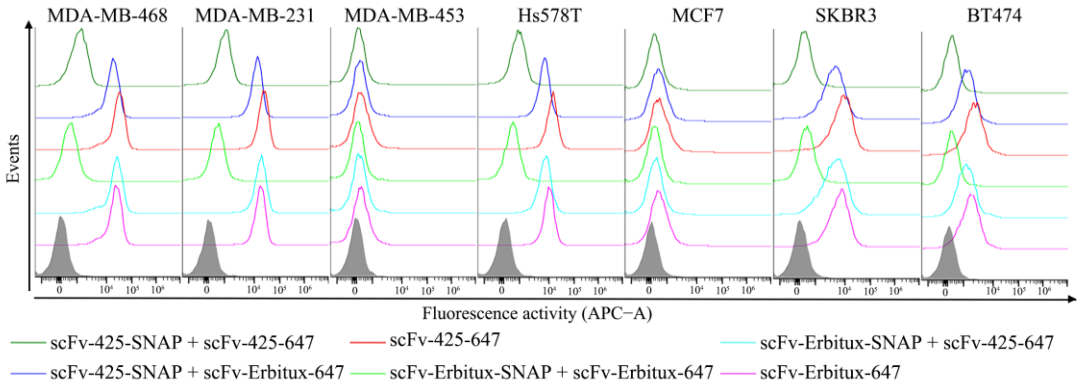

Figure 4.7. The 425 and Erbitux antibodies has distinct binding epitopes of EGFR. Cells were incubated with 10 µg of scFv-425-SNAP or scFv-Erbitux-SNAP to block 425 or Erbitux binding sites, followed by incubation with 1 µg of scFv-425-647 or scFv-Erbitux-647to confirm the block, or scFv-Erbitux-647 or scFv-425-647 to confirm the distinct binding sites. The binding ability of scFv-425-647 and scFv-Erbitux-647 was also showed without block.

4.5.3 Binding and colocalization of pre-targeting complex in breast cancer

The specific binding property of pre-targeting complex was confirmed by flow cytometry. Zip1-SNAP was conjugated with SNAP-Surface® Alexa Fluor® 647 (Zip1-647) to allow visualization of the binding. The flow cytometry results in **figure 4.8a-4.12a** indicate the specific binding of the pre-targeting complexes, which is consistent with the EGFR, EpCAM, Her2 and Trop2 expression confirmed by commercial antibodies (**4.5.1**). Compared to directly conjugated antibodies (scFv-425-647, scFv-Erbitux-647, scFv-αEpCAM-647, scFv-Herceptin-647 and scFv-Sacit-647), the pre-

targeting complexes exhibited comparable binding capability, while the Zip1-647 showed minimal unspecific binding.

The binding and colocalization of the scFv-Zip2 and Zip1-SNAP were further validated by fluorescent microscopy using the Zip1-647 and Alexa Fluor® 488 labeled scFv-Zip2 (scFv-Zip2-488) by direct functionalization of lysine side chains using N-hydroxysuccinimide ester Alexa Fluor® 488.

The results of fluorescent microscopy in **figure 4.8b-4.12b** shows the green-488, red-647, blue-DAPI channels along with the merged images. Both scFv-Zip2-488 and Zip1-647 signals were observed on the cell membrane of EGFR-expressing cells (MDA-MB-468, MDA-MB-231, Hs578T and SKBR3) (**Figure 4.8b**, **Figure 4.9b**), EpCAM-expressing cells (MDA-MB-468, MDA-MB-453, MCF7, SKBR3 and BT474) (**Figure 4.10b**), Her2-expressing cells (MDA-MB-453, SKBR3 and BT474) (**Figure 4.11b**) and Trop2-expressing cells (MDA-MB-468, MDA-MB-231, MDA-MB-453, MCF7, SKBR3 and BT474) (**Figure 4.12b**) but not observed in $EGFR^{low}$ (MDA-MB-453 and MCF7) (**Figure 4.8b**, **Figure 4.9b**), $EpCAM^{low}$ (MDA-MB-231 and Hs578T) (**Figure 4.10b**), $Her2^{low}$ (MDA-MB-468, MDA-MB231 and Hs578T) (**Figure 4.11b**) and $Trop2^{low}$ (Hs578T) (**Figure 4.12b**) cell lines or cells treated with Zip1-647 (**Figure 4.8b**) alone. However, while the binding in $EGFR^{medium}$ (BT474) cell line was confirmed by flow cytometry, there was no binding and colocalization by fluorescent microscopy, which might due to the different sensitivity of each experiment method. The merged figure shows the overlapped signals from scFv-Zip2-488 and Zip1-647, indicating the colocalization of the two probes, which further validated the interaction between the scFv-Zip2 and Zip1-SNAP. In addition, the fluorescence intensity of scFv-Zip2-488 and Zip1-647, plotted along the white arrow in merged figures was calculated by Image J software **(Figure 4.8c-4.12c**). The Zip1-647 fluorescent intensity consistently followed the peak of scFv-Zip2-488, providing another strong evidence for the colocalization.

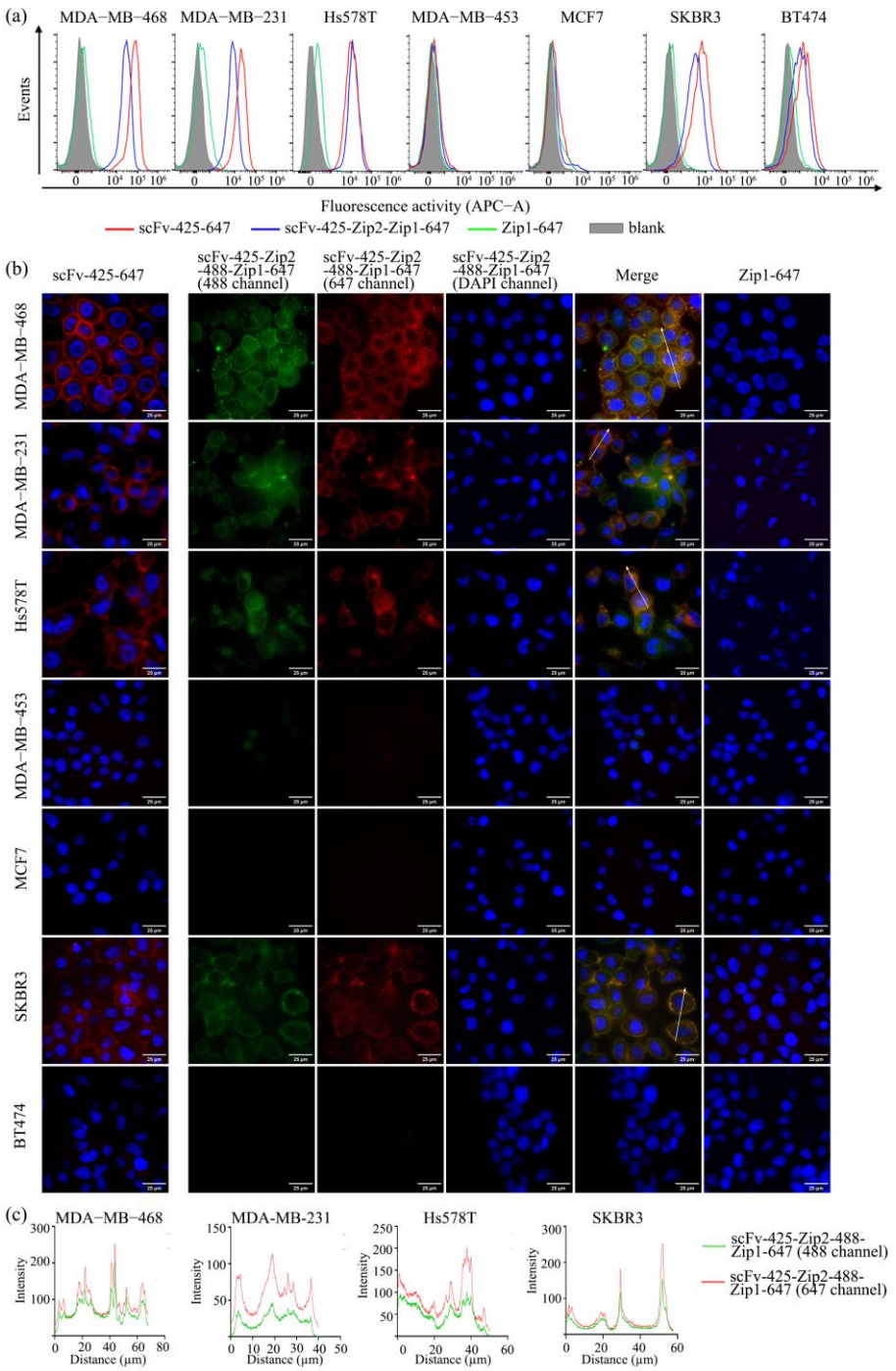

Figure 4.8. EGFR-targeting complex specific binds to EGFR-expressing cells and colocalize on cell membranes. (a) Specific targeting of pre-targeting complex to breast cancer cell lines and comparison with direct conjugated antibody by flow cytometry.(b) The binding and colocalization of scFv-425-Zip2-488 and Zip1-647 were visualized by fluorescence microscopy. The binding process was carried out at 4°C. The fluorescence intensity along the white arrow in EGFR-expressing cell lines was shown in (c) and calculated by Image J software.

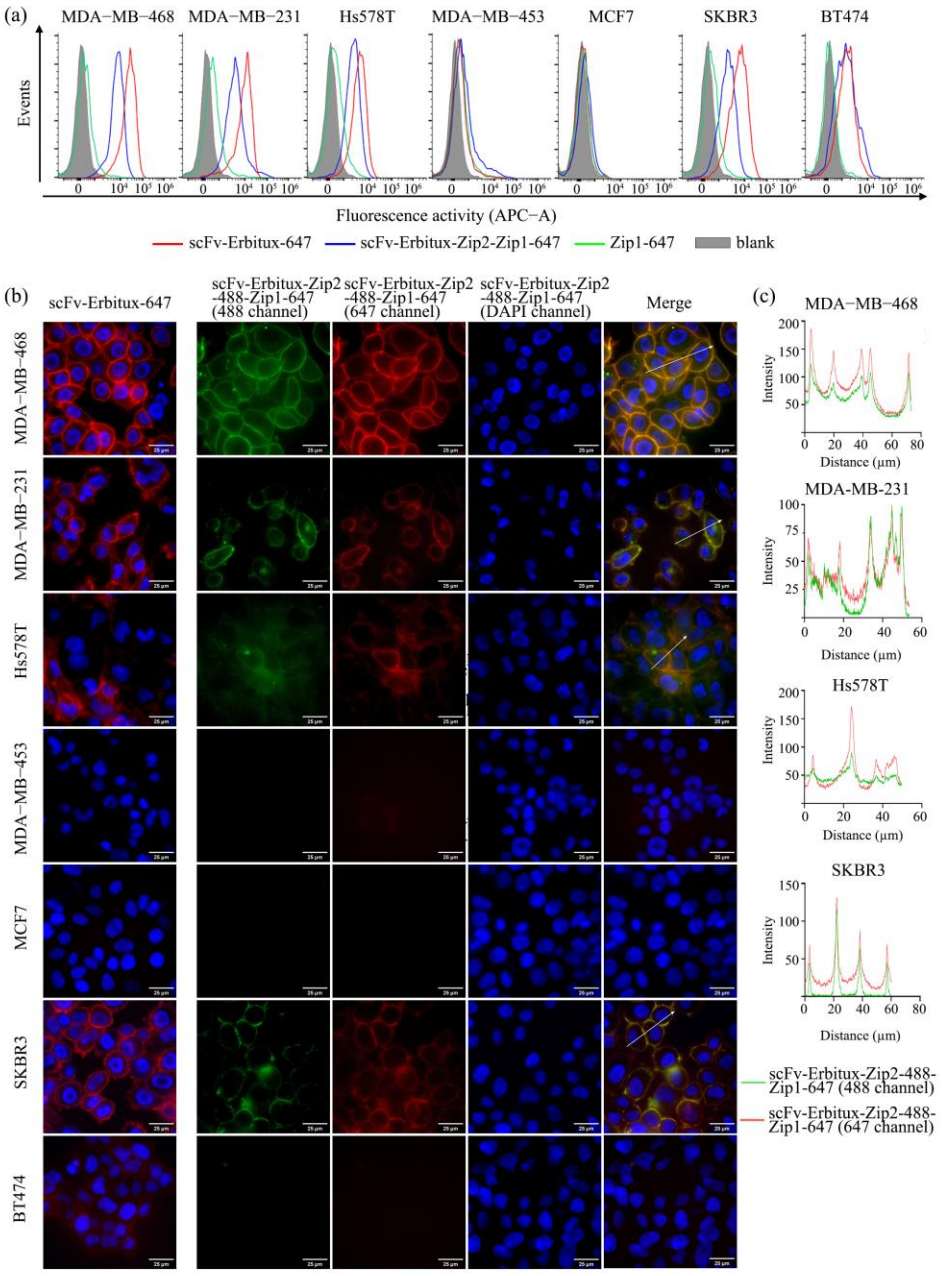

Figure 4.9. EGFR-targeting complex specific binds to EGFR-expressing cells and colocalize on cell membranes. (a) Specific targeting of pre-targeting complex to breast cancer cell lines and comparison with direct conjugated antibody by flow cytometry. (b) The binding and colocalization of scFv-Erbitux-Zip2-488 and Zip1-647 were visualized by fluorescence microscopy. The binding process was carried out at 4°C. The fluorescence intensity along the white arrow in EGFR-expressing cell lines was shown in (c) and calculated by Image J software. Cells treated with Zip1-647 to confirm no unspecific binding were shown in figure 4.8.

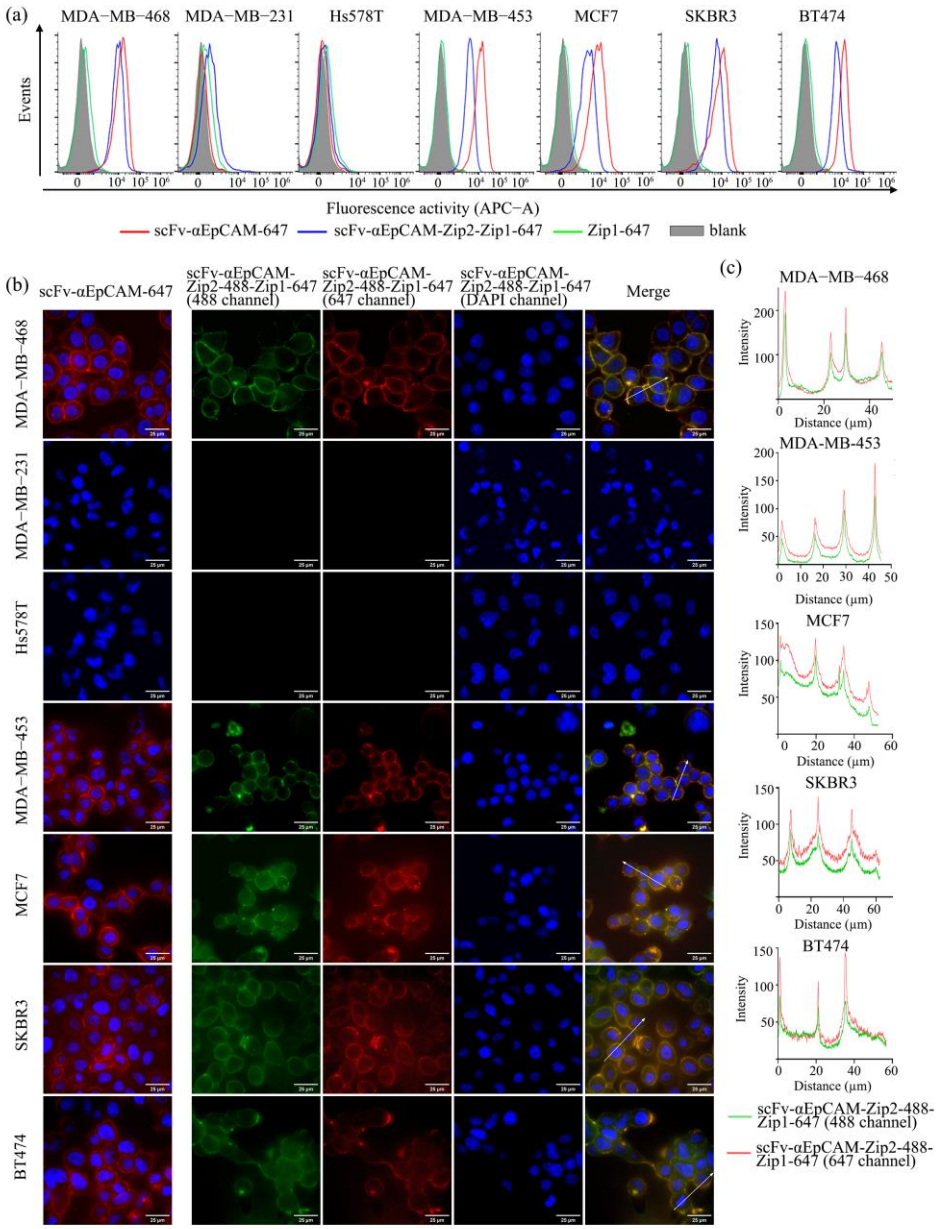

Figure 4.10. The αEpCAM-targeting complex specific binds to αEpCAM-expressing cells and colocalize on cell membranes. (a) Specific targeting of pre-targeting complex to breast cancer cell lines and comparison with direct conjugated antibody by flow cytometry. (b) The binding and colocalization of scFv-αEpCAM-Zip2-488 and Zip1-647 were visualized by fluorescence microscopy. The binding process was carried out at 4°C. The fluorescence intensity along the white arrow in EpCAM-expressing cell lines was shown in (c) and calculated by Image J software. The cells treated with Zip1-647 alone to confirm no unspecific binding were shown in figure 4.8.

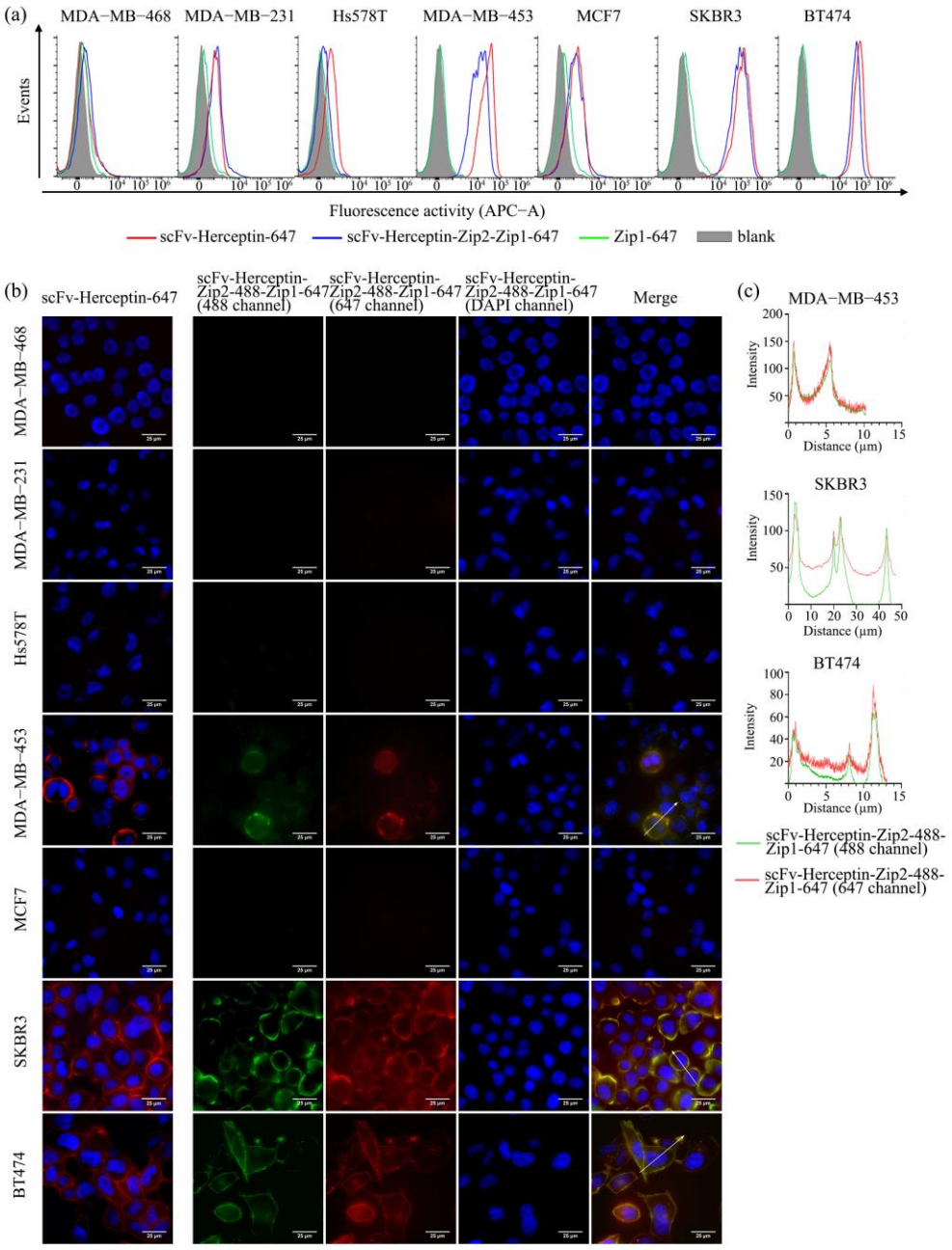

Figure 4.11. The Her2-targeting complex specific binds to Her2-expressing cells and colocalize on cell membranes. (a) Specific targeting of pre-targeting complex to breast cancer cell lines and comparison with direct conjugated antibody by flow cytometry. (b) The binding and colocalization of scFv-Herceptin-Zip2-488 and Zip1-647 were visualized by fluorescence microscopy. The binding process was carried out at 4°C. The fluorescence intensity along the white arrow in Her2-expressing cell lines was shown in (c) and calculated by Image J software. The cells treated with Zip1-647 alone to confirm no unspecific binding were shown in figure 4.8.

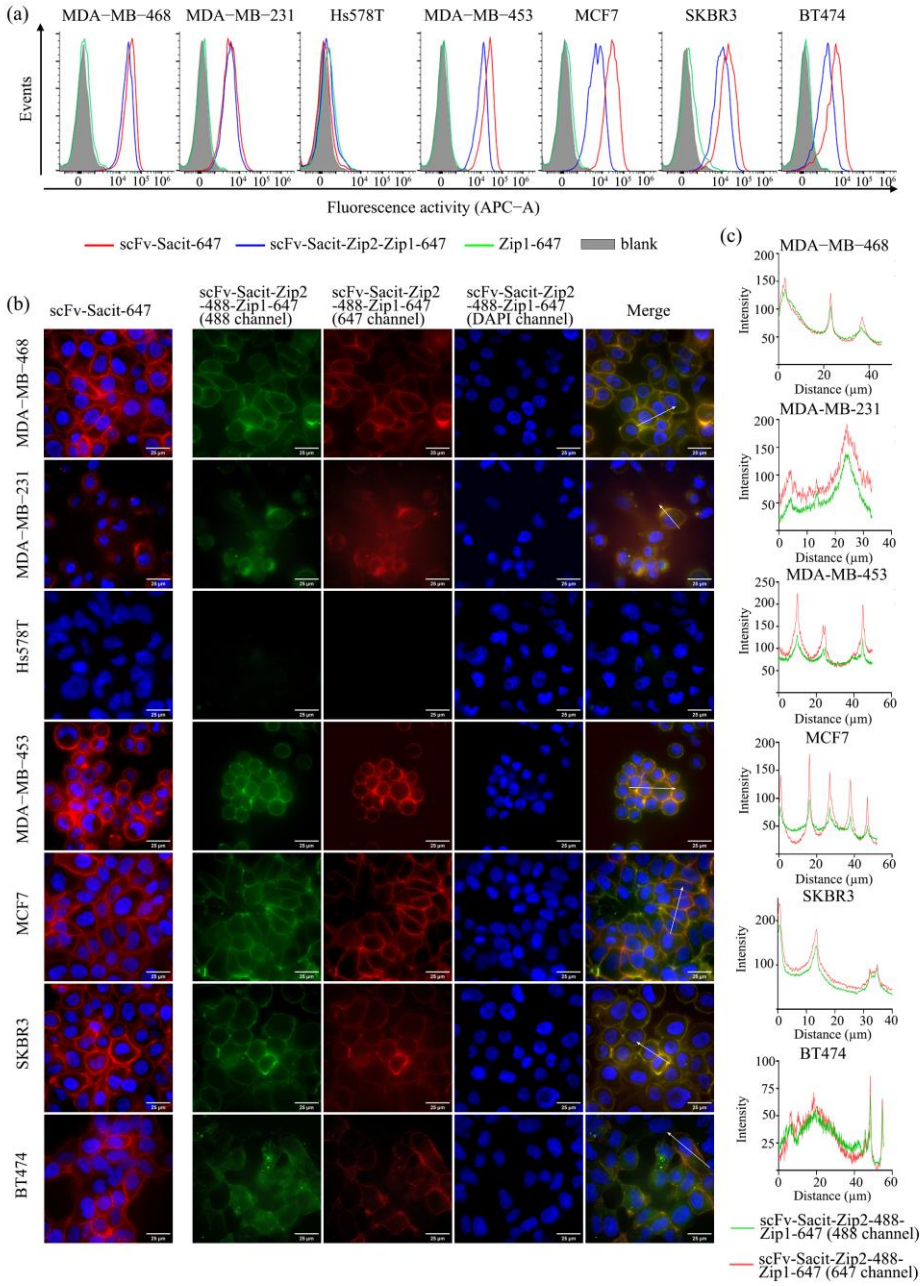

Figure 4.12. The Trop2-targeting complex specific binds to Trop2-expressing cells and colocalize on cell membranes. (a) Specific targeting of pre-targeting complex to breast cancer cell lines and comparison with direct conjugated antibody by flow cytometry. (b) The binding and colocalization of scFv-Sacit-Zip2-488 and Zip1-647 were visualized by fluorescence microscopy. The binding process was carried out at 4°C. The fluorescence intensity along the white arrow in Trop2-expressing cell lines was shown in (c) and calculated by Image J software. The cells treated with Zip1-647 alone to confirm no unspecific binding were shown in figure 4.8.

4.5.4 Internalization property of pre-targeting complex in breast cancer

As the main mechanism of ADC is drug delivery into cells, the fast and adequate internalization is one of the key points in ADC design. The internalization property of

pre-targeting complex was confirmed by fluorescence microscopy and experiment was carried out at 37°C to maintain cellular activity (**Figure 4.13-4.17**). The internalization process was visualized by green-488, red-647 and blue-DAPI channels, and merged figures were also showed to better visualize the internalization.

For instance, the **figure 4.13** shows the internalization of EGFR-targeting ADCs, in which both complex and directly conjugated antibody have started to be internalized into EGFR-expressing cells except BT474 within 3 h (white arrow indicated) and still some remain bound to the cell membrane. Meanwhile, Zip1-647 was not internalized nonspecifically into cells. Given the fact that BT474 have relatively limited EGFR and the complex have relatively weaker binding affinity due to the two-step binding compared to direct conjugation, the internalization was weakly observed in cells treated with directly conjugated antibodies but was not seen in the cells treated with pre-targeting complex. Other complexes targeting EGFR, EpCAM, Her2 and Trop2 also showed homogeneous and clear internalization in antigen-expressing cell lines, consisting to the aforementioned results by flow cytometry and fluorescence microscopy (**Figure 4.14-4.17**).

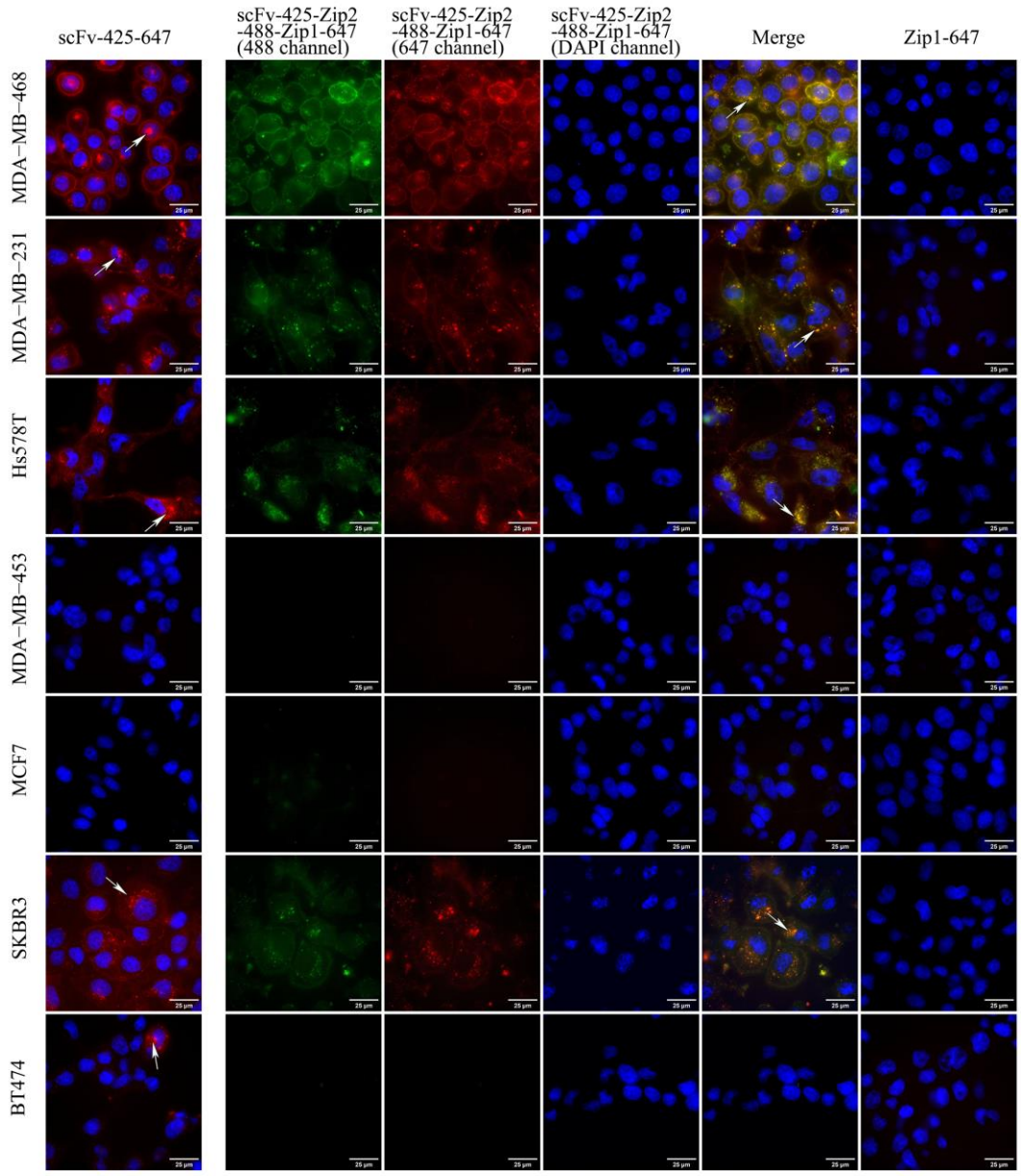

Figure 4.13. Fast internalization of the scFv-425-Zip2-488 and Zip1-647 complex. Breast cancer cells were incubated with scFv-425-Zip2-488 for 1h followed by post-incubation with Zip1-647 for 3h, or with scFv-425-647 for 3h. The internalization process was carried out at 37°C. The green represents 488 channel, the red represents 647 channel, and the blue represents DAPI channel. The internalized molecules were indicated by white arrows.

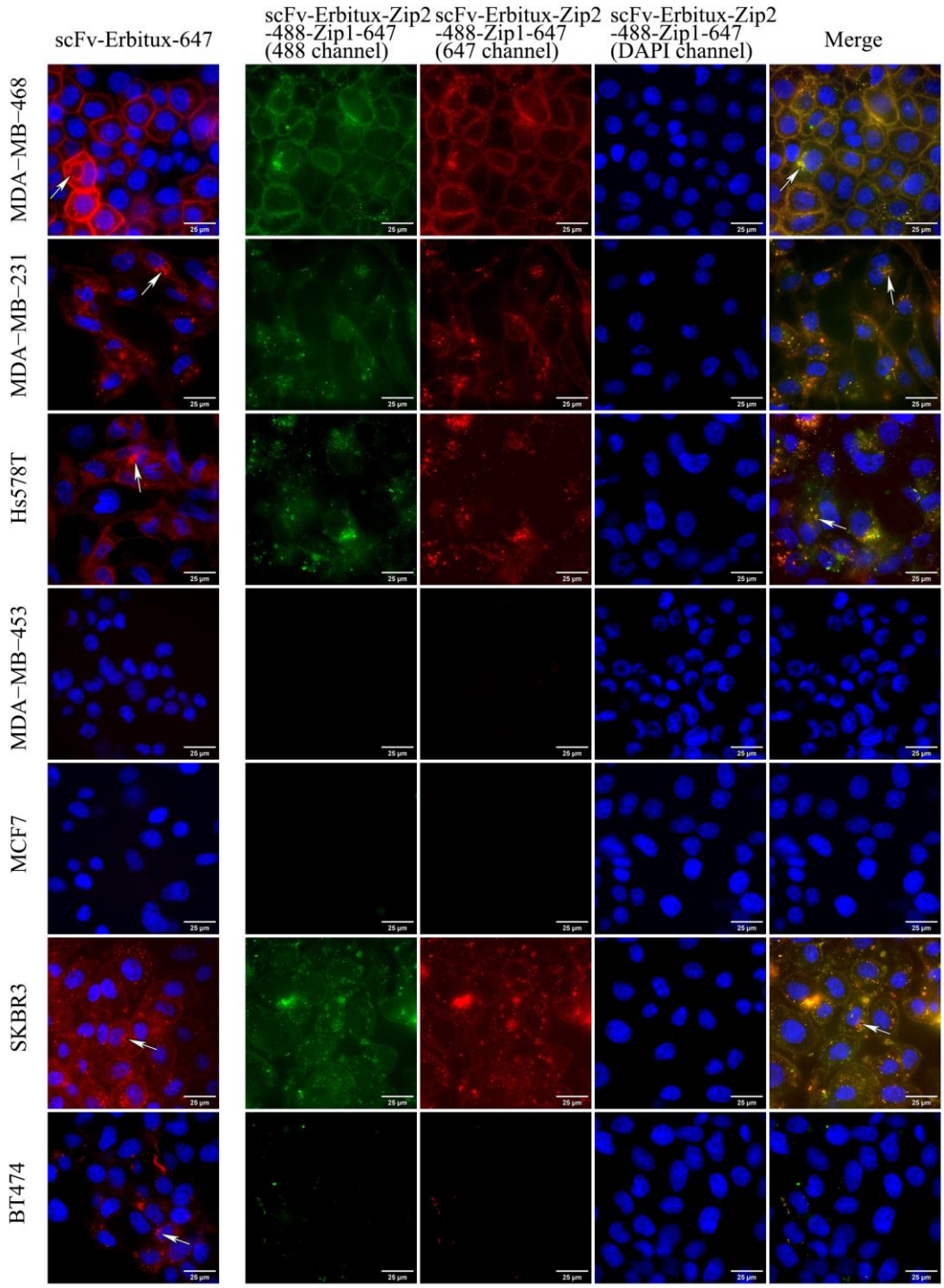

Figure 4.14. Fast internalization of the scFv-Erbitux-Zip2-488 and Zip1-647 complex. Breast cancer cells were incubated with scFv-Erbitux-Zip2-488 for 1h followed by post-incubation with Zip1-647 for 3h, or with scFv- Erbitux -647 for 3h. The internalization process was carried out at 37°C. The green represents 488 channel, the red represents 647 channel, and the blue represents DAPI channel. The internalized molecules were indicated by white arrows. The cells treated with Zip1-647 alone were shown in figure 4.13.

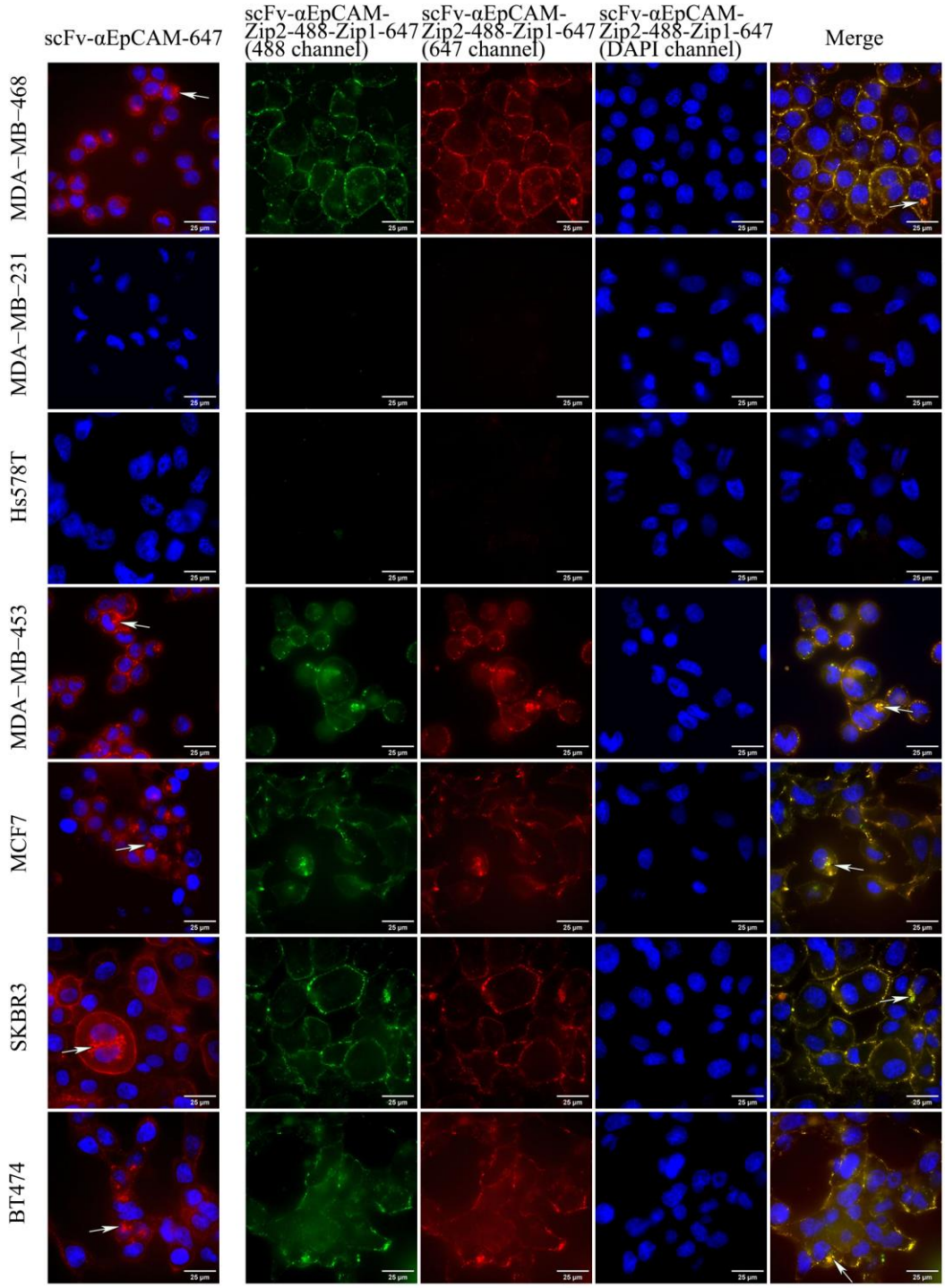

Figure 4.15. Fast internalization of the scFv-αEpCAM-Zip2-488 and Zip1-647 complex. Breast cancer cells were incubated with scFv-αEpCAM-Zip2-488 for 1h followed by post-incubation with Zip1-647 for 3h, or with scFv-αEpCAM-647 for 3h. The internalization process was carried out at 37°C. The green represents 488 channel, the red represents 647 channel, and the blue represents DAPI channel. The internalized molecules were indicated by white arrows. The cells treated with Zip1-647 alone were shown in figure 4.13.

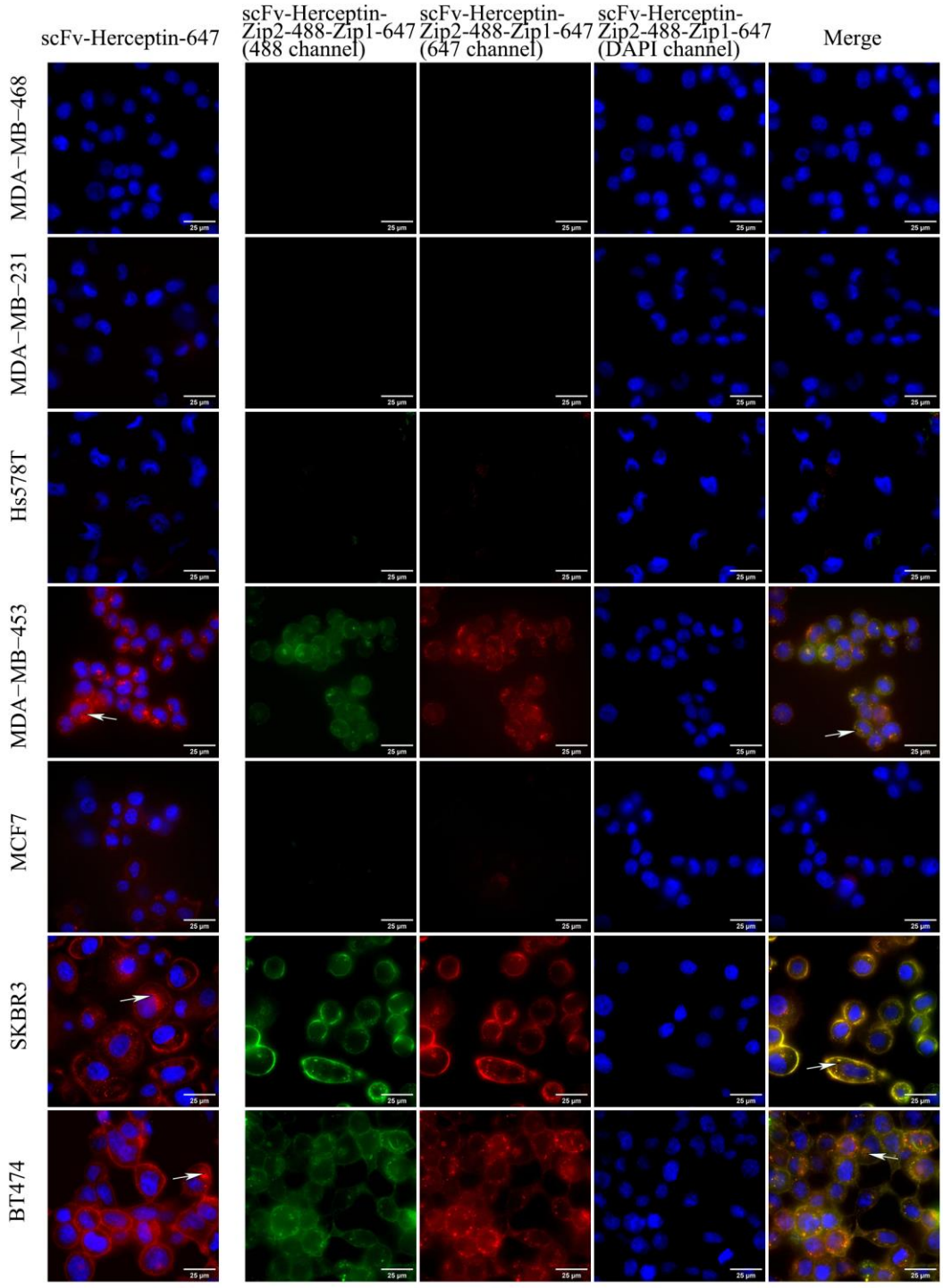

Figure 4.16. Fast internalization of the scFv-Herceptin-Zip2-488 and Zip1-647 complex. Breast cancer cells were incubated with scFv-Herceptin-Zip2-488 for 1h followed by post-incubation with Zip1-647 for 3h, or with scFv-Herceptin-647 for 3h. The internalization process was carried out at 37°C. The green represents 488 channel, the red represents 647 channel, and the blue represents DAPI channel. The internalized molecules were indicated by white arrows. The cells treated with Zip1-647 alone were shown in figure 4.13.

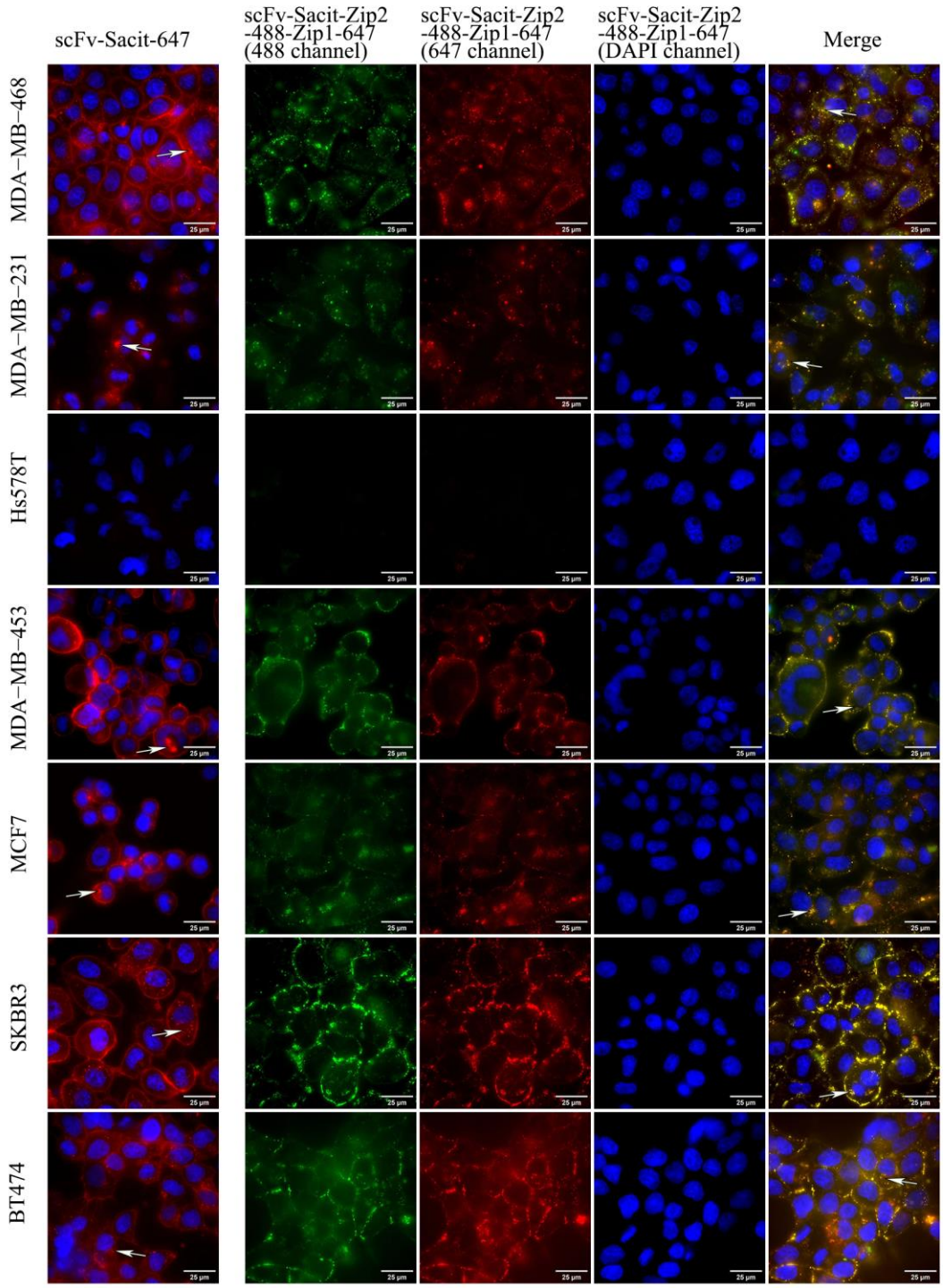

Figure 4.17. Fast internalization of the scFv-Sacit-Zip2-488 and Zip1-647 complex. Breast cancer cells were incubated with scFv-Sacit-Zip2-488 for 1h followed by post-incubation with Zip1-647 for 3h, or with scFv-Sacit-647 for 3h. The internalization process was carried out at 37°C. The green represents 488 channel, the red represents 647 channel, and the blue represents DAPI channel. The internalized molecules were indicated by white arrows. The cells treated with Zip1-647 alone were shown in figure 4.13.

4.5.5 Specific cytotoxicity of MMAE based pre-targeting complex

The cytotoxicity of an ADC centers on the payloads, which are usually high potent small molecules and kill cells indiscriminately. Since the specific binding, colocalization and internalization property of pre-targeting complex have been confirmed by flow cytometry and fluorescence microscopy, these properties were expected to be retained after conjugation with BG-MMAE. Zip1-SNAP and scFv-SNAP were modified with MMAE by SNAP-tag technology, generating Zip1-MMAE and scFv-MMAE as mentioned in **3.2.3.2**, and their specific cytotoxicity was confirmed by cytotoxicity assay using Cell Proliferation (XTT) Kit II.

The specific cytotoxicity was confirmed by incubating breast cancer cells (MDA-MB-468, MDA-MB-231, MDA-MB-453, Hs758T, MCF-7, SKBR3 and BT474) with increasing concentration of scFv-MMAE, pre-targeting complexes (scFv-Zip2-Zip1-MMAE), unconjugated antibodies (scFv-Zip2-Zip1-SNAP or scFv-SNAP), Zip1-MMAE or MMAE at 37°C for 72 h (**Figure 4.18**). After treating the cells with MMAE, all the cell lines showed reduced cell proliferation and different levels of sensitivity according to the half maximal inhibitory concentration (IC_{50}) (**Table 4.2**). Both pre-targeting complex and scFv-MMAE displayed specific cytotoxicity in EGFR-, EpCAM-, Her2- or Trop2-expressing cell lines but spared low expressing cell lines. Compared to scFv-MMAE, the complex exhibited relatively lower cytotoxicity, consistent with flow cytometry and fluorescence microscopy results. Meanwhile, the up to 640 nM of unconjugated antibodies and Zip1-MMAE showed limited cytotoxicity in all treated cell lines. Interestingly, the scFv-Herceptin-MMAE presented extremely strong cytotoxicity in SKBR3, with IC_{50} (2.049 ± 0.1969 nM) even 19 times lower than MMAE (38.65 ± 2.712 nM), but the scFv-Herceptin-Zip2-Zip1-MMAE did not achieve the same efficacy. Full data about IC_{50} was listed in **table 4.2**.

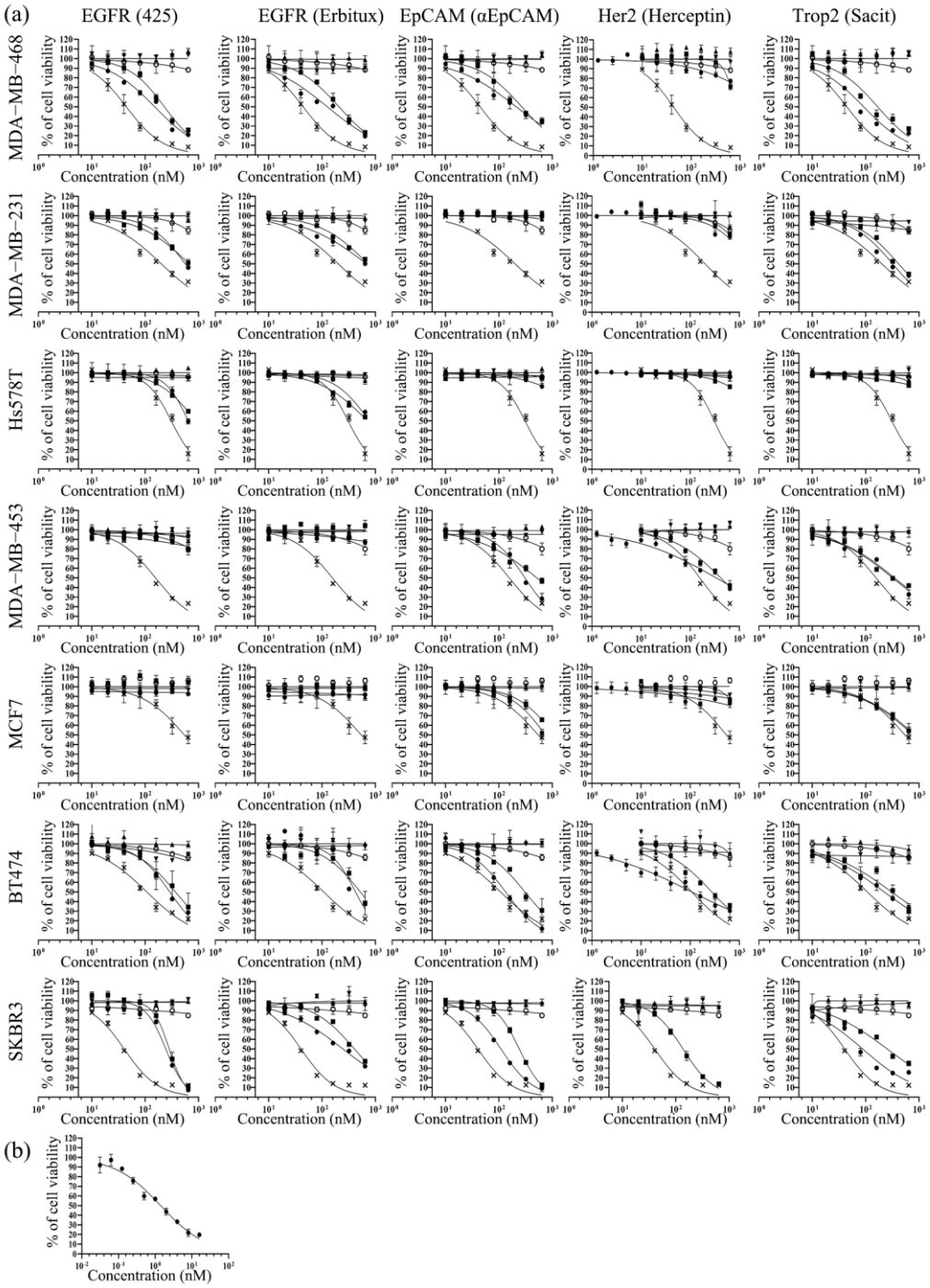

Figure 4.18. Specific cytotoxicity was triggered by pre-targeting complex. (a) Breast cancer cell lines were treated with increasing concentration of scFv-Zip2-Zip1-MMAE (■), scFv-MMAE (●) (except SKBR3 treated with scFv-Herceptin-MMAE), scFv-Zip2-Zip1-SNAP (▼) scFv-SNAP (▲), Zip1-MMAE (○) or MMAE (×) at 37°C for 72 h. (b) SKBR3 was incubated with increasing concentration (0.03125, 0.0625, 0.125, 0.25, 0.5, 1, 2, 4, 8, 16 nM) of scFv-Herceptin-MMAE at 37°C for 72 h. Cell viability was determined by Cell Proliferation (XTT) Kit II, and the experiment was carried out in triplicates for three times. One independent experiment was shown with the mean ±SD.

Table 4.2 Table of IC_{50} values (nM)

	MDA-MB-468	MDA-MB-231	Hs578T	MDA-MB-453	MCF7	SKBR3	BT474
scFv-425-MMAE	111.9±6.639	665.9±28.84	645.5±29.53	-	-	201.4±16.34	311±31.66
scFv-425-Zip2-Zip1-MMAE	188.9±28.28	715.4±36.24	894.3±37.25	-	-	268.4±13.72	372.4±33.43
scFv-425-SNAP	-	-	-	-	-	-	-
scFv-425-Zip2-Zip1-SNAP	-	-	-	-	-	-	-
scFv-Erbitux-MMAE	130.5±22.43	676.9±35.93	694.2±38.97	-	-	265.8±28.19	383.9±37.19
scFv-Erbitux-Zip2-Zip1-MMAE	256.1±11.84	720.9±33.11	784±35.81	-	-	398.3±15.36	474.9±39.71
scFv-Erbitux-SNAP	-	-	-	-	-	-	-
scFv-Erbitux-Zip2-Zip1-SNAP	-	-	-	-	-	-	-
scFv-αEpCAM-MMAE	185±12.04	-	-	329.3±30.77	808.7±45.55	104.5±3.58	135.4±25.22
scFv-αEpCAM-Zip2-Zip1-MMAE	242.6±33.79	-	-	402.3±34.74	1012±46.94	241.3±8.807	260.3±11.19
scFv-αEpCAM-SNAP	-	-	-	-	-	-	-
scFv-αEpCAM-Zip2-Zip1-SNAP	-	-	-	-	-	-	-

Continued table 4.2 Table of IC_{50} values (nM)

	MDA-MB-468	MDA-MB-231	Hs578T	MDA-MB-453	MCF7	SKBR3	BT474
scFv-Herceptin-MMAE	-	-	-	324.1±36.76	-	2.049±0.1969	104.1±8.161
scFv-Herceptin-Zip2-Zip1-MMAE	-	-	-	358.9±23.6	-	133±14.85	270±23.72
scFv-Herceptin -SNAP	-	-	-	-	-	-	-
scFv-Herceptin-Zip2-Zip1-SNAP	-	-	-	-	-	-	-
scFv-Sacit-MMAE	84.35±4.519	311.1±12.99	-	283.3±39.09	708.1±39.57	99.73±9.154	146.1±18.91
scFv-Sacit-Zip2-Zip1-MMAE	187.7±14.12	421.9±21.58	-	306.2±39.5	768.5±39.49	184.7±18.21	305.9±35.84
scFv-Sacit-SNAP	-	-	-	-	-	-	-
scFv-Sacit-Zip2-Zip1-SNAP	-	-	-	-	-	-	-
Zip1-MMAE	-	-	-	-	-	-	-
MMAE	60.78±3.114	287.8±14.17	290.6±11.04	264.2±36.15	599.5±36.16	38.65±2.712	108.3±18.97

The IC_{50} values indicate the concentration that inhibit cell viability by 50% relative to untreated control cells. The data represented three independent experiments carried out in triplicate and were presented as mean ± standard error of the mean (SEM).

4.5.6 Induction of apoptosis by MMAE based pre-targeting complex

Apoptosis is one of the major kinds of programmed cell death to get rid of damaged cells. Propidium iodide (PI) is a membrane-impermeable fluorescent nuclear stain that can distinguish necrotic and late apoptotic cell which lost membrane integrity from living and early apoptotic cell [120]. Phosphatidylserine predominantly locates at the cytoplasmic face, but the asymmetry distribution is broken since the initiation of apoptosis as the phosphatidylserine moves to express at the outer plasma membrane [121]. Annexin V is found to specifically bind to phosphatidylserine at the extracellular membrane leaflet [122], and therefore in conjunction of annexin V and PI has been widely used to detect apoptotic cells by conjugating annexin V with fluorescent dyes. Woitok *et.al* has reported an economical method using fluorescent dye labeled Annexin V-SNAP for apoptosis, which shows comparable results to the commercial staining kit [112].

Here, the apoptosis triggered by MMAE-based ADCs was successfully visualized by flow cytometry using SNAP-Surface® Alexa Fluor® 647 conjugated Annexin V-SNAP (Annexin V-647) and PI (**Figure 4.19-4.23**). Negative and positive controls were set up by treating cells with PBS or camptothecin (apoptosis inducer). The **figure 4.19-4.23** depict the living (Q4), early apoptotic (Q3), late apoptotic (Q2) and necrotic (Q1) cells, and the sum of early and late apoptotic cells were used for statistical analysis. In comparison to negative control, apoptosis was triggered in all cell lines after treatment with camptothecin or MMAE ($p < 0.001$). Compatible with cytotoxicity assay results, the fractions of apoptotic cells in EGFR- (MDA-MB-468, MDA-MB-231, Hs578T, SKBR3 and BT474), EpCAM- (MDA-MB-468, MDA-MB-453, MCF7, SKBR3 and BT474), Her2- (MDA-MB-453 and BT474) or Trop2- (MDA-MB-468, MDA-MB-231, MDA-MB-453, MCF7, SKBR3 and BT474) expressing cell lines were significantly increased after incubating them with 640 nM of either scFv-Zip2-Zip1-MMAE or scFv-MMAE for 48 h. The 16 nM of scFv-Herceptin-MMAE was enough to trigger apoptosis in SKBR3 under the same conditions. Unconjugated antibodies (scFv-Zip2-Zip1-SNAP or scFv-SNAP) and Zip1-MMAE did not induce apoptosis in all breast cancer

cell lines.

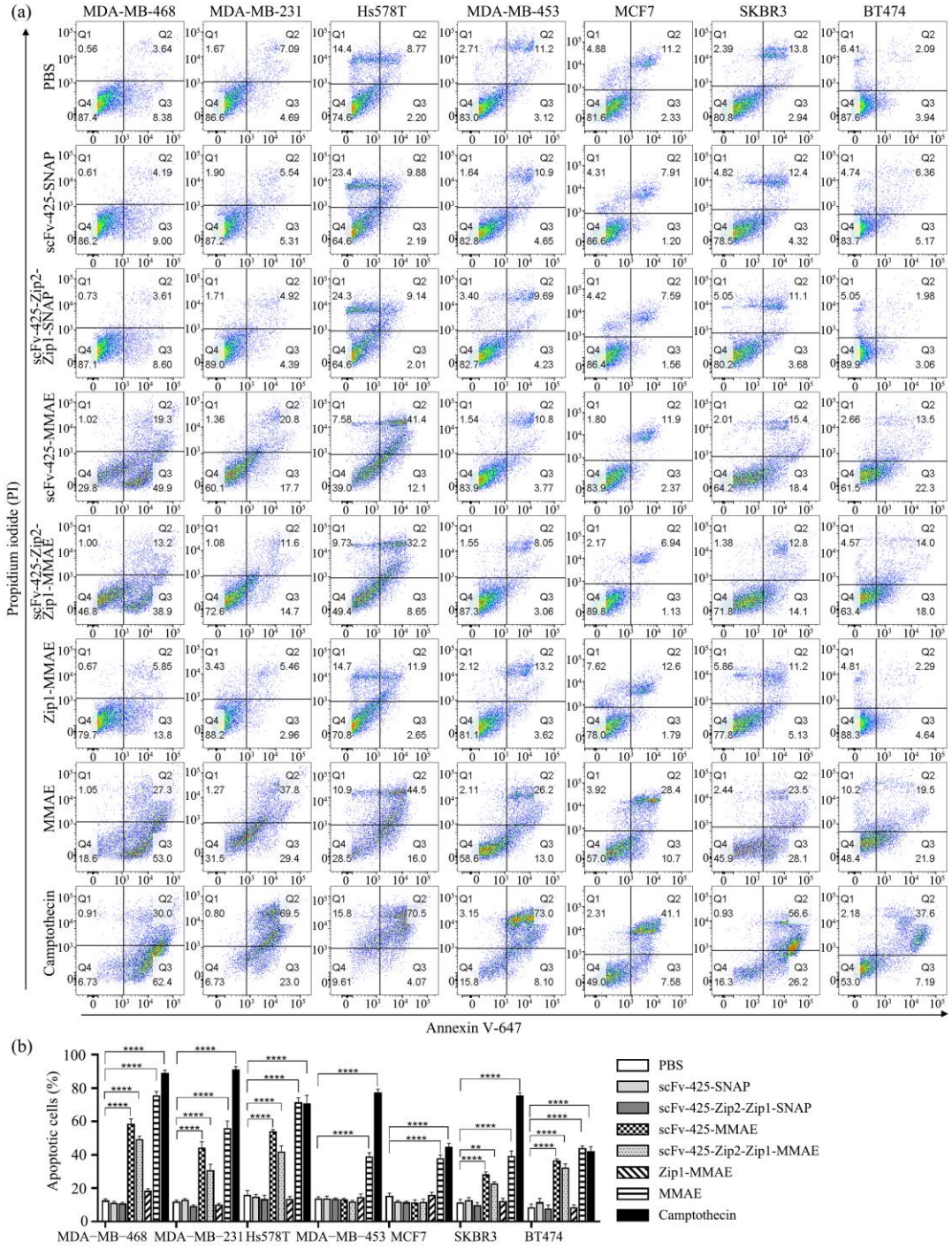

Figure 4.19. EGFR-targeting ADCs induced apoptosis. (a) Scatter plot of one measurement as an example. (b) Statistic analysis of apoptotic cells including early (Q3) and late (Q2) apoptotic cells. The experiment was carried out independently in triplicates for three times. Data were shown as mean±SEM. The statistical analysis was carried out using one-way ANOVA and corrected by Tukey's test (** $p < 0.01$, **** $p < 0.0001$).

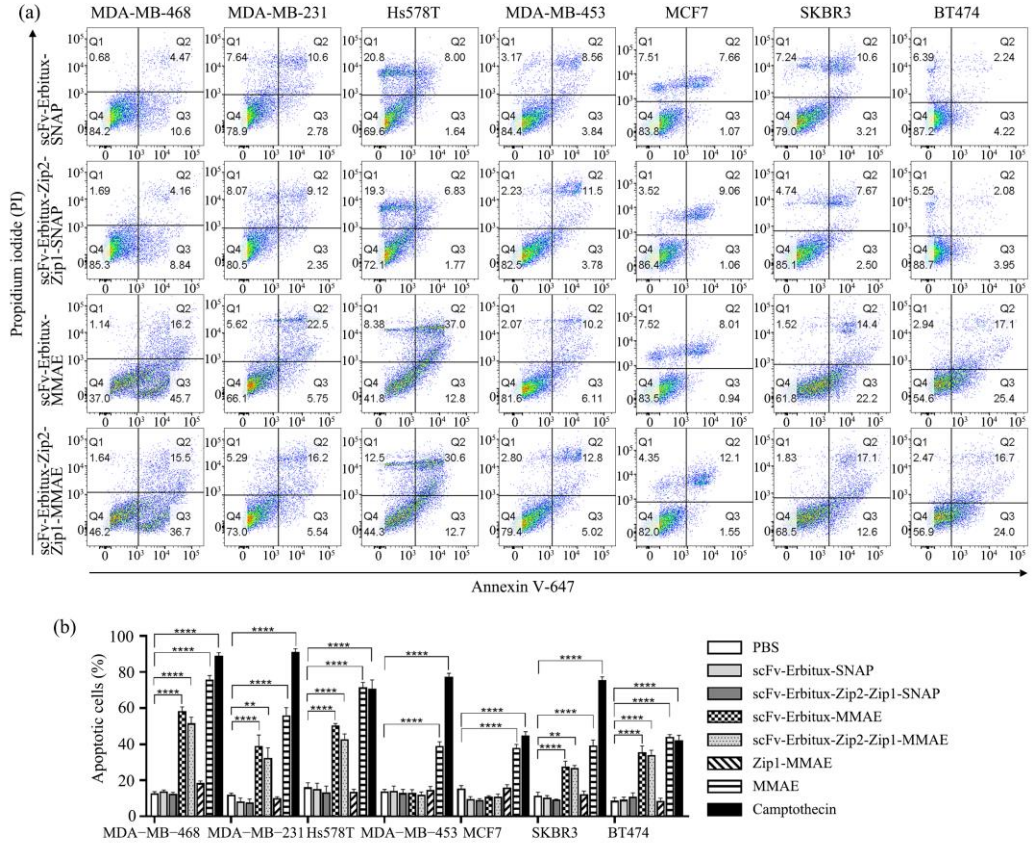

Figure 4.20. EGFR-targeting ADCs induced apoptosis. (a) Scatter plot of one measurement as an example. (b) Statistic analysis of apoptotic cells including early (Q3) and late (Q2) apoptotic cells. The experiment was carried out independently in triplicates for three times. Data were shown as mean±SEM. The statistical analysis was carried out using one-way ANOVA and corrected by Tukey's test (** $p < 0.01$, **** $p < 0.0001$). The cells treated with PBS, MMAE, camptothecin or Zip1-MMAE were shown in figure 4.19.

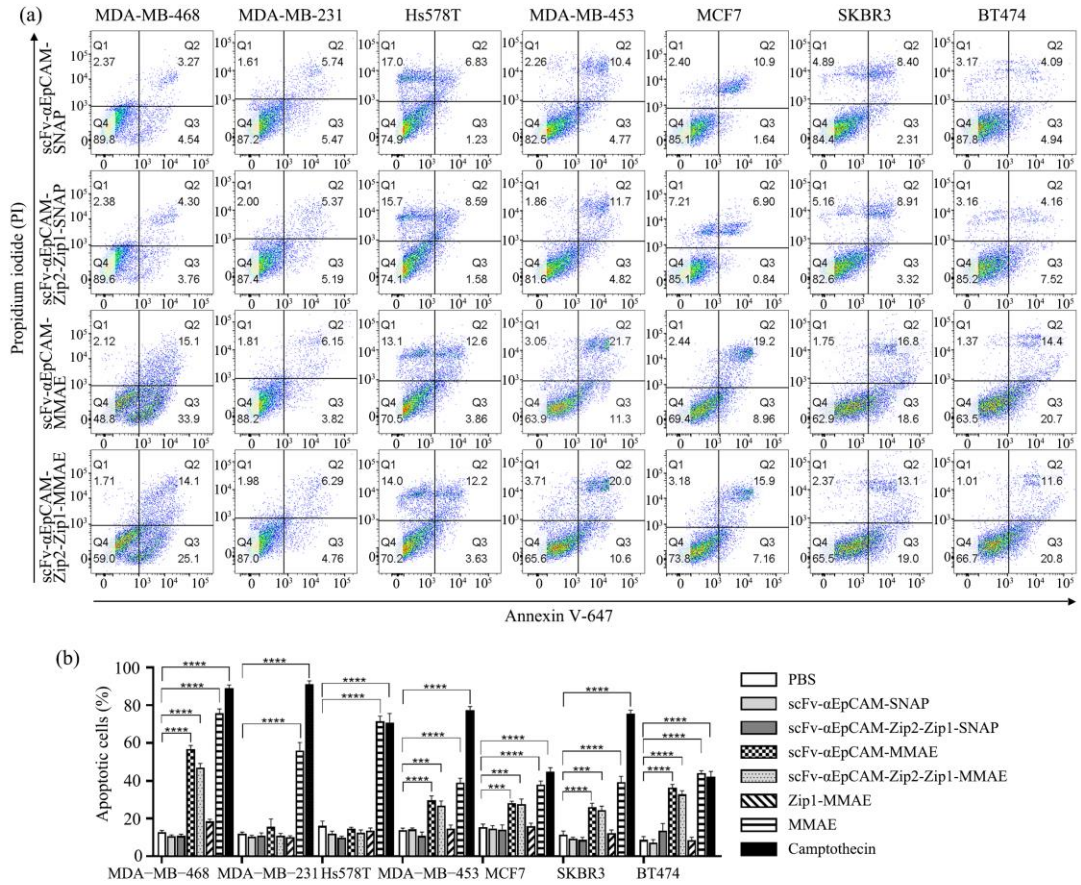

Figure 4.21. EpCAM-targeting ADCs induced apoptosis. (a) Scatter plot of one measurement as an example. (b) Statistic analysis of apoptotic cells including early (Q3) and late (Q2) apoptotic cells. The experiment was carried out independently in triplicates for three times. Data were shown as mean±SEM. The statistical analysis was carried out using one-way ANOVA and corrected by Tukey's test (*** $p < 0.001$, **** $p < 0.0001$). The cells treated with PBS, MMAE, camptothecin or Zip1-MMAE were shown in figure 4.19.

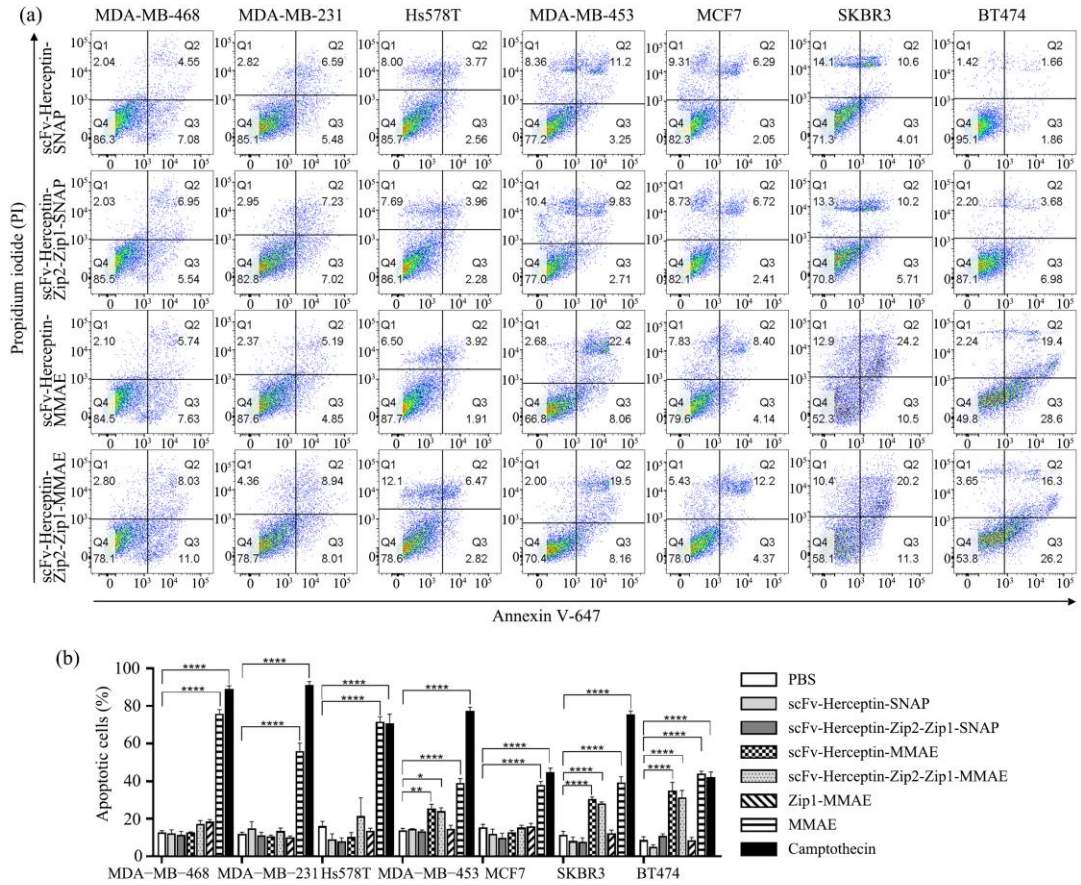

Figure 4.22. Her2-targeting ADCs induced apoptosis. (a) Scatter plot of one measurement as an example. (b) Statistic analysis of apoptotic cells including early (Q3) and late (Q2) apoptotic cells. The experiment was carried out independently in triplicates for three times. Data were shown as mean±SEM. The statistical analysis was carried out using one-way ANOVA and corrected by Tukey's test (*$p < 0.05$, ** $p < 0.01$, **** $p < 0.0001$). The cells treated with PBS, MMAE, camptothecin or Zip1-MMAE were shown in figure 4.19.

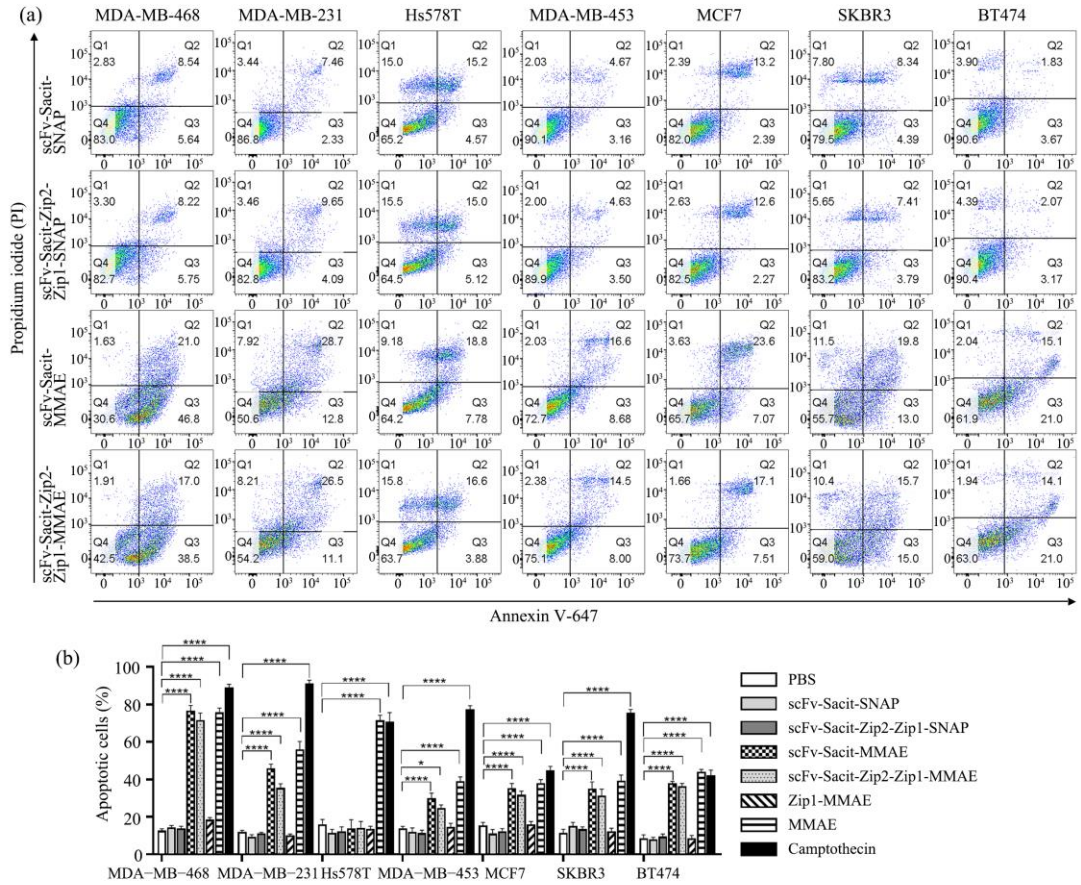

Figure 4.23. Trop2-targeting ADCs induced apoptosis. (a) Scatter plot of one measurement as an example. (b) Statistic analysis of apoptotic cells including early (Q3) and late (Q2) apoptotic cells. The experiment was carried out independently in triplicates for three times. Data were shown as mean±SEM. The statistical analysis was carried out using one-way ANOVA and corrected by Tukey's test (*$p < 0.05$, **** $p < 0.0001$). The cells treated with PBS, MMAE, camptothecin or Zip1-MMAE were shown in figure 4.19.

4.6 Functional assay in ovarian cancer

4.6.1 Expression of targets in ovarian cancer

The ovarian cancer cell lines (SKOV3, OVCAR3, A2780 and Hey) were confirmed to express different levels of EGFR, Her2 and Trop2 on cell membrane by flow cytometry (**Figure 4.24, Table 4.3**). The EGFR and Her2 were highly expressed on SKOV3 and OVCAR3, moderately presented on Hey, and relatively low expressed on A2780. A2780 and SKOV3 had low expression of Trop2, while OVCAR3 and Hey presented extremely high expression of Trop2.

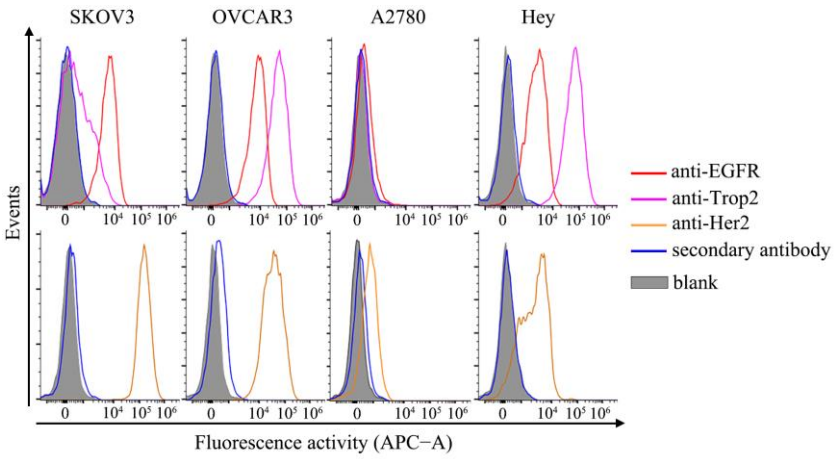

Figure 4.24. EGFR, Her2 and Trop2 were differently expressed in ovarian cancer cell lines. The EGFR, Her2 and Trop2 expression in breast cancer cell lines were determined by flow cytometry. The cells were treated with anti-EGFR (EGFR Monoclonal Antibody, H11), anti-Her2 (ErbB2 monoclonal antibody, 3B5) and anti-Trop2 (Trop2 monoclonal antibody, MR54) antibodies, respectively, followed by incubation with secondary antibody (Goat anti-Mouse IgG Highly Cross-Adsorbed Secondary Antibody, Alexa Fluor™ Plus 647).

Table 4.3 Expression profile of EGFR, Her2 and Trop2 in ovarian cancer cell lines

	SKOV3	OVCAR3	A2780	Hey
EGFR	high	high	low	medium
Her2	high	high	low	medium
Trop2	low	high	low	high

The expression levels of EGFR, Her2 and Trop2 were determined by flow cytometry.

4.6.2 Binding and colocalization of pre-targeting complex in ovarian cancer

The specific binding and colocalization of pre-targeting complex in ovarian cancer cell lines were confirmed by flow cytometry (**Figure 4.25a-4.28a**) and fluorescence microscopy (**Figure 4.25b-4.28b**). The flow cytometry showed that both scFv-Zip2-Zip1-647 and scFv-647 specifically bound to EGFR- (SKOV3, OVCAR3 and Hey), Her2- (SKOV3, OVCAR3 and Hey) or Trop2- (OVCAR3 and Hey) expressing cell lines, while Zip1-647 showed no unspecific binding. The binding process was further visualized by fluorescence microscopy as the fluorescence was observed on the cell membrane. However, the binding of EGFR- and Her2-targeting scFv-647 was weakly observed in Hey, but the scFv-425-Zip2-488-Zip1-647 and scFv-Herceptin-Zip2-488-Zip1-647 fluorescence was not detected in either green-488 or red-647 channel by fluorescence microscope due to the relatively low expression and the different

sensitivity of each experiment method, which also happened in breast cancer cell lines. In addition to the validation of binding property, the **figure 4.25b-4.28b** and **figure 4.25c-4.28c** further proved the colocalization and interaction of scFv-Zip2-488 and Zip1-647. As an example, the scFv-425-Zip2-488 and Zip1-647 fluorescence signals were detected on the cell membranes of SKOV3 and OVCAR3 by green-488 and red-647 channels individually, and the localities were totally overlapped in merged figures (**Figure 4.25b**). No binding was observed by incubating cells with Zip1-647, indicating that the red-647 signal detected on SKOV3 and OVCAR3 was from the combined complex rather than unspecific binding. The intensity of scFv-425-Zip2-488 and Zip1-647 increased and decreased simultaneously along the white arrow in merged figures further confirmed the colocalization (**Figure 4.25c**).

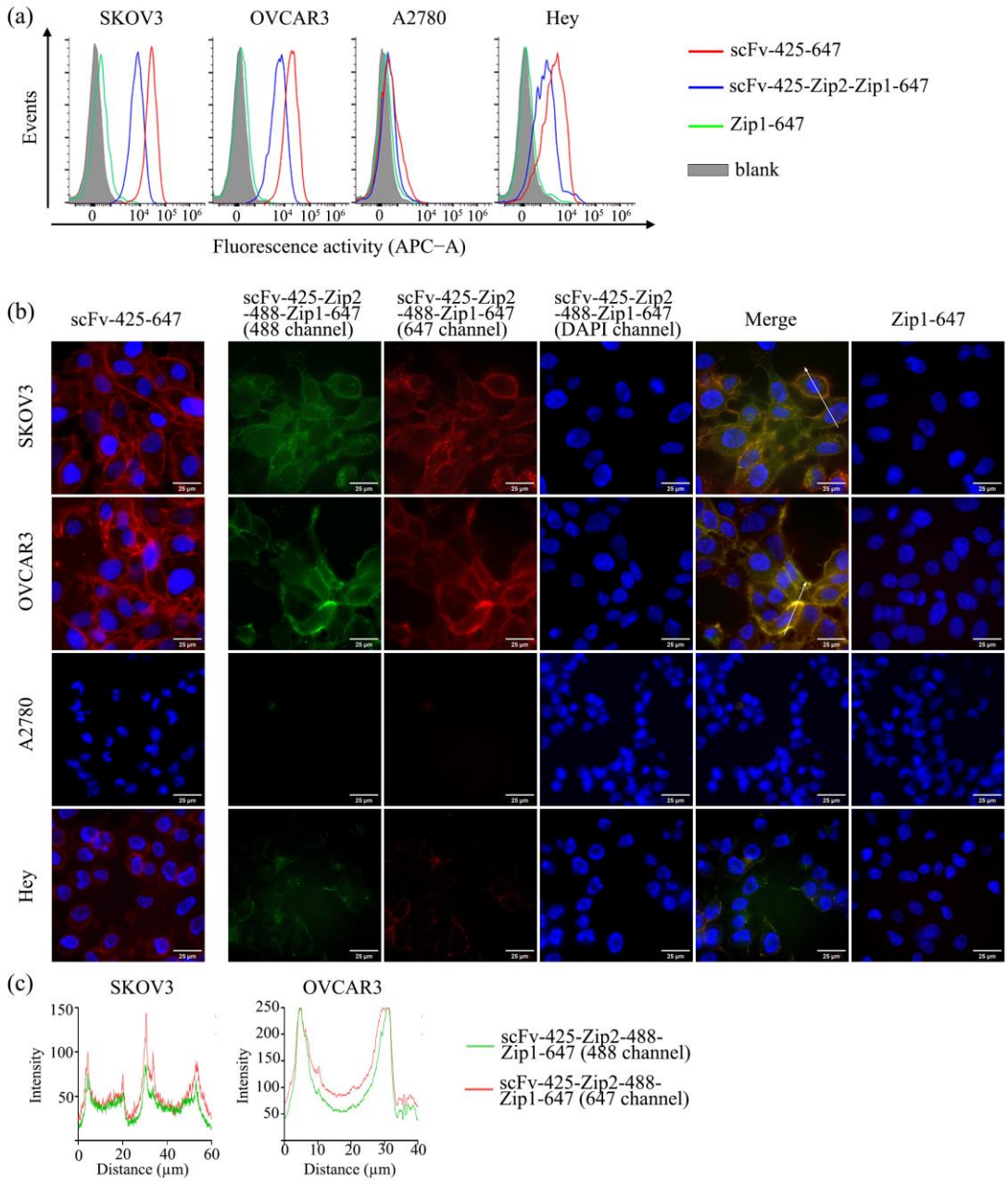

Figure 4.25. The EGFR-targeting complex specific binds to EGFR-expressing cells and colocalize on cell membranes. (a) Specific targeting of pre-targeting complex to ovarian cancer cell lines and comparison with direct conjugated antibody by flow cytometry. (b) The binding and colocalization of scFv-425-Zip2-488 and Zip1-647 were visualized by fluorescence microscopy. The binding process was carried out at 4°C. The fluorescence intensity along the white arrow in EGFR-expressing cell lines was shown in (c) and calculated by Image J software.

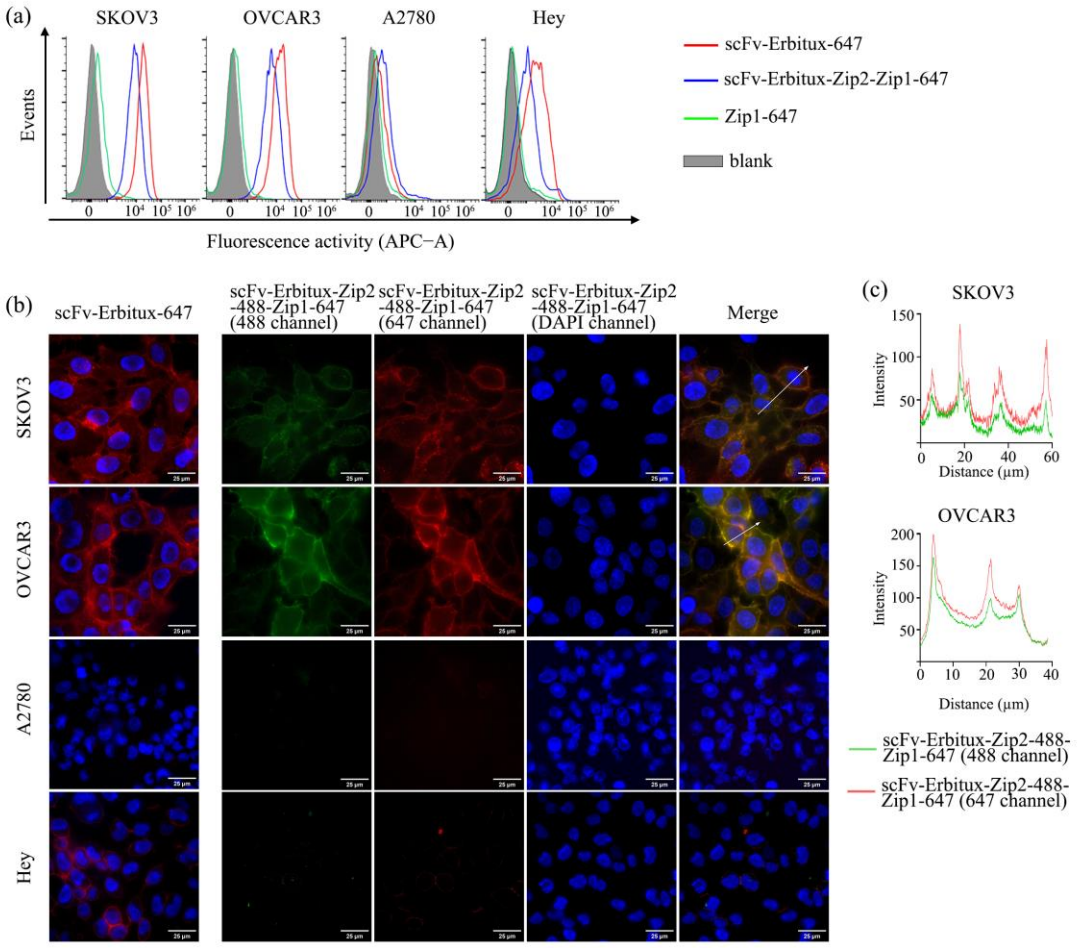

Figure 4.26. The EGFR-targeting complex specific binds to EGFR-expressing cells and colocalize on cell membranes. (a) Specific targeting of pre-targeting complex to ovarian cancer cell lines and comparison with direct conjugated antibody by flow cytometry. (b) The binding and colocalization of scFv-Erbitux-Zip2-488 and Zip1-647 were visualized by fluorescence microscopy. The binding process was carried out at 4°C. The fluorescence intensity along the white arrow in EGFR-expressing cell lines was shown in (c) and calculated by Image J software. The cells treated with Zip1-647 alone to confirm no unspecific binding were shown in figure 4.25.

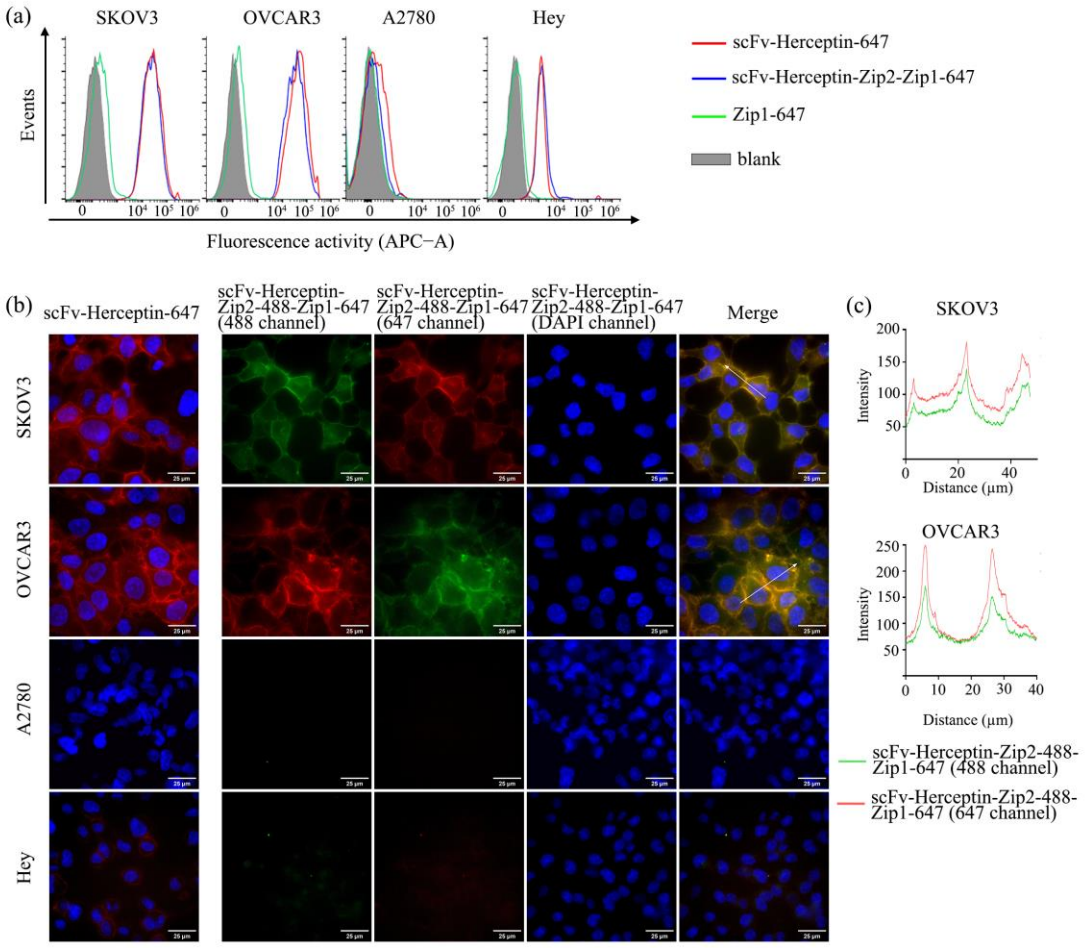

Figure 4.27. The Her2-targeting complex specific binds to Her2-expressing cells and colocalize on cell membranes. (a) Specific targeting of pre-targeting complex to ovarian cancer cell lines and comparison with direct conjugated antibody by flow cytometry. (b) The binding and colocalization of scFv-Herceptin-Zip2-488 and Zip1-647 were visualized by fluorescence microscopy. The binding process was carried out at 4°C. The fluorescence intensity along the white arrow in Her2-expressing cell lines was shown in (c) and calculated by Image J software. The cells treated with Zip1-647 alone to confirm no unspecific binding were shown in figure 4.25.

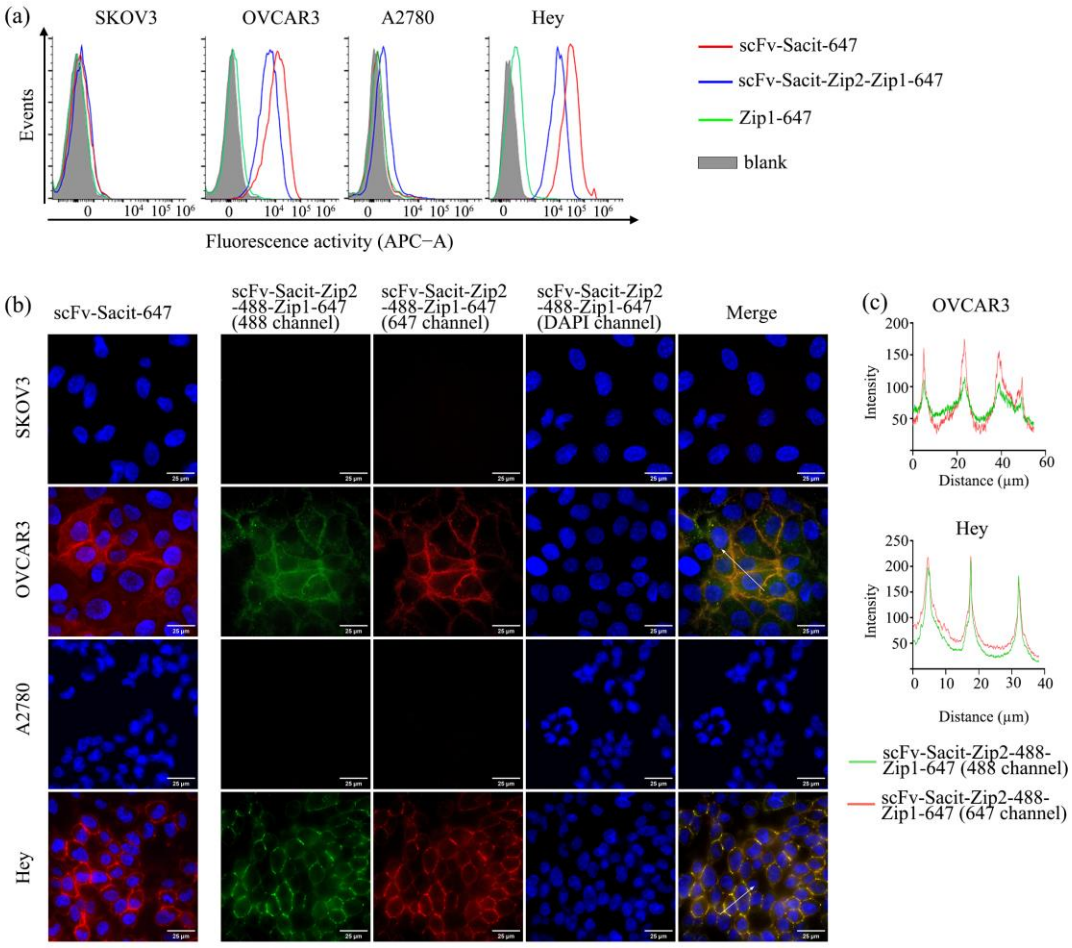

Figure 4.28. The Trop2-targeting complex specific binds to Trop2-expressing cells and colocalize on cell membranes. (a) Specific targeting of pre-targeting complex to ovarian cancer cell lines and comparison with direct conjugated antibody by flow cytometry. (b) The binding and colocalization of scFv-Sacit-Zip2-488 and Zip1-647 were visualized by fluorescence microscopy. The binding process was carried out at 4°C. The fluorescence intensity along the white arrow in Trop2-expressing cell lines was shown in (c) and calculated by Image J software. The cells treated with Zip1-647 alone to confirm no unspecific binding were shown in figure 4.25.

4.6.3 Internalization property of pre-targeting complex in ovarian cancer

Compatible to the aforementioned results, scFv-Zip2-488-Zip1-647 and scFv-647 were internalized into the cells, and its binding and colocalization properties were observed by fluorescence microscopy (**Figure 4.29-4.32**). Similarly, the internalization of scFv-425-Zip2-488-Zip1-647, scFv-Erbitux-Zip2-488-Zip1-647 and scFv-Herceptin-Zip2-488-Zip1-647 were not detected in Hey, but scFv-425-647, scFv-Erbitux-647 and scFv-Herceptin-647 were weakly detected. No unspecific internalization of Zip1-647 was

observed.

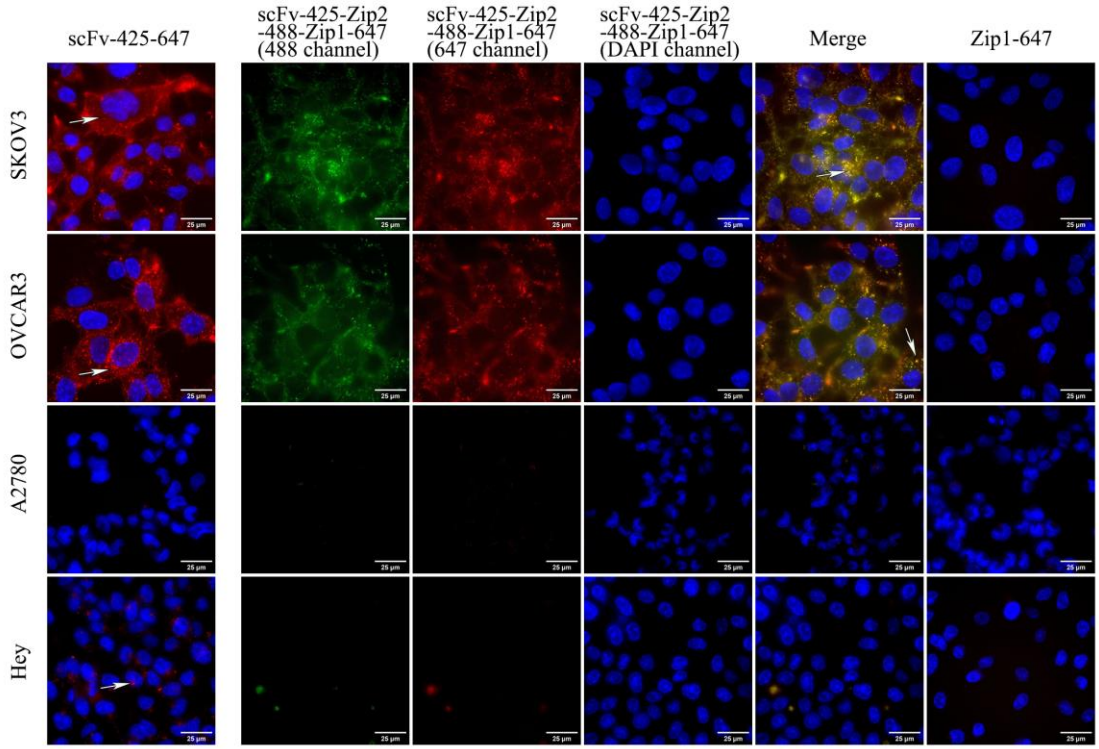

Figure 4.29. Fast internalization of the scFv-425-Zip2-488 and Zip1-647 complex. Ovarian cancer cells were incubated with scFv-425-Zip2-488 for 1h followed by post-incubation with Zip1-647 for 3h, or with scFv-425-647 for 3h. The internalization process was carried out at 37°C. The green represents 488 channel, the red represents 647 channel, and the blue represents DAPI channel. The internalized molecules were indicated by white arrows.

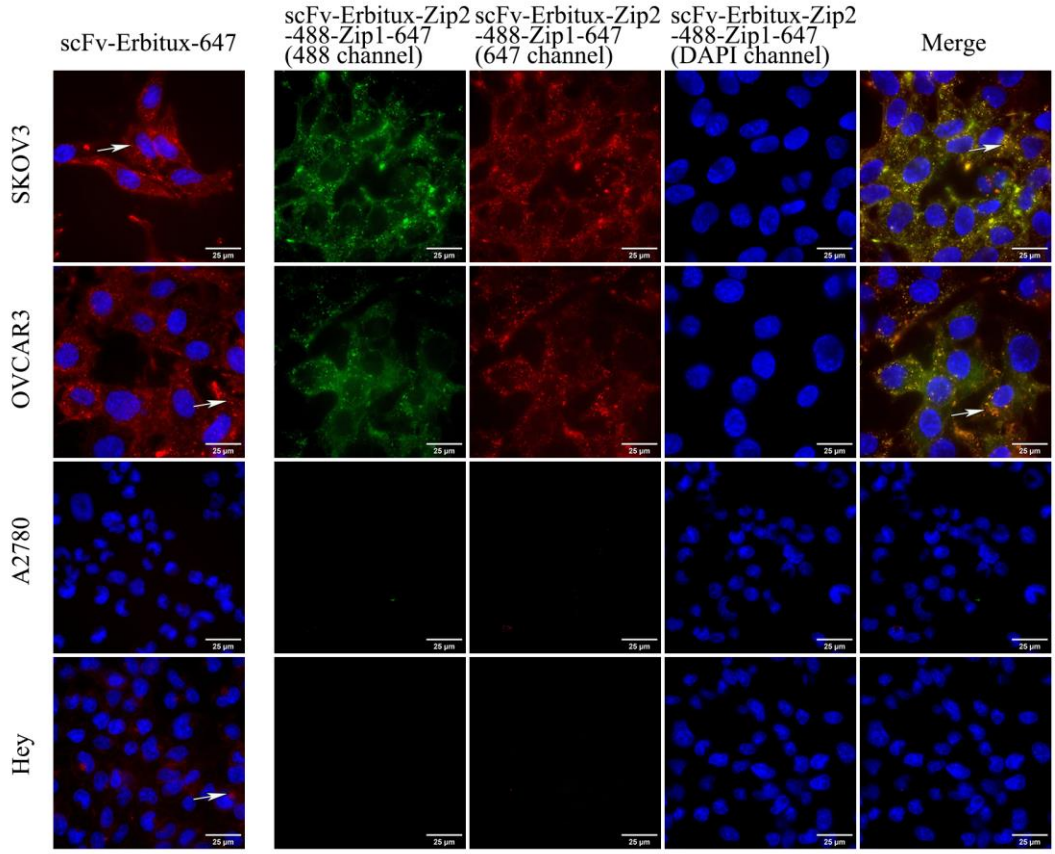

Figure 4.30. Fast internalization of the scFv-Erbitux-Zip2-488 and Zip1-647 complex. Ovarian cancer cells were incubated with scFv-Erbitux-Zip2-488 for 1h followed by post-incubation with Zip1-647 for 3h, or with scFv-Erbitux-647 for 3h. The internalization process was carried out at 37°C. The green represents 488 channel, the red represents 647 channel, and the blue represents DAPI channel. The internalized molecules were indicated by white arrows. The cells treated with Zip1-647 alone were shown in figure 4.29.

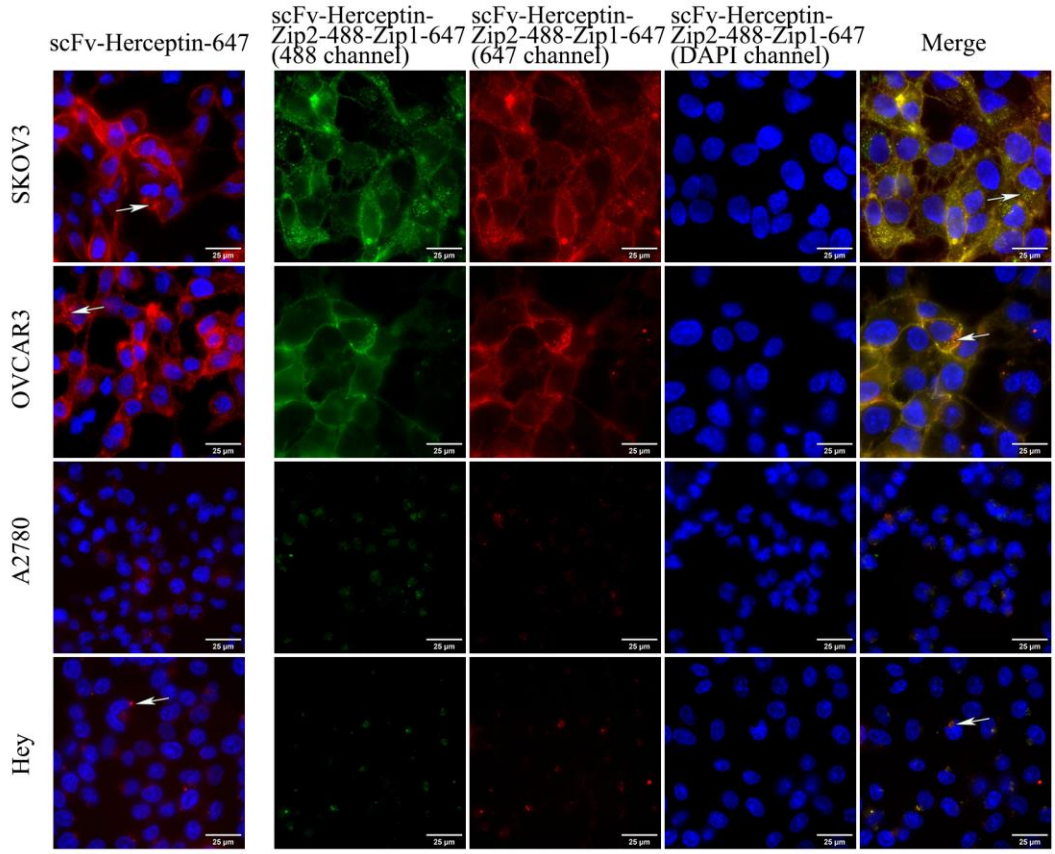

Figure 4.31. Fast internalization of the scFv-Herceptin-Zip2-488 and Zip1-647 complex. Ovarian cancer cells were incubated with scFv-Herceptin-Zip2-488 for 1h followed by post-incubation with Zip1-647 for 3h, or with scFv-Herceptin-647 for 3h. The internalization process was carried out at 37°C. The green represents 488 channel, the red represents 647 channel, and the blue represents DAPI channel. The internalized molecules were indicated by white arrows. The cells treated with Zip1-647 alone were shown in figure 4.29.

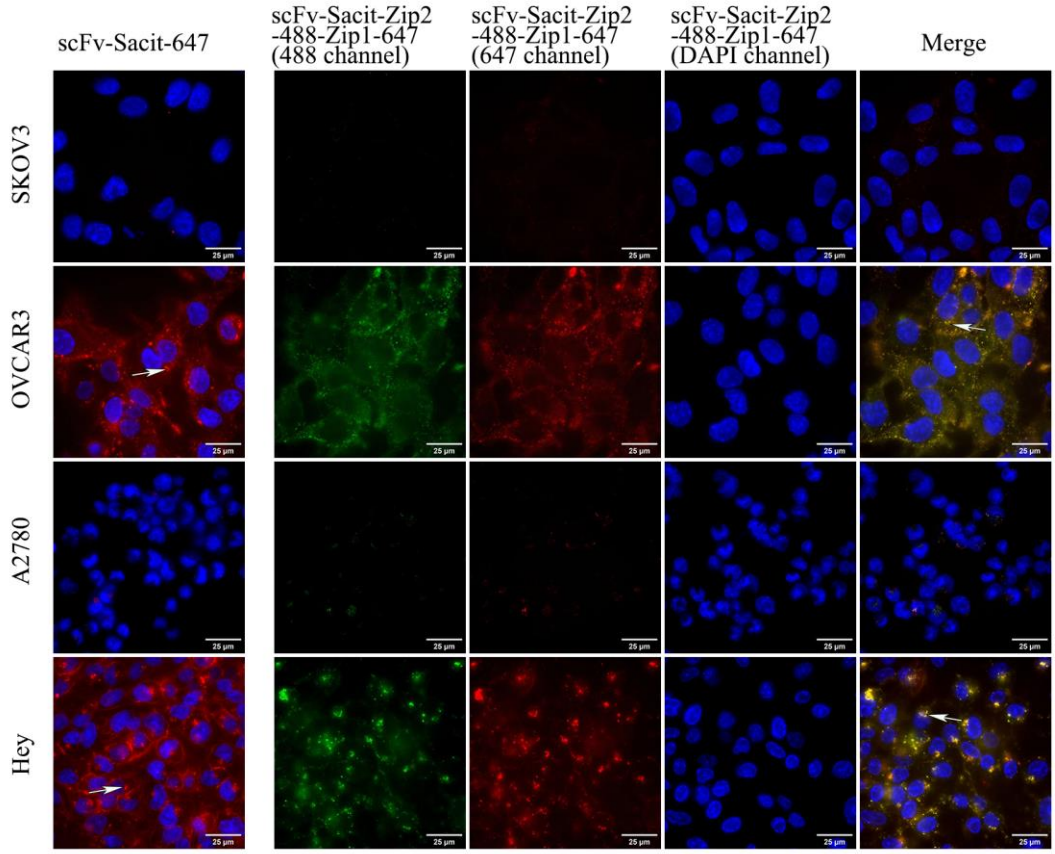

Figure 4.32. Fast internalization of the scFv-Sacit-Zip2-488 and Zip1-647 complex. Ovarian cancer cells were incubated with scFv-Sacit-Zip2-488 for 1h followed by post-incubation with Zip1-647 for 3h, or with scFv-Sacit-647 for 3h. The internalization process was carried out at 37°C. The green represents 488 channel, the red represents 647 channel, and the blue represents DAPI channel. The internalized molecules were indicated by white arrows. The cells treated with Zip1-647 alone were shown in figure 4.29.

4.6.4 Specific cytotoxicity of MMAE based pre-targeting complex

The specific cytotoxicity of MMAE-based ADCs was validated by determining cell viability after treating cells with increasing concentration (10, 20, 40, 80, 160, 320, 640 nM) of scFv-MMAE, pre-targeting complex (scFv-Zip2-Zip1-MMAE), unconjugated antibodies (scFv-Zip2-Zip1-SNAP or scFv-SNAP), Zip1-MMAE or MMAE at 37°C for 72 h (**Figure 4.33**). All ovarian cancer cell lines showed high sensitivity to MMAE with IC_{50} around 100 nM. After tethering MMAE to antibodies or Zip1-SNAP, the sensitivity reduced but specificity profoundly improved: cytotoxicity was observed in EGFR- (SKOV3, OVCAR3 and Hey), Her2- (SKOV3, OVCAR3 and Hey) and Trop2- (OVCAR3 and Hey) expressing cells, but not in $EGFR^{low}$ (A2780), $Her2^{low}$ (A2780)

and Trop2^{low} (SKOV3 and A2780) cell lines. The scFv-SNAP and Zip1-MMAE showed no or minimal cytotoxicity up to 640 nM. The range of IC_{50} differed in different cell lines influenced by various factors such as sensitivity to MMAE and the expression of the antigens. Full details are listed in **table 4.4**.

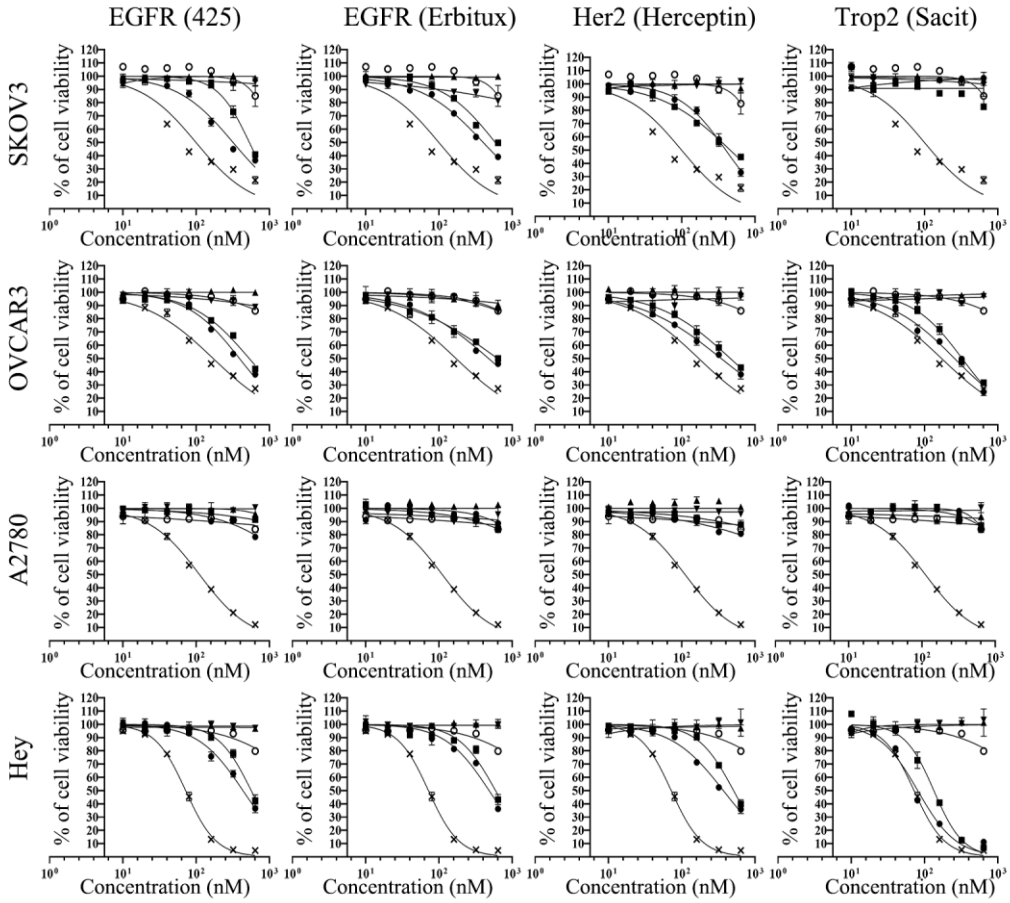

Figure 4.33. Specific cytotoxicity was triggered by pre-targeting complex. Ovarian cancer cell lines were treated with increasing concentration (10, 20, 40, 80, 160, 320, 640 nM) of scFv-Zip2-Zip1-MMAE (■), scFv-MMAE (●), scFv-Zip2-Zip1-SNAP (▼) scFv-SNAP (▲), Zip1-MMAE (○) or MMAE (×) at 37°C for 72 h. Cell viability was determinized by Cell Proliferation (XTT) Kit II, and the experiment was carried out in triplicates for three times. One independent experiment was shown with the mean±SD.

Table 4.4 Table of IC_{50} values (nM)

	SKOV3	OVCAR3	A2780	Hey
scFv-425-MMAE	318.9±19.04	398.3±27.42	-	459.8±36.65
scFv-425-Zip2-Zip1-MMAE	555.4±23.11	538.6±36.21	-	588.6±38.94
scFv-425-SNAP	-	-	-	-
scFv-425-Zip2-Zip1-SNAP	-	-	-	-
scFv-Erbitux-MMAE	409.3±36.87	415.4±28.3	-	507.8±37.96
scFv-Erbitux-Zip2-Zip1-MMAE	565.5±39.39	540.5±38.72	-	596.8±39.58
scFv-Erbitux-SNAP	-	-	-	-
scFv-Erbitux-Zip2-Zip1-SNAP	-	-	-	-
scFv-Herceptin-MMAE	407±31.03	387.9±21.63	-	426.7±34.77
scFv-Herceptin-Zip2-Zip1-MMAE	432.2±22.28	455.8±20.8	-	513.6±39.72
scFv-Herceptin -SNAP	-	-	-	-
scFv-Herceptin-Zip2-Zip1-SNAP	-	-	-	-

Continued table 4.4 Table of IC_{50} values (nM)

	SKOV3	OVCAR3	A2780	Hey
scFv-Sacit-MMAE		271±13.93	-	97.65±5.491
scFv-Sacit-Zip2-Zip1-MMAE		282.7±12.31	-	106.8±6.105
scFv-Sacit-SNAP	-	-	-	-
scFv-Sacit-Zip2-Zip1-SNAP	-	-	-	-
Zip1-MMAE	-	-	-	-
MMAE	96.6±8.85	166±12.26	127.2±8.226	77.13±3.326

The IC_{50} values indicate the concentration that inhibit cell viability by 50% relative to untreated control cells. The data represented three independent experiments carried out in triplicate and were presented as mean ± standard error of the mean (SEM).

4.6.5 Induction of apoptosis by MMAE based pre-targeting complex

The specific cytotoxicity was further validated by apoptosis assay. The **figure 4.34-4.37** shows the proportion of apoptotic cells in EGFR- (SKOV3, OVCAR3 and Hey), Her2- (SKOV3, OVCAR3 and Hey) and Trop2- (OVCAR3 and Hey) expressing cells significantly increased after treating them with 640 nM of scFv-MMAE, scFv-Zip2-Zip1-MMAE or MMAE, but not in $EGFR^{low}$ (A2780), $Her2^{low}$ (A2780) and $Trop2^{low}$ (SKOV3 and A2780) cell lines and cells treated with unconjugated antibodies (scFv-Zip2-Zip1-SNAP or scFv-SNAP) or Zip1-MMAE. The detailed statistical analysis is

showed in figure **4.34b-4.37b**.

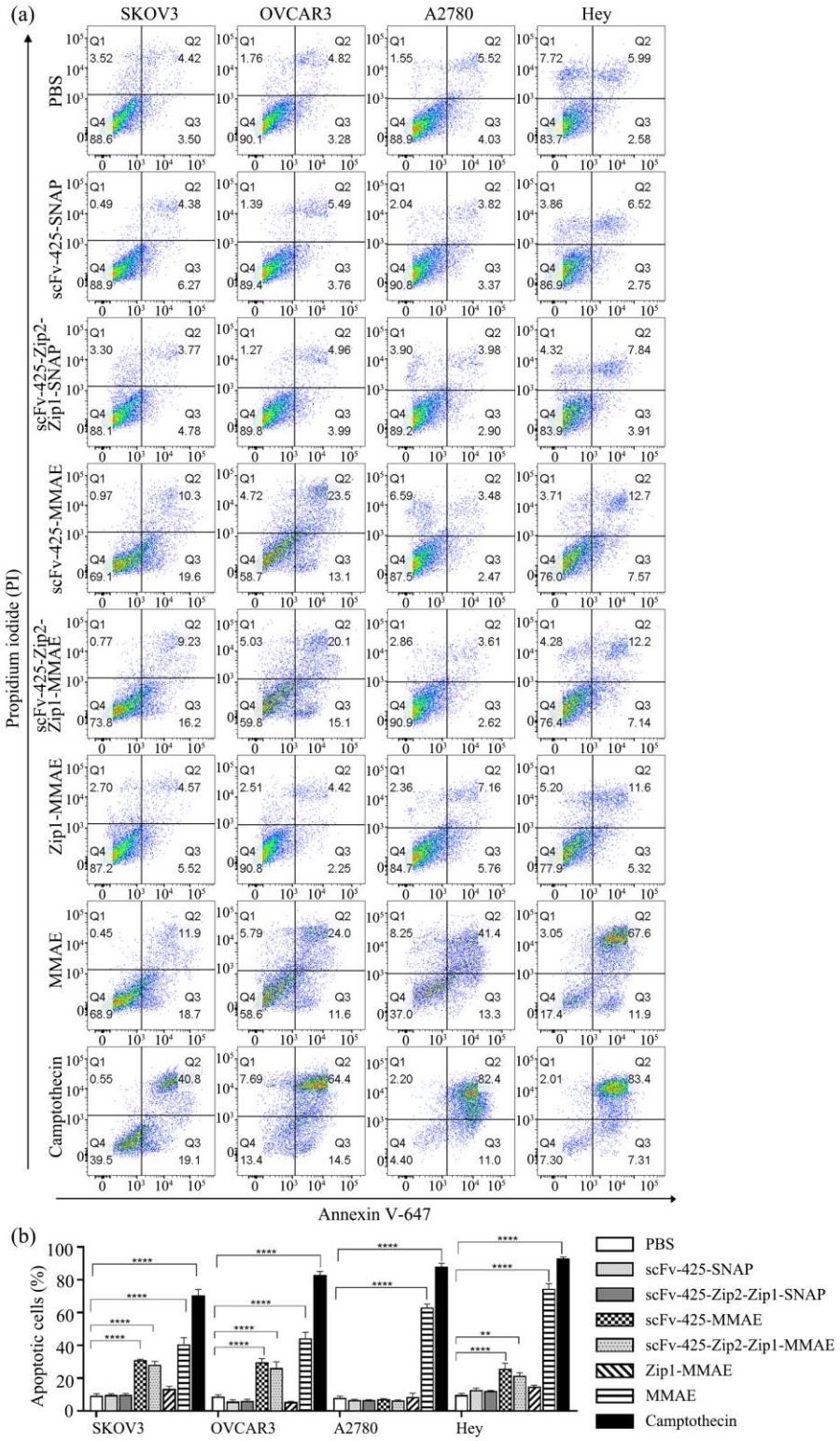

Figure 4.34. EGFR-targeting ADCs induced apoptosis. (a) Scatter plot of one measurement as an example. (b) Statistic analysis of apoptotic cells including early (Q3) and late (Q2) apoptotic cells. The experiment was carried out independently in triplicates for three times. Data were shown as mean±SEM. The statistical analysis was carried out using one-way ANOVA and corrected by Tukey's test (** $p < 0.01$, **** $p < 0.0001$).

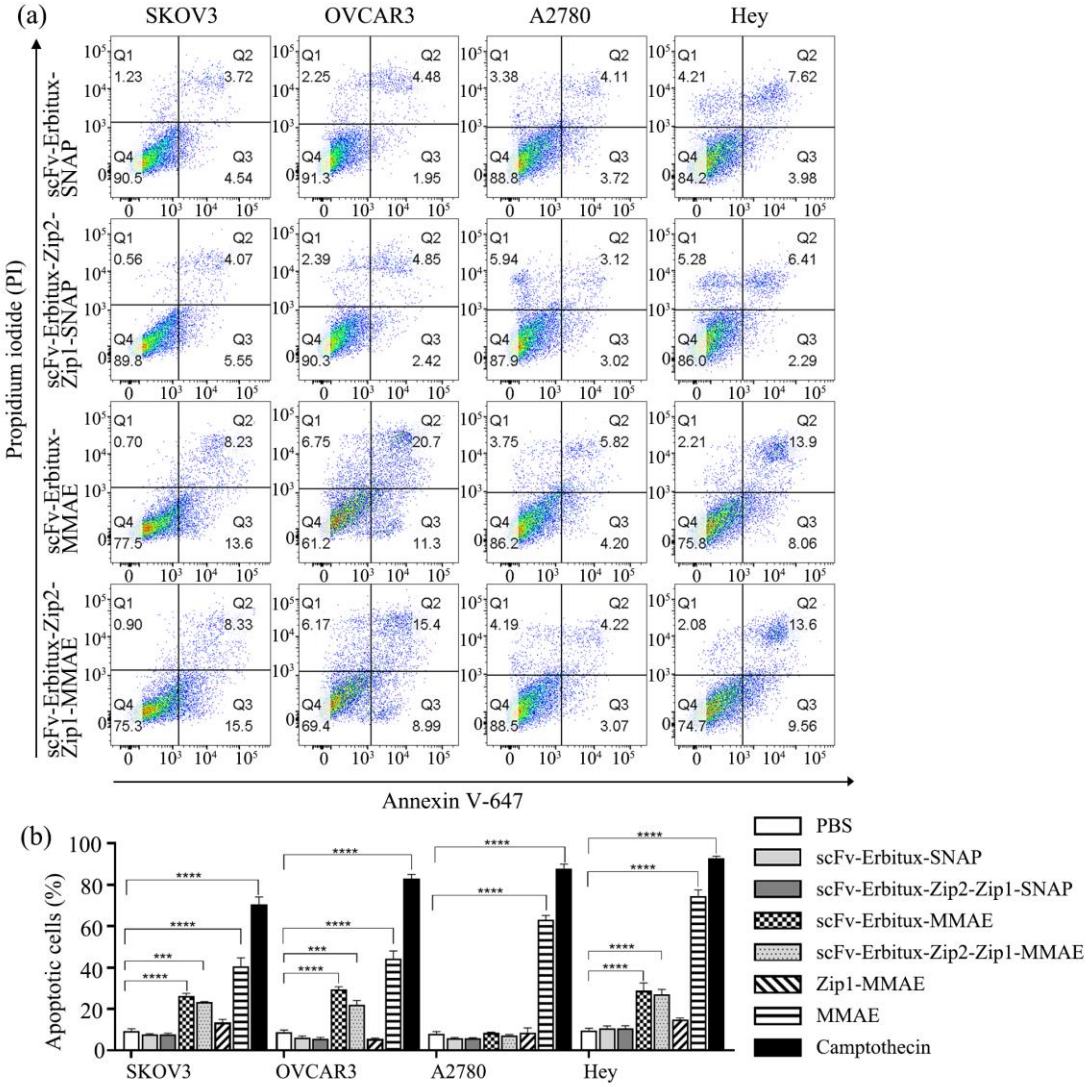

Figure 4.35. EGFR-targeting ADCs induced apoptosis. (a) Scatter plot of one measurement as an example. (b) Statistic analysis of apoptotic cells including early (Q3) and late (Q2) apoptotic cells. The experiment was carried out independently in triplicates for three times. Data were shown as mean±SEM. The statistical analysis was carried out using one-way ANOVA and corrected by Tukey's test (*** $p < 0.001$, **** $p < 0.0001$). The cells treated with PBS, MMAE, camptothecin or Zip1-MMAE were shown in figure 4.34.

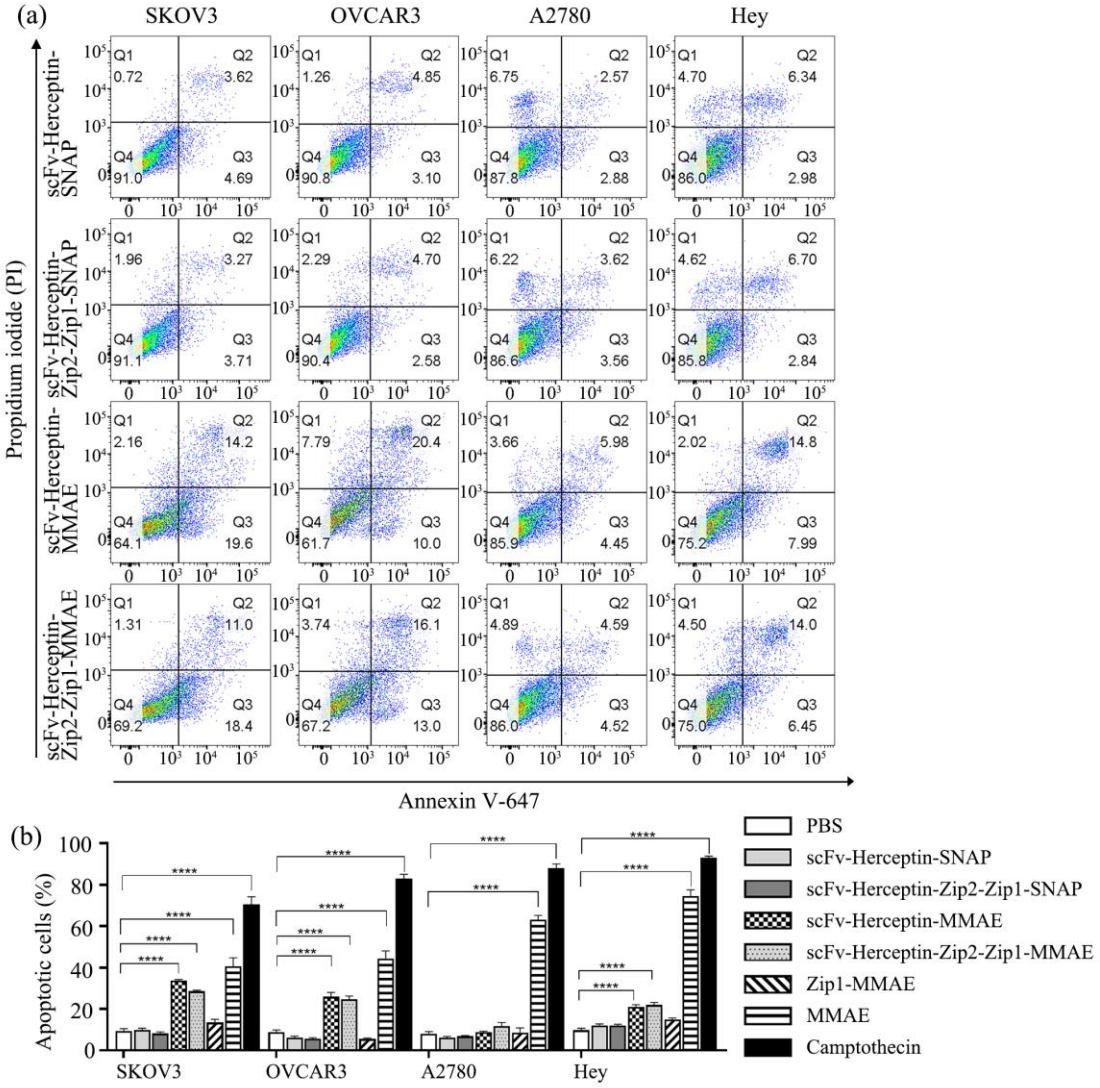

Figure 4.36. Her2-targeting ADCs induced apoptosis. (a) Scatter plot of one measurement as an example. (b) Statistic analysis of apoptotic cells including early (Q3) and late (Q2) apoptotic cells. The experiment was carried out independently in triplicates for three times. Data were shown as mean ± SEM. The statistical analysis was carried out using one-way ANOVA and corrected by Tukey's test (**** $p < 0.0001$). The cells treated with PBS, MMAE, camptothecin or Zip1-MMAE were shown in figure 4.34.

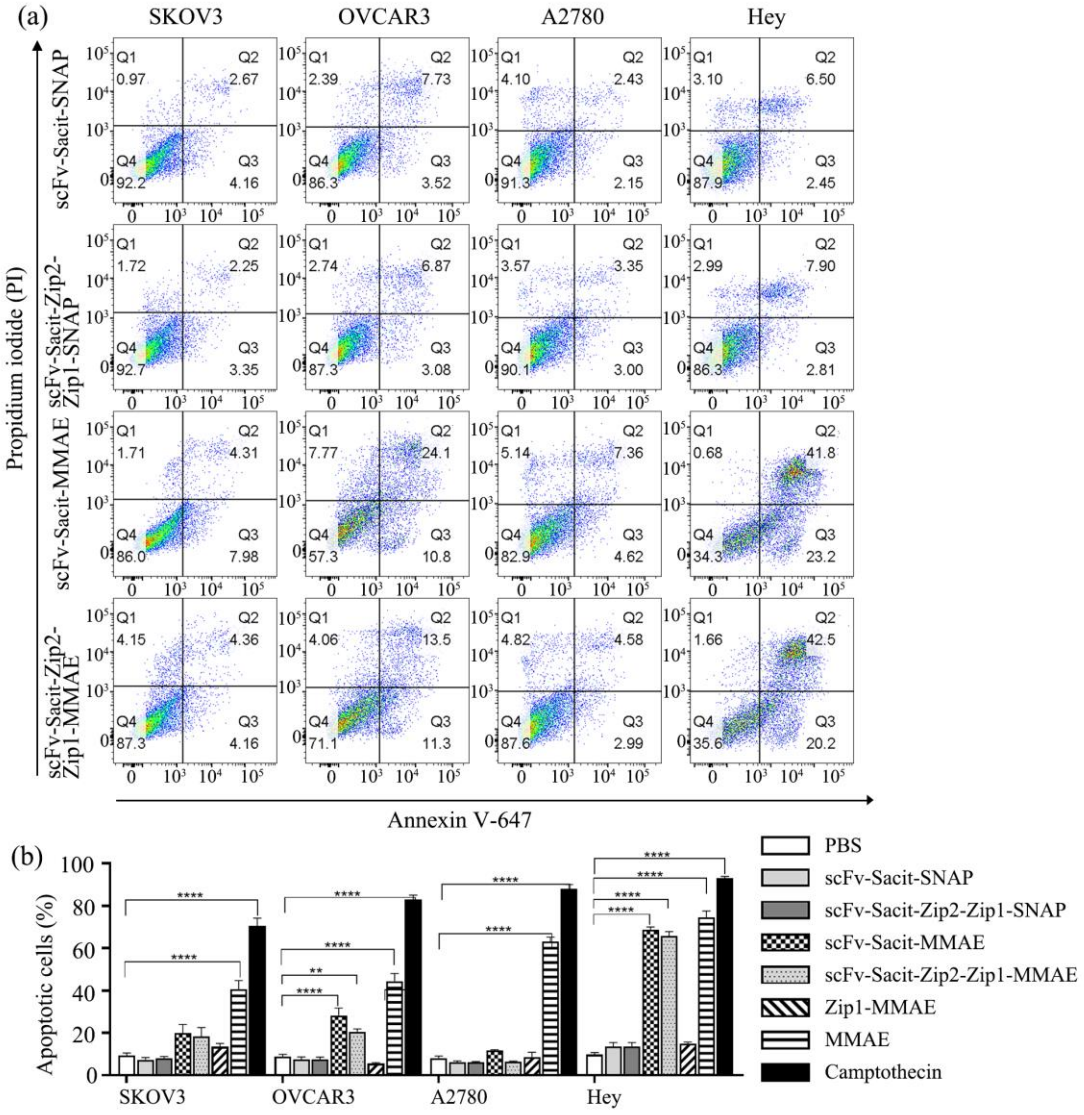

Figure 4.37. Trop2-targeting ADCs induced apoptosis. (a) Scatter plot of one measurement as an example. (b) Statistic analysis of apoptotic cells including early (Q3) and late (Q2) apoptotic cells. The experiment was carried out independently in triplicates for three times. Data were shown as mean±SEM. The statistical analysis was carried out using one-way ANOVA and corrected by Tukey's test (** $p < 0.01$, **** $p < 0.0001$). The cells treated with PBS, MMAE, camptothecin or Zip1-MMAE were shown in figure 4.34.

5. Discussion

The construction of ADC perfectly fits the concept of "magic bullet" by combining the specificity of antibody and cytotoxicity of small molecules. Undoubtedly, the targeted delivery of drug expands the therapeutic window by lowering the minimum effective dose and increasing the maximum tolerated dose, as the drugs increase the toxicity of mAbs and the mAbs reduce the drug toxicity in normal or non-target cells [123]. However, even the 13 approved ADCs have achieved tremendous success in improving clinical outcomes as adjuvant therapy, it is still in the early stage of the development, especially for solid tumor treatment.

This study focuses on establishing a novel pre-targeting drug delivery system to improve the design of the ADC, enhance the ADC efficacy, and provide more alternative treatment options for breast cancer and ovarian cancer. The scFv-based ADCs, which were directly conjugated with MMAE via SNAP-tag, has been confirmed to bind and eliminate the EGFR- or EpCAM-expressing TNBC cells specifically [124]. Here, the corresponding scFv-SNAP of pre-targeting system was also generated to compare the efficacy.

5.1 ADC design

Antibody, linker and payload are three core components for constructing an ADC. Once the ADC have entered human body, each step including blood circulation, ADC accumulation, antigen recognition and binding, ADC-antigen complex internalization, drug releasing and cell killing, can be the "rate-limiting step" for a successful therapy. The growing number of tumor associated antigens, the diversification of the optional components and the fast development of conjugation methods nowadays make the ADC design like an endlessly intricate puzzle. Therefore, choosing suitable components to maximize the function of ADC and minimize the side effect is one of the most challenging tasks.

This study involved EGFR, EpCAM, Her2 and Trop2 as targets, scFv as backbone, Val-Cit dipeptide as cleavable linker, MMAE as payload and SNAP-tag technology as

conjugation method to establish the novel ADCs.

5.1.1 EGFR, EpCAM, Her2 and Trop2 as potential targets for breast and ovarian cancers

Breast cancer is the most common and ovarian cancer is the most mortal cancer among the gynecologic cancers. There are already three ADCs have been approved for breast cancer but only one that was just recently approved for ovarian cancer. However, many ADCs either approved or in clinical trial are focusing on Her2 in breast cancer and FRα in ovarian cancer. Although a wide range of clinical trials have displayed favorable efficacy results of Her2-targeing ADCs in Her2-positive or even Her2-low breast cancer, most of patients with advanced or metastatic tumor ineluctably progressed [85, 125]. Besides, the drug resistance issue also limits patients to benefit from long-term treatment, which is reported to be associated, but not limited with Her2 down-regulation, epitope masking and ADC recycling after internalization [126, 127]. Apparently, selecting more breast or ovarian cancer related antigens to develop new ADCs is in urgent need.

In this study, EGFR and EpCAM were selected as potential targets for breast cancer except Her2 and Trop2, while EGFR, Her2 and Trop2 were selected for ovarian cancer after extensive literature survey. A plethora of researches have shown that EGFR is overexpressed in breast cancer, especially in TNBC, associating with higher proliferation, recurrence and poor survival [128-130]. Immunohistochemistry result indicates that EGFR-overexpressing patients range from 13% to 76% in TNBC depending on the detection methods and antibodies used [131]. This study included four TNBC cell lines (MDA-MB-468, MDA-MB-231, Hs578T and MDA-MB-453), among which three fourths of the cell lines showed high expression of EGFR (**Figure 4.6**). Similarly, EpCAM is also reported to be upregulated in breast cancer and is related to unfavorable outcomes and metastases [132-135]. In particular, the high expression of EpCAM can lead to poor neoadjuvant chemotherapy, indicating the importance to eliminate EpCAM-overexpressing tumor cells [136]. Her2 and Trop2 have already been

used as targets for ADCs, but they are mainly focusing on special types of breast cancer. The application of T-DXd in patients with Her2-low breast cancer have achieved impressive results (clinical trial, NCT03734029) [83], and now more studies (clinical trials, NCT05831878, NCT04400695 and NCT04742153) are ongoing to evaluate the efficacy and safety of Her2-targeting ADCs in Her2-low breast cancer. Trodelvy® is a Trop2-targeting ADC approved for TNBC, but high level of Trop2 is detected in all breast cancer types (50% ER+, 74% HER2+, and 93% TNBC) [89]. Considering that this study not only focuses on exploring new targets, but also aims to establish and estimate a novel drug delivery system, Her2 and Trop2 are also included as targets. The two Her2-positive cell line (SKBR3 and BT474) presented high expression level of Her2 as expected and all breast cancer cell lines except Hs578T showed overexpression of Trop2 (**Figure 4.6**). However, the MDA-MB-453 is officially defined as a TNBC cell line but exhibited high Her2 expression (**Figure 4.6**). As there are conflicting results on MDA-MB-453 that some research groups use it as TNBC cell line, some report low gene amplification and protein expression, some confirm the high mRNA level, and others find high Her2 expression [137-140], the MDA-MB-453 was used as a Her2-expressing cell line in this study according to the flow cytometry result (**Figure 4.6**).

Apart from the potency or confirmed efficacy in breast cancer, EGFR, Her2 and Trop2 are also candidate targets for ovarian cancer. These antigens have been confirmed to be overexpressed in ovarian cancer and correlated with aggressive clinical features by many studies [141-146]. While the results of Her2- and Trop2-targting ADCs in clinical trials are still awaited (clinical trials, NCT04965519 and NCT04152499), unfortunately, the previous clinical trials using anti-EGFR mAbs show no significant or limited clinical activity in ovarian cancer [147-149], and no EGFR-targeting ADC is in clinical trial by far. The wide range of EGFR expression (4-100%) [150] on ovarian cancer cells and limited toxicity of mAbs might be reasons to some degree. Given the importance of EGFR in tumorigenesis and cancer progress in ovarian cancer, it remains the potential to be the target for ADC.

Some studies have reported that the EGFR epitope for mAb Erbitux is distinct from mAb 425 [116, 151]. Thus, EGFR-specific scFv-SNAP and scFv-Zip2 derived from mAb Erbitux and mAb 425 are both generated. These scFvs were also confirmed to bind distinct epitopes of EGFR as their parental antibodies by blocking the epitopes using 10 μg of naked scFv-425-SNAP or scFv-Erbitux-SNAP, followed by post-incubation with scFv-Erbitux-647 or scFv-425-647, respectively (**Figure 4.7**). As the binding site for 425 was blocked by scFv-425-SNAP, the scFv-425-647 could not bind anymore, but the scFv-Erbitux-647 were still able to bind EGFR, and vice versa.

5.1.2 Application of scFv in ADC design

ADC accumulation is one of the limiting factors to exert full activity of ADCs. The majority of ADCs either approved or under development are using IgG scaffold. In spite of the wide application and mature technology of full-length antibody in ADC field, there still remains demerits. On the one hand, researchers indicate that the size of intact antibody (approximately 150 kDa) might be the reason for the low accumulation (less than 0.01%) in tumor site due to its poor penetration capability [31, 152]. On the other hand, the interaction between the Fc region and Fc receptor (FcR) can lead to Fc-mediated side effects. For example, the thrombocytopenia which is a common adverse effect of T-DM1 can be partially caused by FcγRIIa-mediated internalization into megakaryocytes to affect production of platelets [153]; ADC aggregates can be internalized into non-target cells to cause off-target toxicity by FcγR-dependent cellular uptake [154]; and the Fc domain also contributes to inter-individual variation as the Fc-FcR interaction varies from person to person [155]. The antitumor activity of therapeutic mAb is driven by antibody-dependent cellular cytotoxicity, complement-dependent cytotoxicity, signal transduction change, immunomodulation and antibody-dependent cellular phagocytosis [156, 157]. These immune reactions mediated by Fc region increase the cytotoxicity of mAb but may be superfluous for ADC, since the toxicity of ADC mainly relies on payload not antibody [158]. Furthermore, the toxicity of these immune reactions is doubted to be limited. An assessment from European

Medicine Agency in 2012 indicates that Adcetris® exhibits no complement dependent cytotoxicity and limited antibody-dependent cell-mediated cytotoxicity *in vitro* [32].

In the course of time, many small antibody fragments such as scFv, Fab, nanobodies have been developed to supersede full-length antibodies, among which scFvs have gained attention and achieved impressive results. The scFv is about 30 kDa and made up of the variable regions of heavy chain and light chain connected by a flexible peptide linker [159]. The scFv has smaller size compared to intact antibody but still retains the antigen-binding fragment which is responsible for specific antibody binding. Thus, scFv obtains better tissue penetration property to diffuse to tumor site more efficiently. While the scFv is able to reach the maximum accumulation after 0.5 to 6 h in tumor model, the full-length antibody takes 48 to 96 h to meet the equivalent distribution [160, 161]. Also, the small size results in fast clearance. For example, the Beovu® (brolucizumab-dbll), which is a FDA-approved scFv as vascular endothelial growth factor inhibitor, can reach maximum serum concentration after 24 h and the systemic half-life is 4.4 ± 2.0 days, whereas most therapeutic full-length antibodies exhibit much longer serum half-life (around 21 days) [162]. The increased tissue permeability, fast accumulation and clearance lead to the low concentration of scFv in blood circulation, which can further help to reduce side effects due to less accumulation in non-target cells [161].

The recombinant antibody technology boosts the development of protein expression technique without animal immunization and hybridoma, and it also enables the genetic manipulation of antibodies [163]. Most of the marketed full-length antibodies are expressed by mammalian cells as they have better folding, secretion and post-translation function compared to other expression system [164]. Without Fc fragment which requires for glycosylation and disulfide bond which needs folding function of host, the scFv can be produced in *E. coli*, yeast, mammalian cells, plant and insect cells [163, 165]. Another advantage of scFv is that the antibody allows diversified modification such as generating tandem scFv to target two different antigens or adding tags [166, 167]. While manipulating intact antibody might further increase the size to

cause worse pharmacokinetics, these manipulation in scFv might even improve the therapeutic index. For example, the molecular weight of scFv-SNAP is around 52 kDa, and some researchers have reported that the protein around 50 kDa can achieve the maximum tumor-to-plasma exposure ratio for Fc-independent targeted protein therapeutics [168]. Given the advantages and disadvantages of *E. coli* and mammalian expression system, the expression systems of scFv varies in different studies: the marketed Beovu® is expressed by *E. coli* BL21(DE3) bacteria, but Blincyto® is produced by mammalian expression system using chinese hamster ovary cells. As the scFvs in this study were modified with SNAP-tag or Zip2, the mammalian expression system might be a better choice to maintain the full activity of protein. The HEK293T protein expression system has been well established in this lab. Even though this mammalian expression system is difficult to scale up for manufacturing compared to chinese hamster ovary cells, it is a commonly used method to produce protein in research settings as it allows transiently transfection and is cost-saving.

The insertion of IgK leader (**Figure 4.1**) allowed the secretion of the protein to culture medium, which simplified the protein purification to some extend by skipping cell lysis and reducing the intracellular protein in the initial collected medium by the way. After the protein enrichment, almost only the interest proteins were in final collection (**Figure 4.2**, **Supplementary Figure 1**), and this expression system was proved to be high-yield as up to 10 mg of SNAP-fusion proteins and 5 mg of Zip2-fusion proteins were produced per liter of culture medium. These SNAP- or Zip2-modified scFvs retained full activity to bind BG-derivatives (**Figure 4.4b**, **Supplementary Figure 2**) or Zip1-SNAP (**Figure 4.5b**), and the specific targeting property of antibody was remained, which was further confirmed by flow cytometry and fluorescence microscopy (**Figure 4.8-4.12**, **Figure 4.25-4.28**).

Taking these advantages, the scFv has been widely applied in medicine field for research, diagnosis and treatment. Apart from the antitumor effect from the scFv itself [169-171], researchers have conjugated scFv with various agents, for example, chelating agent [172], fluorescence [173] or radionuclide as imaging probes for

diagnosis or treatment. However, most of the scFv-based therapy now are focusing on generating bispecific antibody as engager to facilitate T cells to tumor cells (Kimmtrak® and Blincyto®) or CAR T-cell therapy, and most of the scFv-based ADCs are still in pre-clinical research. Theoretically, using the scFv as backbone can be a promising way to overcome the limitations of full-length antibody-based ADCs. Therefore, this study investigated the potential of the scFv as vehicle or as target protein to deliver fluorescence or cytotoxic agent by either direct conjugation or pre-targeting system. The three core procedures of ADC antitumor mechanism were estimated: 1) the specific antigen binding ability of scFv was confirmed by both flow cytometry and fluorescence microscopy as fluorescence is only detected on antigen-expressing cell lines (**Figure 4.8-4.12**, **Figure 4.25-4.28**); 2) fast internalization of scFv-antigen complex was achieved within 3 h (**Figure 4.13-4.17**, **Figure 4.29-4.32**), evincing that scFv could efficiently deliver therapeutic agent into cells; 3) specific cell death was observed on ADC treated cells but not on naked antibody treated cells (**Figure 4.18**, **Figure 4.33**), indicating that the cytotoxicity was mainly from the MMAE, and the scFv-based ADCs were harmless to antigen-low cells which might reduce side effect caused by off-target effect.

5.1.3 MMAE with cleavable linker

Choosing a potent toxin and a suitable linker to help toxin exert maximum toxicity is of importance as the toxicity of ADC is mainly from payload at low therapeutic doses. MMAE is one of the derivatives of dolastatin 10 which exhibits no significant activity but its derivatives such as MMAE and MMAF are highly potent [46]. Although both MMAE and MMAF have been utilized in approved ADCs, MMAE is the most prevalent one. The MMAE (IC_{50}: 0.47-6.5 nM) is reported to be more toxic than MMAF (IC_{50}: 130 nM-2.7 μM) which may be due to the different ability to penetrate membrane [47, 174]. The MMAE is more permeable than MMAF, so a cleavable linker is preferred so as to exert bystander effect. With cleavable linker, MMAE is able to diffuse to extracellular environment after releasing from antibody. Thus, the free

MMAE can kill the adjacent cells by antigen-independent way. In contrast, non-cleavable linker exhibits higher stability in blood circulation as it relies on the antibody degradation by lysosomal processing to release payload in the target cells. Therefore, the drugs still contain some peptides or amino acids after antibody degradation, which impedes the bystander effect and also may affect the activity of drug [175]. For example, as aforementioned in introduction (**1.3.6.1**), T-DXd contains a cleavable linker and the DAR is approximately 8, while the T-DM1 is designed with uncleavable linker with approximately 3.5 molecules of DM1. Considering the heterogeneous environment of breast cancer with different levels of antigen expression and the membrane permeability of free DXd released by cleavable linker, the high DAR and the bystander effect might be one of the reasons to account for the higher efficacy achieved by T-DXd compared to T-DM1 [176].

The cleavable linker contains chemically cleavable linker (e.g., acid-cleavable linkers and reducible disulfides) and enzyme cleavable linker (e.g., dipeptide-containing linkers and glycosidase-cleavable linkers) [35]. In this work, the well-characterized MMAE with a cleavable linker containing protease-sensitive Val-Cit dipeptide, which is confirmed to have better human or mouse plasma stability than hydrazone-containing linker (acid-cleavable linker) and can also be cleaved in extracellular environment due to the overexpressed lysosomal enzymes, was included to extend the toxicity of the ADCs for the future *in vivo* experiment. In the current *in vitro* experiment, all breast cancer and ovarian cancer cell lines showed different levels of sensitivity to MMAE (**Figure 4.18**, **Figure 4.33**, **Table 4.2**, **Table 4.4**). In breast cancer cell lines, SKBR3 (IC_{50}: 38.65 nM) and MDA-MB-468 (IC_{50}: 60.78 nM) displayed the highest sensitivity, the MCF (IC_{50}: 599.5 nM) showed relatively low sensitivity, and the other cell lines MDA-MB-231, Hs578T, MDA-MB-453 and BT474) exhibited medium level (IC_{50}: 108.3-290.6 nM). Also, MMAE achieved potent cytotoxicity in all ovarian cancer cell lines (SKOV3, OVCAR3, A2780 and Hey) with IC_{50} range of 77.13-166 nM. In addition, this work elucidated that the cell death was driven by the released MMAE rather than the naked antibody as the naked scFv or pre-targeting complex engendered

no effect at least up to 640 nM. The apoptosis assay further proved the result (**Figure 4.19-4.23**, **Figure 4.34-4.37**). The Apoptosis or specific apoptosis was only observed on cells treated with MMAE or MMAE-based ADCs, consistent with previous studies which indicate that MMAE can trigger apoptosis to cause cell death [177, 178].

5.1.4 The site-specific conjugation using SNAP-tag technology

Since the approval of Mylotrag®, ADC has undergone three generations of upgrades. One of the biggest improvement during the development is the conjugation methods. While the first- and second-generation ADC mainly use random conjugation by lysines or reduced interchain cysteines, resulting in heterogeneous products, the third-generation ADC are more focusing on site-specific conjugation to generate homogeneous product with defined DAR [18]. Hitherto, many site-specific conjugation methods have been developed such as using engineered cysteine residues, unnatural amino acids, selenocysteine and enzymatic conjugation [123]. However, some methods still produce relatively heterogeneous ADCs (DAR: 2-4), need some complex steps like redox reaction or require additional materials to catalytic reactions, or consume excess amount of cytotoxic payload [123, 179-181]. While these methods may affect the activity of antibody or be laborious, the SNAP-tag technology, which is a kind of enzymatic method, provides a fast and economical approach to achieve site-specific conjugation. The SNAP-tag, as introduced before (**1.3.5**), is capable to specifically react with BG derivatives so as to produce homogeneous product.

In this work, scFv and Zip1 were genetically modified with SNAP-tag as conjugation site for cytotoxic agent. The SNAP-fusion proteins were successfully expressed by HEK293T cells. With the SNAP-tag, the rapid conjugation was achieved within 2 h with different BG-derivatives, and site-specific conjugation was confirmed by post-incubating SNAP-Surface® Alexa Fluor® 647 or BG-MMAE blocked SNAP-fusion proteins with SNAP-Surface® Alexa Fluor® 488 (**Figure 4.4b**, **Supplementary Figure 2**). The SDS gel visualization showed that once the conjugation site was blocked, BG-derivatives cannot conjugate with the SNAP-fusion proteins anymore. Apart from

saving the time, this technology allows the reaction to occur under physiological conditions ensuring the full activity of the proteins. The conjugation was carried out in PBS at room temperature with a two-fold molar of BG derivatives and the successful conjugation was observed.

The SNAP-tag technology allows to produce homogeneous product in a rapid and economical way. It extremely simplifies the conjugation step in lab and also shows potential to be used for manufacturing. Although the technology is only used to conjugated BG-modified fluorescent dye and MMAE in this study, it can be tagged to any antibody and even cell surface [182], and can react with more kinds of substrates as long as they are BG derivatives such as BG-biotin [183].

5.2 A coil coils-based pre-targeting drug delivery system

The pre-targeting strategy, which is developed from the radioimmunotherapy, requires the pre-localization of antibodies followed by the injection of radiolabeled effectors. This approach is now mainly studied in nuclear medicine, including nuclear imaging and nuclear therapy. The concept of conventional radioimmunotherapy is kind of like ADC, which links mAb with a radioactive substance instead of cytotoxic agent. There are two radiolabeled anti-CD20 mAbs (Bexxar® and Zevalin®) have been approved by FDA for non-Hodgkin lymphoma treatment. However, in the same situation as ADC, the big size of the full-length antibody impedes the rapid accumulation in target site due to the long half-life and poor tissue penetration ability. To circumvent this problem, some studies also engineer small antibody fragments such as Fab and scFv to bear radionuclides [184, 185]. Additionally, to be sure that the radionuclides are still active enough to kill cells after days or even weeks in blood circulation, radionuclides with long half-lives are also required. Some long-lived radionuclides such as ^{89}Zr, ^{124}I and ^{177}Lu have been developed, of whom the half-lives are around 3.3 days, 4 days and 6.7 days, respectively [186, 187]. But every coin has two sides. While the radioactivity is ensured, the healthy cells under exposure are at risk. Thus, the concept of pre-targeting strategy emerges as a promising way. The approach allows the combination of

antibodies and complementary radiolabeled effectors in the tumor site after the sequential administration [188]. Once the antibodies have reached desired biodistribution in the tumor site, the radiolabeled effector molecules can rapidly penetrate the tissue to bind the antibodies and the excess small molecules will be fast cleared from blood circulation. This concept extremely increases the tumor/nontumor ratio of the effector molecules and also allows the use of radionuclides with short half-lives.

Therefore, the problem has switched to find an ideal strategy to achieve the combination of antibodies and radioactive molecules *in vivo*. To date, there are four major bioconjugation methodology harnessed: 1) streptavidin and biotin; 2) bispecific antibodies targeting both tumor associated antigens and radiolabeled haptens; 3) oligonucleotides; 4) click chemistry [186]. The advantages and limitations of each approach have been extensively discussed, but it is difficult to define which is the optimal solution due to the lack of head-to-head competition [186, 189]. In view of the fact that ADC and radioimmunotherapy have the similar concern on long blood circulation and off-target effect, as discussed before, the pre-targeting concept has already moved from radioimmunotherapy to other field such as drug delivery based on these developed bioconjugation approaches [190, 191]. This work introduced a novel binding strategy using coiled coils to achieve the two-step drug delivery process, and the function of the system was fully studied *in vitro*.

5.2.1 The coiled coil can mediate specific interaction between targeting protein and vehicle protein

After Reinke *et al.* introduced 23 heteroassociating synthetic coiled coils in 2010 [107], Thompson *et al.* further studied the biological properties of 14 synthetic Zips and 32 pairs of coiled coil in Reinke's work [105]. In light of Thompson's work, 22 pairs of Zips have relatively strong interaction with low dissociation constant (less than 10), among which some Zips (14, 16, 20 and 21) show homodimers [105]. To avoid the self-interaction of the coiled coil, the coiled coil pairs with these four Zips were filtered out.

After the preliminary screening, five coiled coil pairs (1+2, 2+19, 6+19, 11+19 and 18+19) were deemed to be candidates for the pre-targeting system. However, the yeast two-hybrid assay conducted by Thompson *et al.* demonstrates three autoactivating DNA-binding domain fusions (Zips, 4, 11, and 18) without its partner for some unexplained reasons [105], so 11+19 and 18+19 were also excluded. Among these three remained pairs, the Zip1 and Zip2 pair is the most detailed one in previous work, which is proved to form parallel, dimeric coiled coils with melting temperature at 47°C [105, 107].

Therefore, Zip1 and Zip2 with high specificity and affinity was selected as the first try to establish the pre-targeting drug delivery system. The Zip2 was genetically modified to EGFR-, EpCAM-, Her2- and Trop2-specific scFvs, while Zip1 was modified with SNAP-tag to allow the conjugation with BG derivatives. To estimate the potential of Zip1 and Zip2 to conduct the combination of targeting molecules and effector molecules, far-western blotting was conducted to confirm the specific binding between Zip1 and Zip2. Obviously, the specific interaction between Zip1 and Zip2 was still maintained after fusing it to scFvs or SNAP-tag as all Zip2-labeled antibodies were detected by Zip1-SNAP-488 in PVDF membrane except the scFv-Erbitux-SNAP, which was set as negative control (**Figure 4.5**). In addition, the binding property of Zip2 to Zip1 was not affected by being labeled to different antibodies. Compared to direct conjugation, the pre-targeting drug delivery system also simplifies the generation of ADC, which means that this two-step system has no need to repeat conjugation step if the target antigen is switched as the payload is conjugated to the vehicle protein instead of the targeting protein.

5.2.2 The specific delivery property of pre-targeting system

Delivering the drugs to the targeted tumor site is a pivotal step of achieving targeting therapy, which is also the main difference between pre-targeting drug delivery system and directly conjugated ADCs. With the aim of illustrating the potential of the coiled coil-mediated drug delivery to be used in pre-targeting therapy, scFv-SNAP, Zip1-

SNAP and scFv-Zip2 were conjugated with fluorescent dyes instead of MMAE to visualize the binding and internalization processes of the pre-targeting complex and compare its specificity and sensitivity with direct conjugation.

Some studies have calculated that only 1.56% of the administered cytotoxic agent can finally reach the tumor site if each step of ADC mechanism (accumulation in tumor site, binding to the target, ADC-antigen complex internalization, drug releasing and drug reaching the target) achieves 50% efficiency [44]. In fact, the efficiency is even much lower in practical implementation due to various factors [31]. In the pre-targeting therapy, even though the reduced size of targeting proteins in this study were supposed to increase the accumulation efficiency, the additional binding step might lose efficiency to some degree. Fortunately, the specific targeting property in all pre-targeting complexes and the comparable fluorescence activity between pre-targeting complexes and directly conjugated antibodies in breast and ovarian cancer cell lines were confirmed by flow cytometry, demonstrating the efficient binding between scFv-Zip2 and Zip1-647 (**Figure 4.8a-4.12a**, **Figure 4.25a-4.28a**). The similar result was also observed in colocalization analysis by fluorescence microscopy. The experiment was conducted at 4°C to reduce the cellular internalization processes. While both scFv-Zip2-SNAP-488 and Zip1-647 were detected on the cell membrane (**Figure 4.8b-4.12b**, **Figure 4.25b-4.28b**) which were expressing targeting antigens, Zip1-647 did not show any binding to tested cells without the pre-incubation with scFv-Zip2-488, indicating that the detected red-647 signal was entirely from the complex rather than unspecific binding. However, the EGFR- and Her2-targeting pre-targeting complexes showed binding to BT474 and Hey in flow cytometry but none or very weak in fluorescence microscopy. Considering the scFv-425-647, scFv-Erbitux-647 and scFv-Her2-647 also exhibited none or weak binding in fluorescence microscopy, this was more likely due to the different sensitivity of methods rather than the loss of binding efficiency. In the antigen-expressing cell lines, the colocalization was better presented by tracing the intensity of the fluorescence (**Figure 4.8c-4.12c**, **Figure 4.25c-4.28c**). The Zip1-647 showed good overall agreement with scFv-Zip2-488, and the intensity of Zip1-647 was

generally higher than scFv-Zip2-488 as the Alexa Fluor® 647 usually is brighter than Alexa Fluor® 488. In some cases, the scFv-Zip2-488 showed more rapid or gentle change of intensity than Zip1-647 such as SKBR3 in **figure 4.11c** and MDA-MB-231 in **figure 4.8c,** or sometimes stronger intensity than Zip1-647 such as OVCAR3 in **figure 4.28c**. This might be caused by the random conjugation of scFv-Zip2 with fluorescence using the lysine side chains of antibody, leading to heterogeneous mixture with different fluorescence intensity of each molecule.

After showing the membrane localization of the pre-targeting complex, exploring its internalization property is essential to estimate the efficacy of an ADC as the targets chosen in this study are all depending on intracellular trafficking and processing to release the drug. Cells were incubated at 37°C instead of 4°C to retain the cellular uptake activity. In contrast with colocalization analysis, more punctiform signals were observed in cytoplasm (**Figure 4.13-4.17**, **Figure 4.29-4.32**) after 3h. While the colocalization at 4°C showed great merged signal of scFv-Zip2-488 and Zip1-647, the gree-488 and red-647 detected in cytoplasm at 37°C were sometimes separated on the ground that some 647 molecules have already been cleaved. Even though all the pre-targeting complexes showed internalization within 3 h, the internalization speed varied, depending on the antigen target, the antibody and cell line itself [192]. For example, EGFR-targeting ADCs were relatively fast internalized, while Her2-specific complex was less internalized into cells within 3 h (**Figure 4.13**, **4.14** and **4.16**). In consistent with this result, studies have reported that the internalization of Ab033 (anti-EGFR antibody) is detected after 1 h in A431 and H441 cell lines [193]. Also, almost 20-30% of cetuximab is internalized in SW1573 and H292 cell lines within 1 h and the rate increases only around 10% for another three-hour incubation [194]. However, the trastuzumab just starts to be internalized after 4h in SKBR3, BT474 and MDA-MB-453, and so does T-DM1 in BT474 and MDA-MB-453 [195, 196].

Overall, this coiled coil-based pre-targeting system could specifically deliver the payload to the target cells and be internalized into cells as required by the classical mechanism of ADC.

5.2.3 The specific cytotoxicity of pre-targeting system

The ADC widens the scope of mAb-based targeting therapy by endowing mAb with cytotoxic agent while retaining its specificity. Some small molecules such as DM1 and MMAE (IC_{50}: 10^{-11} and 10^{-9} M) are too toxic to be used in chemotherapy [197, 198]. Loading these toxic molecules to mAbs definitely increases the maximum tolerated dose. Meanwhile, the ADC also reduces the minimum effective dose of the mAb. For example, while the standard dose of trastuzumab for Her2-overexpressing breast cancer as adjuvant treatment is 4 or 8 mg/kg as initial dose followed by 6 or 2 mg/kg weekly for 52 weeks, the standard dose of its ADC (T-DM1) is 3.6 mg/kg every 3 weeks (prescribing information from FDA). As the pre-targeting system has been confirmed to have comparable binding and internalization property with directly conjugated ADCs in this study, the specific cytotoxicity was further validated (**Figure 4.18**, **Figure 4.33**, **Table 4.2**, **Table 4.4**). The scFvs were labeled with fluorescent dyes instead of cytotoxic agent to visualize the binding and internalization. Although there was a possibility that conjugating with different molecules might change the protein property, it was more inclined that these properties would be retained after conjugation with BG-MMAE and the specific toxicity observed also proved the scenario.

The free drug inhibited the cell proliferation in all cell lines in the nanomolar range as expected. Once the MMAE was tethered to scFv-SNAP or Zip1-SNAP, both directly conjugated ADC and pre-targeting complex showed specific cytotoxicity in EGFR-, EpCAM-, Her2- and Trop2-expressing cell lines. The toxicity of ADCs varies (**Table 4.2**, **Table 4.4**) in different cell lines or using different antibody for several reasons. First of all, cell lines have different sensitivity to MMAE, for example, MCF7 showed relatively low sensitivity to MMAE, so the EpCAM- and Trop2-based ADCs also exhibited weak cytotoxicity in MCF7 even it expressed EpCAM and Trop2. Secondly, cell lines express different amounts of antigens. For instance, while the MDA-MB-468 expresses 1.9×10^6 EGFR per cell, the MCF7 only expresses about 10^4 EGFR per cell [199, 200]. Also, the SKBR3 expresses 1.26×10^6 Her2 per cell but only expresses 2.2×10^5 EGFR per cell [201, 202]. Thus, the ADCs showed different efficacy in different

cell lines and also the cell viability was consequentially inhibited to different extent. Thirdly, the high turnover rate of the antigen can increase the ADC efficacy by increasing the internalization [203]. Last, for some unknown reason, the ADC can achieve extremely potent toxicity in specific cell lines. The scFv-Herceptin-MMAE exhibited superior activity in SKBR3 with 19 times lower IC_{50} than free MMAE. This phenomenon is also noticed in other studies. Gail *et al.* have revealed that once the DM1 is conjugated to trastuzumab, its IC_{50} is about 5 times lower than free DM1 [204]. However, this special issue was not observed when using pre-targeting complex to deliver MMAE, indicating that this system could have more universal mechanism of action.

Moreover, compared to the directly conjugated scFvs, the pre-targeting system showed relatively lower toxicity due to the additional binding step. Even though the flow cytometry and fluorescence microscopy confirmed the high efficiency of the interaction between Zip1 and Zip2, there is no doubt that any additional step will influence the efficacy of ADC. However, most of the complexes still exhibited the IC_{50} in the nanomolar range, and the main purpose of the pre-targeting system was to accelerate the accumulation and reduce off-target effect. As discussed before, the full-length antibody has long circulation time, so it is more likely to bind healthy tissue. For example, the major side effect of EGFR-targeting therapy such as cetuximab is skin toxicity as the skin tissues also widely express EGFR [205, 206]. This study introduced the small antibody fragment scFv instead of full-length antibody to accelerate accumulation in cancerous tissue and shorten its circulation in blood. The drug delivery vehicle Zip1-SNAP was only about 32 kDa, which further reduced the exposure of healthy cells to drug. The limited cytotoxicity of Zip1-MMAE without scFv-Zip2 confirmed the safety of this system.

With the fast development of the ADC, there are innumerable new reported ADC models. The efficacy of ADCs varies in studies due to the different cell lines, conjugation methods, targets, payloads, DAR and incubation time, leading to a wide range of IC_{50} from subnanomolar to nanomolar [207-209]. This pre-targeting system,

in most cases, has lower toxicity than these ADC models, but the efficacy was influenced by many factors. The pre-targeting complex generated here was a 1:1 conjugation method, while most ADC models are with a DAR around 2-8. Study has revealed that the toxicity of ADC increases with increasing DAR *in vitro*, but the mAb with two MMAE molecules exhibits the best response after doubling the dose to reach an equal amount of mAb with 4 or 8 molecules of MMAE *in vivo* [210]. Researchers also indicate that the high DAR may result in fast clearance due to the increased hydrophobicity [211]. Considering that Zip1-SNAP was a small molecule, increasing the DAR would further accelerate the clearance, which might be actually adverse. Furthermore, the scFv has lower affinity than intact antibody since it only contains one antigen-binding fragment rather than two in its parental antibody, which may also be one of the reasons for the lower cytotoxicity. Misfortune might be a blessing in disguise. Antibodies have high affinity can be trapped in the tumor surface or around the blood vessel but less penetrate to the deep-seated tumor cells or tumor far away from the vessels [18].

This study confirmed the specific toxicity of the pre-targeting system, with minimal effect by the Zip1-MMAE and stable mechanism of action. Even though the cytotoxicity was relatively compromised but still comparable with directly conjugated ADCs, the system was supposed to reduce the side effect and target deep part of the tumor. Further work needs to be performed *in vivo* to confirm the therapeutic and safety properties of this pre-targeting approach.

6. Summary

The target therapy has ushered in a new generation of cancer treatment, but it still confronts to some limitations, for example, most of the mAbs lack enough cytotoxicity to be translated into clinical fruition. The ADC comes of age as a novel and promising antineoplastic therapy on the grounds that it combines the specificity of mAb and potent toxicity of small molecules. As the cytotoxicity of ADCs mainly comes from the payload rather than mAb, it allows more mAbs to be applied into target therapy and also endows the possibility of these small molecules to be used in patients. Although the approved ADCs have achieved tremendous success in clinical outcomes, still there are obstacles such as the low accumulation in tumor site, off-target cytotoxicity and heterogeneous products after conjugation. To overcome these problems and optimize the ADC design, a pre-targeting drug delivery system was established in this study.

The pre-targeting system is based on the specific interaction between a pair of synthetic coiled coils proteins named Zip1 and Zip2. Compared to the conventional drug delivery system, the two-step drug delivery approach, first, is designed to reduce the size of the antibody to improve the tissue penetration so the antibodies are more likely to reach the deep-seated tumor. Second, in virtue of the small size of the Zip1-labeled effector molecule, the pre-targeting system is supposed to accelerate the accumulation of drug in the target site and increase the tumor/nontumor ratio of drug by fast clearance of the excess effector molecules in the circulation. Additionally, a site-specific conjugation method using the SNAP-tag was introduced to achieve effortless and rapid labelling and also to produce homogeneous product. To evaluate the potential of the pre-targeting system for drug delivery, functional assays were carried out. The specific interaction between the Zip1 and Zip2 was confirmed by far-western blotting, and the EGFR-, EpCAM-, Her2- and Trop2-specific pre-targeting complex exhibited the rapid and high specific drug or fluorescence delivery ability as well as the comparable cytotoxicity with direct conjugation in breast cancer and ovarian cancer cell lines. However, the *in vivo* experiment which is not involved in this study should be further performed to assess the therapeutic and safety property and *in vivo* efficacy.

In conclusion, this study firstly demonstrated the pre-targeting drug delivery system using scFv, SNAP-tag technology and interaction between coiled coils. Even though this pre-targeting drug delivery system was just assessed in breast and ovarian cancers, the application is never limited in these four antigens or in these two cancer types. This novel drug delivery system can be broadened to treat various types of cancers, target suitable tumor associated antigens and bearing different BG-modified drugs.

7. Zusammenfassung

Obwohl die zielgerichtete Therapie eine neue Generation der Krebs-Behandlung einleitet, gibt es immer noch einigen Grenzen, die es zu überwinden gilt. Zum Beispiel, dass den meisten monoklonalen Antikörper (mAbs) die nötige Zytotoxizität fehlt, um einen klinischen Einsatz zu ermöglichen. Mit Medikamenten konjugierte Antikörper (ADC) stellen eine neue und vielversprechende antineoplastische Therapieoption da, indem die spezifische Bindung der mAbs genutzt und mit der potenten, zytotoxischen Wirkung kleiner Moleküle kombiniert wird. Da die zytotoxische Wirkung der ADCs hauptsächlich von ihrer gebundenen Ladung kommt, ermöglichen diese den Einsatz von mehr mAbs und ebenfalls potenteren kleinen Molekülen für die Anwendung an Patienten. Obwohl ADCs schon in klinischen Studien erfolgreich getestet wurden, gibt es auch hier noch einige Hindernisse zu überwinden, wie zum Beispiel eine schlechte Akkumulation in Tumorgewebe, die Off-target-Zytotoxizität und unterschiedliche Verhältnisse von Antikörper zu Medikament nach Konjugation. Um diese Hürden zu überwinden und die ADC zu optimieren, entwickelten wir eine zweizeitiges System zur Applikation von Medikamenten.

In dieser Studie basiert das Vorauswahlsystem auf der spezifischen Bindung der Doppelwindungsproteinen Zip1 und Zip2. Verglichen mit den konventionellen Systemen zur Applikation von Medikamenten verfolgt der Zwei-Schritt-Ansatz zwei Ziele: (a) Die Größe der Antikörper zu reduzieren, um so die Gewebepenetranz zu erhöhen, damit die Antikörper auch tiefere Tumorzellen erreichen können und (b) die Beschleunigung der Akkumulation im Zielgewebe zur Erhöhung des Verhältnisses der Medikamentenbindung von Tumor zu Nichttumor, um überschüssigen Effektor Molekülen im Blutstrom schneller zu beseitigen. Zusätzlich stellen wir eine ortsspezifische Konjugationsmethode vor, die die SNAP-tag benutzt um eine reibungslose und schnelle Konjugation zu ermöglichen und außerdem ein homogenes Produkt zu erzeugen. Um die Effektivität der zweizeitiges Systems zur Medikamenten-Applikation zu testen, wurden Funktions-Assays durchgeführt. Die spezifische Interaktion zwischen Zip1 und Zip2 wurde mittels Western Blot verifiziert und

exemplarisch mittels EGFR-, EpCAM-, HER2- und Trop2-spezifischen zweizeitigen Applikations-Systemen angewendet. Es zeigte sich eine hochspezifische Abgabe von Medikamenten oder Fluoreszenz; auch die Zytotoxizität war mit direkter Konjugation vergleichbar. Allerdings muss noch in einer künftigen *in vivo* Studie, gezeigt werden, dass die Methode *in vivo* ebenso effektiv funktioniert und die nötigen Sicherheitsbestimmungen erfüllt.

Zusammengefasst zeigen wir erstmalig ein zweizeitiges System zur Applikation von Medikamenten unter Verwendung von scFv, SNAP-tag-Technologie und der Interaktion zwischen Doppelwindungsproteinen.

Obwohl das zweizeitige System nur an Brust- und Eierstockkrebszellen getestet wurde, könnte diese neue Methode in verschiedensten Arten von Krebs Anwendung finden.

8. References

1. Coffey, J.C., et al., *Excisional surgery for cancer cure: therapy at a cost.* Lancet Oncol, 2003. **4**(12): p. 760-8.
2. Wang, M., et al., *Neoadjuvant Chemotherapy Creates Surgery Opportunities For Inoperable Locally Advanced Breast Cancer.* Sci Rep, 2017. **7**: p. 44673.
3. Damen, M.P.F., J. van Rheenen, and C. Scheele, *Targeting dormant tumor cells to prevent cancer recurrence.* FEBS J, 2021. **288**(21): p. 6286-6303.
4. Altun, I. and A. Sonkaya, *The Most Common Side Effects Experienced by Patients Were Receiving First Cycle of Chemotherapy.* Iran J Public Health, 2018. **47**(8): p. 1218-1219.
5. Epstein, R.S., et al., *Patient Burden and Real-World Management of Chemotherapy-Induced Myelosuppression: Results from an Online Survey of Patients with Solid Tumors.* Adv Ther, 2020. **37**(8): p. 3606-3618.
6. Strebhardt, K. and A. Ullrich, *Paul Ehrlich's magic bullet concept: 100 years of progress.* Nat Rev Cancer, 2008. **8**(6): p. 473-80.
7. Yan, L., N. Rosen, and C. Arteaga, *Targeted cancer therapies.* Chin J Cancer, 2011. **30**(1): p. 1-4.
8. Bedard, P.L., et al., *Small molecules, big impact: 20 years of targeted therapy in oncology.* Lancet, 2020. **395**(10229): p. 1078-1088.
9. An, S. and L. Fu, *Small-molecule PROTACs: An emerging and promising approach for the development of targeted therapy drugs.* EBioMedicine, 2018. **36**: p. 553-562.
10. Zhong, L., et al., *Small molecules in targeted cancer therapy: advances, challenges, and future perspectives.* Signal Transduct Target Ther, 2021. **6**(1): p. 201.
11. Kohler, G. and C. Milstein, *Continuous cultures of fused cells secreting antibody of predefined specificity.* Nature, 1975. **256**(5517): p. 495-7.
12. Geskin, L.J., *Monoclonal Antibodies.* Dermatol Clin, 2015. **33**(4): p. 777-86.
13. Weiner, G.J., *Building better monoclonal antibody-based therapeutics.* Nat Rev Cancer, 2015. **15**(6): p. 361-70.
14. Mullard, A., *FDA approves 100th monoclonal antibody product.* Nat Rev Drug Discov, 2021. **20**(7): p. 491-495.
15. Li, Z., et al., *Influence of molecular size on tissue distribution of antibody fragments.* MAbs, 2016. **8**(1): p. 113-9.
16. Slastnikova, T.A., et al., *Targeted Intracellular Delivery of Antibodies: The State of the Art.* Front Pharmacol, 2018. **9**: p. 1208.
17. Marei, H.E., C. Cenciarelli, and A. Hasan, *Potential of antibody-drug conjugates (ADCs) for cancer therapy.* Cancer Cell Int, 2022. **22**(1): p. 255.
18. Fu, Z., et al., *Antibody drug conjugate: the "biological missile" for targeted cancer therapy.* Signal Transduct Target Ther, 2022. **7**(1): p. 93.
19. Li, W.Q., et al., *The promising role of antibody drug conjugate in cancer therapy: Combining targeting ability with cytotoxicity effectively.* Cancer Med, 2021. **10**(14): p. 4677-4696.
20. Abdollahpour-Alitappeh, M., et al., *Antibody-drug conjugates (ADCs) for cancer therapy: Strategies, challenges, and successes.* J Cell Physiol, 2019. **234**(5): p. 5628-5642.
21. Chau, C.H., P.S. Steeg, and W.D. Figg, *Antibody-drug conjugates for cancer.* Lancet, 2019.

394(10200): p. 793-804.

22. Diamantis, N. and U. Banerji, *Antibody-drug conjugates--an emerging class of cancer treatment.* Br J Cancer, 2016. **114**(4): p. 362-7.
23. Hafeez, U., et al., *Antibody-Drug Conjugates for Cancer Therapy.* Molecules, 2020. **25**(20).
24. Esapa, B., et al., *Target Antigen Attributes and Their Contributions to Clinically Approved Antibody-Drug Conjugates (ADCs) in Haematopoietic and Solid Cancers.* Cancers (Basel), 2023. **15**(6).
25. Casi, G. and D. Neri, *Noninternalizing targeted cytotoxics for cancer therapy.* Mol Pharm, 2015. **12**(6): p. 1880-4.
26. Hoffman, W., F.G. Lakkis, and G. Chalasani, *B Cells, Antibodies, and More.* Clin J Am Soc Nephrol, 2016. **11**(1): p. 137-54.
27. Baah, S., M. Laws, and K.M. Rahman, *Antibody-Drug Conjugates-A Tutorial Review.* Molecules, 2021. **26**(10).
28. Khongorzul, P., et al., *Antibody-Drug Conjugates: A Comprehensive Review.* Mol Cancer Res, 2020. **18**(1): p. 3-19.
29. Sau, S., et al., *Advances in antibody-drug conjugates: A new era of targeted cancer therapy.* Drug Discov Today, 2017. **22**(10): p. 1547-1556.
30. Hock, M.B., et al., *Immunogenicity of antibody drug conjugates: bioanalytical methods and monitoring strategy for a novel therapeutic modality.* AAPS J, 2015. **17**(1): p. 35-43.
31. Drago, J.Z., S. Modi, and S. Chandarlapaty, *Unlocking the potential of antibody-drug conjugates for cancer therapy.* Nat Rev Clin Oncol, 2021. **18**(6): p. 327-344.
32. Richards, D.A., *Exploring alternative antibody scaffolds: Antibody fragments and antibody mimics for targeted drug delivery.* Drug Discov Today Technol, 2018. **30**: p. 35-46.
33. Tsuchikama, K. and Z. An, *Antibody-drug conjugates: recent advances in conjugation and linker chemistries.* Protein Cell, 2018. **9**(1): p. 33-46.
34. Jain, N., et al., *Current ADC Linker Chemistry.* Pharm Res, 2015. **32**(11): p. 3526-40.
35. Bargh, J.D., et al., *Cleavable linkers in antibody-drug conjugates.* Chem Soc Rev, 2019. **48**(16): p. 4361-4374.
36. McCombs, J.R. and S.C. Owen, *Antibody drug conjugates: design and selection of linker, payload and conjugation chemistry.* AAPS J, 2015. **17**(2): p. 339-51.
37. Tong, J.T.W., et al., *An Insight into FDA Approved Antibody-Drug Conjugates for Cancer Therapy.* Molecules, 2021. **26**(19).
38. Dal Corso, A., et al., *Protease-Cleavable Linkers Modulate the Anticancer Activity of Noninternalizing Antibody-Drug Conjugates.* Bioconjug Chem, 2017. **28**(7): p. 1826-1833.
39. Gebleux, R., et al., *Non-internalizing antibody-drug conjugates display potent anti-cancer activity upon proteolytic release of monomethyl auristatin E in the subendothelial extracellular matrix.* Int J Cancer, 2017. **140**(7): p. 1670-1679.
40. Staudacher, A.H. and M.P. Brown, *Antibody drug conjugates and bystander killing: is antigen-dependent internalisation required?* Br J Cancer, 2017. **117**(12): p. 1736-1742.
41. Kovtun, Y.V., et al., *Antibody-drug conjugates designed to eradicate tumors with homogeneous and heterogeneous expression of the target antigen.* Cancer Res, 2006. **66**(6): p. 3214-21.
42. Sheyi, R., B.G. de la Torre, and F. Albericio, *Linkers: An Assurance for Controlled Delivery of Antibody-Drug Conjugate.* Pharmaceutics, 2022. **14**(2).

43. Nasiri, H., et al., *Antibody-drug conjugates: Promising and efficient tools for targeted cancer therapy.* J Cell Physiol, 2018. **233**(9): p. 6441-6457.
44. Teicher, B.A. and R.V. Chari, *Antibody conjugate therapeutics: challenges and potential.* Clin Cancer Res, 2011. **17**(20): p. 6389-97.
45. Chari, R.V., *Targeted cancer therapy: conferring specificity to cytotoxic drugs.* Acc Chem Res, 2008. **41**(1): p. 98-107.
46. Akaiwa, M., J. Dugal-Tessier, and B.A. Mendelsohn, *Antibody-Drug Conjugate Payloads; Study of Auristatin Derivatives.* Chem Pharm Bull (Tokyo), 2020. **68**(3): p. 201-211.
47. Birrer, M.J., et al., *Antibody-Drug Conjugate-Based Therapeutics: State of the Science.* J Natl Cancer Inst, 2019. **111**(6): p. 538-549.
48. Kupchan, S.M., et al., *Maytansine, a novel antileukemic ansa macrolide from Maytenus ovatus.* J Am Chem Soc, 1972. **94**(4): p. 1354-6.
49. Kupchan, S.M., et al., *The maytansinoids. Isolation, structural elucidation, and chemical interrelation of novel ansa macrolides.* J Org Chem, 1977. **42**(14): p. 2349-57.
50. Chen, H., et al., *Tubulin Inhibitor-Based Antibody-Drug Conjugates for Cancer Therapy.* Molecules, 2017. **22**(8).
51. Appelbaum, F.R. and I.D. Bernstein, *Gemtuzumab ozogamicin for acute myeloid leukemia.* Blood, 2017. **130**(22): p. 2373-2376.
52. Dahl, J., K. Marx, and E. Jabbour, *Inotuzumab ozogamicin in the treatment of acute lymphoblastic leukemia.* Expert Rev Hematol, 2016. **9**(4): p. 329-34.
53. Damle, N.K., *Tumour-targeted chemotherapy with immunoconjugates of calicheamicin.* Expert Opin Biol Ther, 2004. **4**(9): p. 1445-52.
54. Hartley, J.A., et al., *Pre-clinical pharmacology and mechanism of action of SG3199, the pyrrolobenzodiazepine (PBD) dimer warhead component of antibody-drug conjugate (ADC) payload tesirine.* Sci Rep, 2018. **8**(1): p. 10479.
55. Calabretta, E., et al., *The antibody-drug conjugate loncastuximab tesirine for the treatment of diffuse large B-cell lymphoma.* Blood, 2022. **140**(4): p. 303-308.
56. Okamoto, H., et al., *Pharmacokinetics of trastuzumab deruxtecan (T-DXd), a novel anti-HER2 antibody-drug conjugate, in HER2-positive tumour-bearing mice.* Xenobiotica, 2020. **50**(10): p. 1242-1250.
57. Conilh, L., et al., *Payload diversification: a key step in the development of antibody-drug conjugates.* J Hematol Oncol, 2023. **16**(1): p. 3.
58. Yao, H., et al., *Methods to Design and Synthesize Antibody-Drug Conjugates (ADCs).* Int J Mol Sci, 2016. **17**(2).
59. Haque, M., N. Forte, and J.R. Baker, *Site-selective lysine conjugation methods and applications towards antibody-drug conjugates.* Chem Commun (Camb), 2021. **57**(82): p. 10689-10702.
60. Hamann, P.R., et al., *Gemtuzumab ozogamicin, a potent and selective anti-CD33 antibody-calicheamicin conjugate for treatment of acute myeloid leukemia.* Bioconjug Chem, 2002. **13**(1): p. 47-58.
61. Vollmar, B.S., et al., *Calicheamicin Antibody-Drug Conjugates with Improved Properties.* Mol Cancer Ther, 2021. **20**(6): p. 1112-1120.
62. Jackson, D.Y., *Processes for Constructing Homogeneous Antibody Drug Conjugates.* Organic Process Research & Development, 2016. **20**(5): p. 852-866.

63. Kline, T., et al., *Methods to Make Homogenous Antibody Drug Conjugates.* Pharm Res, 2015. **32**(11): p. 3480-93.
64. Kolberg, K., et al., *SNAP-tag technology: a general introduction.* Curr Pharm Des, 2013. **19**(30): p. 5406-13.
65. Hussain, A.F., et al., *One-step site-specific antibody fragment auto-conjugation using SNAP-tag technology.* Nat Protoc, 2019. **14**(11): p. 3101-3125.
66. Dreyer, R., et al., *The Evolution of SNAP-Tag Labels.* Biomacromolecules, 2023. **24**(2): p. 517-530.
67. Bojkowska, K., et al., *Measuring in vivo protein half-life.* Chem Biol, 2011. **18**(6): p. 805-15.
68. Bosch, P.J., et al., *Evaluation of fluorophores to label SNAP-tag fused proteins for multicolor single-molecule tracking microscopy in live cells.* Biophys J, 2014. **107**(4): p. 803-14.
69. Zhang, X., et al., *Novel development strategies and challenges for anti-Her2 antibody-drug conjugates.* Antib Ther, 2022. **5**(1): p. 18-29.
70. Dan, N., et al., *Antibody-Drug Conjugates for Cancer Therapy: Chemistry to Clinical Implications.* Pharmaceuticals (Basel), 2018. **11**(2).
71. Nervig, C.S. and S.C. Owen, *Affinity-bound antibody-drug conjugates.* Nat Biomed Eng, 2019. **3**(11): p. 850-851.
72. Sung, H., et al., *Global Cancer Statistics 2020: GLOBOCAN Estimates of Incidence and Mortality Worldwide for 36 Cancers in 185 Countries.* CA Cancer J Clin, 2021. **71**(3): p. 209-249.
73. Perou, C.M., et al., *Molecular portraits of human breast tumours.* Nature, 2000. **406**(6797): p. 747-52.
74. Sorlie, T., et al., *Gene expression patterns of breast carcinomas distinguish tumor subclasses with clinical implications.* Proc Natl Acad Sci U S A, 2001. **98**(19): p. 10869-74.
75. Yersal, O. and S. Barutca, *Biological subtypes of breast cancer: Prognostic and therapeutic implications.* World J Clin Oncol, 2014. **5**(3): p. 412-24.
76. Garrido-Castro, A.C., N.U. Lin, and K. Polyak, *Insights into Molecular Classifications of Triple-Negative Breast Cancer: Improving Patient Selection for Treatment.* Cancer Discov, 2019. **9**(2): p. 176-198.
77. Foulkes, W.D., I.E. Smith, and J.S. Reis-Filho, *Triple-negative breast cancer.* N Engl J Med, 2010. **363**(20): p. 1938-48.
78. Bando, Y., et al., *Triple-negative breast cancer and basal-like subtype : Pathology and targeted therapy.* J Med Invest, 2021. **68**(3.4): p. 213-219.
79. Chen, L., et al., *In-depth structural characterization of Kadcyla(R) (ado-trastuzumab emtansine) and its biosimilar candidate.* MAbs, 2016. **8**(7): p. 1210-1223.
80. Verma, S., et al., *Trastuzumab emtansine for HER2-positive advanced breast cancer.* N Engl J Med, 2012. **367**(19): p. 1783-91.
81. von Minckwitz, G., et al., *Trastuzumab Emtansine for Residual Invasive HER2-Positive Breast Cancer.* N Engl J Med, 2019. **380**(7): p. 617-628.
82. Modi, S., et al., *Trastuzumab Deruxtecan in Previously Treated HER2-Positive Breast Cancer.* N Engl J Med, 2020. **382**(7): p. 610-621.
83. Modi, S., et al., *Trastuzumab Deruxtecan in Previously Treated HER2-Low Advanced Breast*

Cancer. N Engl J Med, 2022. **387**(1): p. 9-20.

84. Hurvitz, S.A., et al., *Trastuzumab deruxtecan versus trastuzumab emtansine in patients with HER2-positive metastatic breast cancer: updated results from DESTINY-Breast03, a randomised, open-label, phase 3 trial.* Lancet, 2023. **401**(10371): p. 105-117.
85. Cortes, J., et al., *Trastuzumab Deruxtecan versus Trastuzumab Emtansine for Breast Cancer.* N Engl J Med, 2022. **386**(12): p. 1143-1154.
86. Muhlmann, G., et al., *TROP2 expression as prognostic marker for gastric carcinoma.* J Clin Pathol, 2009. **62**(2): p. 152-8.
87. Fang, Y.J., et al., *Elevated expressions of MMP7, TROP2, and survivin are associated with survival, disease recurrence, and liver metastasis of colon cancer.* Int J Colorectal Dis, 2009. **24**(8): p. 875-84.
88. Liu, T., et al., *Overexpression of TROP2 predicts poor prognosis of patients with cervical cancer and promotes the proliferation and invasion of cervical cancer cells by regulating ERK signaling pathway.* PLoS One, 2013. **8**(9): p. e75864.
89. Aslan, M., et al., *Oncogene-mediated metabolic gene signature predicts breast cancer outcome.* NPJ Breast Cancer, 2021. **7**(1): p. 141.
90. Syed, Y.Y., *Sacituzumab Govitecan: First Approval.* Drugs, 2020. **80**(10): p. 1019-1025.
91. Bardia, A., et al., *Sacituzumab Govitecan in Metastatic Triple-Negative Breast Cancer.* N Engl J Med, 2021. **384**(16): p. 1529-1541.
92. Rugo, H.S., et al., *Sacituzumab Govitecan in Hormone Receptor-Positive/Human Epidermal Growth Factor Receptor 2-Negative Metastatic Breast Cancer.* J Clin Oncol, 2022. **40**(29): p. 3365-3376.
93. Berek, J.S., et al., *Cancer of the ovary, fallopian tube, and peritoneum: 2021 update.* Int J Gynaecol Obstet, 2021. **155 Suppl 1**(Suppl 1): p. 61-85.
94. O'Malley, D.M., et al., *PARP Inhibitors in Ovarian Cancer: A Review.* Target Oncol, 2023.
95. Nero, C., et al., *Ovarian Cancer Treatments Strategy: Focus on PARP Inhibitors and Immune Check Point Inhibitors.* Cancers (Basel), 2021. **13**(6).
96. Pujade-Lauraine, E., et al., *Avelumab alone or in combination with chemotherapy versus chemotherapy alone in platinum-resistant or platinum-refractory ovarian cancer (JAVELIN Ovarian 200): an open-label, three-arm, randomised, phase 3 study.* Lancet Oncol, 2021. **22**(7): p. 1034-1046.
97. Dilawari, A., et al., *FDA Approval Summary: Mirvetuximab soravtansine-gynx for FRalpha-positive, Platinum-Resistant Ovarian Cancer.* Clin Cancer Res, 2023.
98. O'Shannessy, D.J., et al., *Expression of folate receptors alpha and beta in normal and cancerous gynecologic tissues: correlation of expression of the beta isoform with macrophage markers.* J Ovarian Res, 2015. **8**: p. 29.
99. Kalli, K.R., et al., *Folate receptor alpha as a tumor target in epithelial ovarian cancer.* Gynecol Oncol, 2008. **108**(3): p. 619-26.
100. Moore, K.N., et al., *Phase III, randomized trial of mirvetuximab soravtansine versus chemotherapy in patients with platinum-resistant ovarian cancer: primary analysis of FORWARD I.* Ann Oncol, 2021. **32**(6): p. 757-765.
101. Shimizu, T., et al., *First-in-Human Phase 1 Study of MORAb-202, an Antibody-Drug Conjugate Comprising Farletuzumab Linked to Eribulin Mesylate, in Patients with Folate Receptor-alpha-Positive Advanced Solid Tumors.* Clin Cancer Res, 2021. **27**(14): p. 3905-

3915.

102. Stolz, M.L. and C. McCormick, *The bZIP Proteins of Oncogenic Viruses.* Viruses, 2020. **12**(7).
103. Jorgensen, M.D. and J. Chmielewski, *Recent advances in coiled-coil peptide materials and their biomedical applications.* Chem Commun (Camb), 2022. **58**(83): p. 11625-11636.
104. Potapov, V., J.B. Kaplan, and A.E. Keating, *Data-driven prediction and design of bZIP coiled-coil interactions.* PLoS Comput Biol, 2015. **11**(2): p. e1004046.
105. Thompson, K.E., et al., *SYNZIP protein interaction toolbox: in vitro and in vivo specifications of heterospecific coiled-coil interaction domains.* ACS Synth Biol, 2012. **1**(4): p. 118-29.
106. Grigoryan, G., A.W. Reinke, and A.E. Keating, *Design of protein-interaction specificity gives selective bZIP-binding peptides.* Nature, 2009. **458**(7240): p. 859-64.
107. Reinke, A.W., R.A. Grant, and A.E. Keating, *A synthetic coiled-coil interactome provides heterospecific modules for molecular engineering.* J Am Chem Soc, 2010. **132**(17): p. 6025-31.
108. Cho, J.H., J.J. Collins, and W.W. Wong, *Universal Chimeric Antigen Receptors for Multiplexed and Logical Control of T Cell Responses.* Cell, 2018. **173**(6): p. 1426-1438 e11.
109. Conticello, V., S. Hughes, and C. Modlin, *Biomaterials Made from Coiled-Coil Peptides.* Subcell Biochem, 2017. **82**: p. 575-600.
110. Amoury, M., et al., *Granzyme B-based cytolytic fusion protein targeting EpCAM specifically kills triple negative breast cancer cells in vitro and inhibits tumor growth in a subcutaneous mouse tumor model.* Cancer Lett, 2016. **372**(2): p. 201-9.
111. Kampmeier, F., et al., *Site-specific, covalent labeling of recombinant antibody fragments via fusion to an engineered version of 6-O-alkylguanine DNA alkyltransferase.* Bioconjug Chem, 2009. **20**(5): p. 1010-5.
112. Woitok, M., et al., *Using the SNAP-Tag technology to easily measure and demonstrate apoptotic changes in cancer and blood cells with different dyes.* PLoS One, 2020. **15**(12): p. e0243286.
113. Gall, V.A., et al., *Trastuzumab Increases HER2 Uptake and Cross-Presentation by Dendritic Cells.* Cancer Res, 2017. **77**(19): p. 5374-5383.
114. Emlet, D.R., et al., *HER2 expression as a potential marker for response to therapy targeted to the EGFR.* Br J Cancer, 2006. **94**(8): p. 1144-53.
115. Bou-Assaly, W. and S. Mukherji, *Cetuximab (erbitux).* AJNR Am J Neuroradiol, 2010. **31**(4): p. 626-7.
116. Kamat, V., et al., *Enhanced EGFR inhibition and distinct epitope recognition by EGFR antagonistic mAbs C225 and 425.* Cancer Biol Ther, 2008. **7**(5): p. 726-33.
117. Kampmeier, F., et al., *Rapid optical imaging of EGF receptor expression with a single-chain antibody SNAP-tag fusion protein.* Eur J Nucl Med Mol Imaging, 2010. **37**(10): p. 1926-34.
118. Bremer, E., et al., *Target cell-restricted and -enhanced apoptosis induction by a scFv:sTRAIL fusion protein with specificity for the pancarcinoma-associated antigen EGP2.* Int J Cancer, 2004. **109**(2): p. 281-90.
119. Gemmete, J.J. and S.K. Mukherji, *Trastuzumab (herceptin).* AJNR Am J Neuroradiol, 2011. **32**(8): p. 1373-4.
120. Rieger, A.M., et al., *Modified annexin V/propidium iodide apoptosis assay for accurate*

assessment of cell death. J Vis Exp, 2011(50).

121. Elmore, S., *Apoptosis: a review of programmed cell death.* Toxicol Pathol, 2007. **35**(4): p. 495-516.
122. van Engeland, M., et al., *Annexin V-affinity assay: a review on an apoptosis detection system based on phosphatidylserine exposure.* Cytometry, 1998. **31**(1): p. 1-9.
123. Panowski, S., et al., *Site-specific antibody drug conjugates for cancer therapy.* MAbs, 2014. **6**(1): p. 34-45.
124. Zhang, C., et al., *EpCAM- and EGFR-Specific Antibody Drug Conjugates for Triple-Negative Breast Cancer Treatment.* Int J Mol Sci, 2022. **23**(11).
125. Vega Cano, K.S., et al., *Systemic Therapy for HER2-Positive Metastatic Breast Cancer: Current and Future Trends.* Cancers (Basel), 2022. **15**(1).
126. Hunter, F.W., et al., *Mechanisms of resistance to trastuzumab emtansine (T-DM1) in HER2-positive breast cancer.* Br J Cancer, 2020. **122**(5): p. 603-612.
127. Barok, M., H. Joensuu, and J. Isola, *Trastuzumab emtansine: mechanisms of action and drug resistance.* Breast Cancer Res, 2014. **16**(2): p. 209.
128. Magkou, C., et al., *Expression of the epidermal growth factor receptor (EGFR) and the phosphorylated EGFR in invasive breast carcinomas.* Breast Cancer Res, 2008. **10**(3): p. R49.
129. Rimawi, M.F., et al., *Epidermal growth factor receptor expression in breast cancer association with biologic phenotype and clinical outcomes.* Cancer, 2010. **116**(5): p. 1234-42.
130. Masuda, H., et al., *Role of epidermal growth factor receptor in breast cancer.* Breast Cancer Res Treat, 2012. **136**(2): p. 331-45.
131. Nakai, K., M.C. Hung, and H. Yamaguchi, *A perspective on anti-EGFR therapies targeting triple-negative breast cancer.* Am J Cancer Res, 2016. **6**(8): p. 1609-23.
132. Soysal, S.D., et al., *EpCAM expression varies significantly and is differentially associated with prognosis in the luminal B HER2(+), basal-like, and HER2 intrinsic subtypes of breast cancer.* Br J Cancer, 2013. **108**(7): p. 1480-7.
133. Abd El-Maqsoud, N.M. and D.M. Abd El-Rehim, *Clinicopathologic implications of EpCAM and Sox2 expression in breast cancer.* Clin Breast Cancer, 2014. **14**(1): p. e1-9.
134. Agboola, A.J., et al., *EpCAM expression is an indicator of recurrence in basal-like breast cancer.* Breast Cancer Res Treat, 2012. **133**(2): p. 575-82.
135. Hiraga, T., S. Ito, and H. Nakamura, *EpCAM expression in breast cancer cells is associated with enhanced bone metastasis formation.* Int J Cancer, 2016. **138**(7): p. 1698-708.
136. Ohashi, R., et al., *Higher expression of EpCAM is associated with poor clinical and pathological responses in breast cancer patients undergoing neoadjuvant chemotherapy.* Pathol Int, 2016. **66**(4): p. 210-7.
137. Subik, K., et al., *The Expression Patterns of ER, PR, HER2, CK5/6, EGFR, Ki-67 and AR by Immunohistochemical Analysis in Breast Cancer Cell Lines.* Breast Cancer (Auckl), 2010. **4**: p. 35-41.
138. Smith, S.E., et al., *Molecular characterization of breast cancer cell lines through multiple omic approaches.* Breast Cancer Res, 2017. **19**(1): p. 65.
139. Stanley, A., et al., *Synergistic effects of various Her inhibitors in combination with IGF-1R, C-MET and Src targeting agents in breast cancer cell lines.* Sci Rep, 2017. **7**(1): p. 3964.

140. Vranic, S., Z. Gatalica, and Z.Y. Wang, *Update on the molecular profile of the MDA-MB-453 cell line as a model for apocrine breast carcinoma studies.* Oncol Lett, 2011. **2**(6): p. 1131-1137.
141. Wang, K., D. Li, and L. Sun, *High levels of EGFR expression in tumor stroma are associated with aggressive clinical features in epithelial ovarian cancer.* Onco Targets Ther, 2016. **9**: p. 377-86.
142. Sheng, Q. and J. Liu, *The therapeutic potential of targeting the EGFR family in epithelial ovarian cancer.* Br J Cancer, 2011. **104**(8): p. 1241-5.
143. Cai, Y., et al., *Expressions of fatty acid synthase and HER2 are correlated with poor prognosis of ovarian cancer.* Med Oncol, 2015. **32**(1): p. 391.
144. Hogdall, E.V., et al., *Distribution of HER-2 overexpression in ovarian carcinoma tissue and its prognostic value in patients with ovarian carcinoma: from the Danish MALOVA Ovarian Cancer Study.* Cancer, 2003. **98**(1): p. 66-73.
145. Bignotti, E., et al., *Trop-2 overexpression as an independent marker for poor overall survival in ovarian carcinoma patients.* Eur J Cancer, 2010. **46**(5): p. 944-53.
146. Wu, B., et al., *Overexpression of TROP2 promotes proliferation and invasion of ovarian cancer cells.* Exp Ther Med, 2017. **14**(3): p. 1947-1952.
147. Schilder, R.J., et al., *Phase II trial of single agent cetuximab in patients with persistent or recurrent epithelial ovarian or primary peritoneal carcinoma with the potential for dose escalation to rash.* Gynecol Oncol, 2009. **113**(1): p. 21-7.
148. Seiden, M.V., et al., *A phase II trial of EMD72000 (matuzumab), a humanized anti-EGFR monoclonal antibody, in patients with platinum-resistant ovarian and primary peritoneal malignancies.* Gynecol Oncol, 2007. **104**(3): p. 727-31.
149. Wagner, U., et al., *Gefitinib in combination with tamoxifen in patients with ovarian cancer refractory or resistant to platinum-taxane based therapy--a phase II trial of the AGO Ovarian Cancer Study Group (AGO-OVAR 2.6).* Gynecol Oncol, 2007. **105**(1): p. 132-7.
150. Wilken, J.A., et al., *EGFR/HER-targeted therapeutics in ovarian cancer.* Future Med Chem, 2012. **4**(4): p. 447-69.
151. Schmiedel, J., et al., *Matuzumab binding to EGFR prevents the conformational rearrangement required for dimerization.* Cancer Cell, 2008. **13**(4): p. 365-73.
152. Shin, T.H., et al., *Enhancement of the tumor penetration of monoclonal antibody by fusion of a neuropilin-targeting peptide improves the antitumor efficacy.* Mol Cancer Ther, 2014. **13**(3): p. 651-61.
153. Uppal, H., et al., *Potential mechanisms for thrombocytopenia development with trastuzumab emtansine (T-DM1).* Clin Cancer Res, 2015. **21**(1): p. 123-33.
154. Aoyama, M., et al., *Fcgamma Receptor-Dependent Internalization and Off-Target Cytotoxicity of Antibody-Drug Conjugate Aggregates.* Pharm Res, 2022. **39**(1): p. 89-103.
155. Hansel, T.T., et al., *The safety and side effects of monoclonal antibodies.* Nat Rev Drug Discov, 2010. **9**(4): p. 325-38.
156. Adams, G.P. and L.M. Weiner, *Monoclonal antibody therapy of cancer.* Nat Biotechnol, 2005. **23**(9): p. 1147-57.
157. Shah, A., et al., *The Current Landscape of Antibody-based Therapies in Solid Malignancies.* Theranostics, 2021. **11**(3): p. 1493-1512.
158. Tolcher, A.W., *The Evolution of Antibody-Drug Conjugates: A Positive Inflexion Point.* Am

Soc Clin Oncol Educ Book, 2020. **40**: p. 1-8.

159. Satheeshkumar, P.K., *Expression of Single Chain Variable Fragment (scFv) Molecules in Plants: A Comprehensive Update.* Mol Biotechnol, 2020. **62**(3): p. 151-167.
160. Yokota, T., et al., *Rapid tumor penetration of a single-chain Fv and comparison with other immunoglobulin forms.* Cancer Res, 1992. **52**(12): p. 3402-8.
161. Kubetzko, S., et al., *PEGylation and multimerization of the anti-p185HER-2 single chain Fv fragment 4D5: effects on tumor targeting.* J Biol Chem, 2006. **281**(46): p. 35186-201.
162. Ko, S., M. Jo, and S.T. Jung, *Recent Achievements and Challenges in Prolonging the Serum Half-Lives of Therapeutic IgG Antibodies Through Fc Engineering.* BioDrugs, 2021. **35**(2): p. 147-157.
163. Ahmad, Z.A., et al., *scFv antibody: principles and clinical application.* Clin Dev Immunol, 2012. **2012**: p. 980250.
164. Jager, V., et al., *High level transient production of recombinant antibodies and antibody fusion proteins in HEK293 cells.* BMC Biotechnol, 2013. **13**: p. 52.
165. Guglielmi, L. and P. Martineau, *Expression of single-chain Fv fragments in E. coli cytoplasm.* Methods Mol Biol, 2009. **562**: p. 215-24.
166. Hornig, N. and A. Farber-Schwarz, *Production of bispecific antibodies: diabodies and tandem scFv.* Methods Mol Biol, 2012. **907**: p. 713-27.
167. Wang, Y., et al., *A 33-residue peptide tag increases solubility and stability of Escherichia coli produced single-chain antibody fragments.* Nat Commun, 2022. **13**(1): p. 4614.
168. Li, Z., et al., *Effect of Size on Solid Tumor Disposition of Protein Therapeutics.* Drug Metab Dispos, 2019. **47**(10): p. 1136-1145.
169. Frigerio, B., et al., *A single-chain fragment against prostate specific membrane antigen as a tool to build theranostic reagents for prostate cancer.* Eur J Cancer, 2013. **49**(9): p. 2223-32.
170. Jalilzadeh-Razin, S., et al., *Phage antibody library screening for the selection of novel high-affinity human single-chain variable fragment against gastrin receptor: an in silico and in vitro study.* Daru, 2019. **27**(1): p. 21-34.
171. Wu, Y., et al., *A Cyclin D1-Specific Single-Chain Variable Fragment Antibody that Inhibits HepG2 Cell Growth and Proliferation.* Biotechnol J, 2020. **15**(8): p. e1900430.
172. Khantasup, K., et al., *Anti-EpCAM scFv gadolinium chelate: a novel targeted MRI contrast agent for imaging of colorectal cancer.* MAGMA, 2018. **31**(5): p. 633-644.
173. Mazzocco, C., et al., *In vivo imaging of prostate cancer using an anti-PSMA scFv fragment as a probe.* Sci Rep, 2016. **6**: p. 23314.
174. Hartmann, R.W., et al., *Rational Design of Azastatin as a Potential ADC Payload with Reduced Bystander Killing.* ChemMedChem, 2020. **15**(24): p. 2500-2512.
175. Su, Z., et al., *Antibody-drug conjugates: Recent advances in linker chemistry.* Acta Pharm Sin B, 2021. **11**(12): p. 3889-3907.
176. Ferraro, E., J.Z. Drago, and S. Modi, *Implementing antibody-drug conjugates (ADCs) in HER2-positive breast cancer: state of the art and future directions.* Breast Cancer Res, 2021. **23**(1): p. 84.
177. Cunningham, D., et al., *Monomethyl Auristatin E Phosphate Inhibits Human Prostate Cancer Growth.* Prostate, 2016. **76**(15): p. 1420-30.
178. Hu, X.Y., et al., *An EGFR-targeting antibody-drug conjugate LR004-VC-MMAE: potential*

in esophageal squamous cell carcinoma and other malignancies. Mol Oncol, 2019. **13**(2): p. 246-263.

179. Strop, P., et al., *Location matters: site of conjugation modulates stability and pharmacokinetics of antibody drug conjugates.* Chem Biol, 2013. **20**(2): p. 161-7.
180. Holder, P.G., et al., *Reconstitution of Formylglycine-generating Enzyme with Copper(II) for Aldehyde Tag Conversion.* J Biol Chem, 2015. **290**(25): p. 15730-15745.
181. Pan, L., et al., *Sortase A-Generated Highly Potent Anti-CD20-MMAE Conjugates for Efficient Elimination of B-Lineage Lymphomas.* Small, 2017. **13**(6).
182. Hoehnel, S. and M.P. Lutolf, *Capturing Cell-Cell Interactions via SNAP-tag and CLIP-tag Technology.* Bioconjug Chem, 2015. **26**(8): p. 1678-86.
183. Renz, C., N. Johnsson, and T. Gronemeyer, *An efficient protocol for the purification and labeling of entire yeast septin rods from E.coli for quantitative in vitro experimentation.* BMC Biotechnol, 2013. **13**: p. 60.
184. Huhalov, A. and K.A. Chester, *Engineered single chain antibody fragments for radioimmunotherapy.* Q J Nucl Med Mol Imaging, 2004. **48**(4): p. 279-88.
185. Suzuki, H., et al., *Copper-64-Labeled Antibody Fragments for Immuno-PET/Radioimmunotherapy with Low Renal Radioactivity Levels and Amplified Tumor-Kidney Ratios.* ACS Omega, 2021. **6**(33): p. 21556-21562.
186. Altai, M., et al., *Pretargeted Imaging and Therapy.* J Nucl Med, 2017. **58**(10): p. 1553-1559.
187. Yoon, J.K., et al., *Current Perspectives on (89)Zr-PET Imaging.* Int J Mol Sci, 2020. **21**(12).
188. Verhoeven, M., Y. Seimbille, and S.U. Dalm, *Therapeutic Applications of Pretargeting.* Pharmaceutics, 2019. **11**(9).
189. Liu, G., *A Revisit to the Pretargeting Concept-A Target Conversion.* Front Pharmacol, 2018. **9**: p. 1476.
190. Khang, M.K., et al., *A pretargeting nanoplatform for imaging and enhancing anti-inflammatory drug delivery.* Bioact Mater, 2020. **5**(4): p. 1102-1112.
191. Gerke, C., et al., *Clickable Albumin Nanoparticles for Pretargeted Drug Delivery toward PD-L1 Overexpressing Tumors in Combination Immunotherapy.* Bioconjug Chem, 2022. **33**(5): p. 821-828.
192. Maass, K.F., et al., *Determination of Cellular Processing Rates for a Trastuzumab-Maytansinoid Antibody-Drug Conjugate (ADC) Highlights Key Parameters for ADC Design.* AAPS J, 2016. **18**(3): p. 635-46.
193. Durbin, K.R., C. Phipps, and X. Liao, *Mechanistic Modeling of Antibody-Drug Conjugate Internalization at the Cellular Level Reveals Inefficient Processing Steps.* Mol Cancer Ther, 2018. **17**(6): p. 1341-1351.
194. Kol, A., et al., *ADCC responses and blocking of EGFR-mediated signaling and cell growth by combining the anti-EGFR antibodies imgatuzumab and cetuximab in NSCLC cells.* Oncotarget, 2017. **8**(28): p. 45432-45446.
195. Liang, K., et al., *Dynamics of Endocytosis and Degradation of Antibody-Drug Conjugate T-DM1 in HER2 Positive Cancer Cells.* Drug Des Devel Ther, 2021. **15**: p. 5135-5150.
196. Sharma, S., et al., *Evaluation of Quantitative Relationship Between Target Expression and Antibody-Drug Conjugate Exposure Inside Cancer Cells.* Drug Metab Dispos, 2020. **48**(5): p. 368-377.
197. Wang, Y., et al., *Antibody-Drug Conjugate Using Ionized Cys-Linker-MMAE as the Potent*

Payload Shows Optimal Therapeutic Safety. Cancers (Basel), 2020. **12**(3).

198. Shen, Y., et al., *Conjugation of DM1 to anti-CD30 antibody has potential antitumor activity in CD30-positive hematological malignancies with lower systemic toxicity.* MAbs, 2019. **11**(6): p. 1149-1161.
199. Filmus, J., et al., *MDA-468, a human breast cancer cell line with a high number of epidermal growth factor (EGF) receptors, has an amplified EGF receptor gene and is growth inhibited by EGF.* Biochem Biophys Res Commun, 1985. **128**(2): p. 898-905.
200. Mamot, C., et al., *Epidermal growth factor receptor (EGFR)-targeted immunoliposomes mediate specific and efficient drug delivery to EGFR- and EGFRvIII-overexpressing tumor cells.* Cancer Res, 2003. **63**(12): p. 3154-61.
201. Costantini, D.L., et al., *Trastuzumab-resistant breast cancer cells remain sensitive to the auger electron-emitting radiotherapeutic agent 111In-NLS-trastuzumab and are radiosensitized by methotrexate.* J Nucl Med, 2008. **49**(9): p. 1498-505.
202. Brockhoff, G., et al., *Epidermal growth factor receptor, c-erbB2 and c-erbB3 receptor interaction, and related cell cycle kinetics of SK-BR-3 and BT474 breast carcinoma cells.* Cytometry, 2001. **44**(4): p. 338-48.
203. de Goeij, B.E., et al., *High turnover of tissue factor enables efficient intracellular delivery of antibody-drug conjugates.* Mol Cancer Ther, 2015. **14**(5): p. 1130-40.
204. Lewis Phillips, G.D., et al., *Targeting HER2-positive breast cancer with trastuzumab-DM1, an antibody-cytotoxic drug conjugate.* Cancer Res, 2008. **68**(22): p. 9280-90.
205. Pinto, C., et al., *Management of skin toxicity associated with cetuximab treatment in combination with chemotherapy or radiotherapy.* Oncologist, 2011. **16**(2): p. 228-38.
206. Lacouture, M.E., et al., *Dermatologic Toxicity Occurring During Anti-EGFR Monoclonal Inhibitor Therapy in Patients With Metastatic Colorectal Cancer: A Systematic Review.* Clin Colorectal Cancer, 2018. **17**(2): p. 85-96.
207. Ho, E.C.H., et al., *Antibody drug conjugates, targeting cancer-expressed EGFR, exhibit potent and specific antitumor activity.* Biomed Pharmacother, 2023. **157**: p. 114047.
208. Chiang, Z.C., et al., *Preparation and characterization of antibody-drug conjugates acting on HER2-positive cancer cells.* PLoS One, 2020. **15**(9): p. e0239813.
209. Damiani, I., et al., *Purification and In Vitro Evaluation of an Anti-HER2 Affibody-Monomethyl Auristatin E Conjugate in HER2-Positive Cancer Cells.* Biology (Basel), 2021. **10**(8).
210. Hamblett, K.J., et al., *Effects of drug loading on the antitumor activity of a monoclonal antibody drug conjugate.* Clin Cancer Res, 2004. **10**(20): p. 7063-70.
211. Zacharias, N., et al., *A homogeneous high-DAR antibody-drug conjugate platform combining THIOMAB antibodies and XTEN polypeptides.* Chem Sci, 2022. **13**(11): p. 3147-3160.

9. Supplementary materials

9.1 Sequences of open reading frames

9.1.1 scFv-Erbitux-SNAP

ATGGAGACAGACACACTCCTGCTATGGGTACTGCTGCTCTGGGTTCCAGGT
TCCACTGGTGACGCGGCCCAGCCGGCCCAGGTGCAGCTGAAGCAGAGCG
GCCCCGGCCTGGTGCAGCCCAGCCAGAGCCTGAGCATCACCTGCACCGTG
AGCGGCTTCAGCCTGACCAACTACGGCGTGCACTGGGTGAGGCAGAGCCC
CGGCAAGGGCCTGGAGTGGCTGGGCGTGATCTGGAGCGGCGGCAACACC
GACTACAACACCCCCTTCACCAGCAGGCTGAGCATCAACAAGGACAACAG
CAAGAGCCAGGTGTTCTTCAAGATGAACAGCCTGCAGAGCAACGACACCG
CCATCTACTACTGCGCCAGGGCCCTGACCTACTACGACTACGAGTTCGCCT
ACTGGGGCCAGGGCACCCTGGTGACCGTGAGCGCCGGTGGAGGCGGTTCA
GGCGGAGGTGGCAGCGGCGGTGGCGGGTCGGACATCCTGCTGACCCAGA
GCCCCGTGATCCTGAGCGTGAGCCCCGGCGAGAGGGTGAGCTTCAGCTGC
AGGGCCAGCCAGAGCATCGGCACCAACATCCACTGGTATCAGCAGAGGAC
CAACGGCAGCCCCAGGCTGCTGATCAAGTACGCCAGCGAGAGCATCAGCG
GCATCCCCAGCAGGTTCAGCGGCAGCGGCAGCGGCACCGACTTCACCCTG
AGCATCAACAGCGTGGAGAGCGAGGACATCGCCGACTACTACTGCCAGCA
GAACAACAACTGGCCCACCACCTTCGGCGCCGGCACCAAGCTGGAGCTGA
AGGGGTCTTCTAGAATGGACAAAGACTGCGAAATGAAGCGCACCACCCTG
GATAGCCCTCTGGGCAAGCTGGAACTGTCTGGGTGCGAACAGGGCCTGCA
CGAGATCAAGCTGCTGGGCAAAGGAACATCTGCCGCCGACGCCGTGGAAG
TGCCTGCCCCAGCCGCCGTGCTGGGCGGACCAGAGCCACTGATGCAGGCC
ACCGCCTGGCTCAACGCCTACTTTCACCAGCCTGAGGCCATCGAGGAGTTC
CCTGTGCCAGCCCTGCACCACCCAGTGTTCCAGCAGGAGAGCTTTACCCGC
CAGGTGCTGTGGAAACTGCTGAAAGTGGTGAAGTTCGGAGAGGTCATCAG
CTACCAGCAGCTGGCGGCCCTGGCGGGCAATCCCGCCGCCACCGCCGCCG
TGAAAACCGCCCTGAGCGGAAATCCCGTGCCCATTCTGATCCCCTGCCACC

GGGTGGTGTCTAGCTCTGGCGCCGTGGGGGGCTACGAGGGCGGGCTCGCC
GTGAAAGAGTGGCTGCTGGCCCACGAGGGCCACAGACTGGGCAAGCCTG
GGCTGGGCGCTGAGCACGAATTTCGAGGAGGGCCCGAACAAAAACTCATC
TCAGAAGAGGATCTGAATAGCGCCGTCGACCATCATCATCATCATCATTGA

9.1.2 scFv-425-SNAP

ATGGAGACAGACACACTCCTGCTATGGGTACTGCTGCTCTGGGTTCCAGGT
TCCACTGGTGACGCGGCCCAGCCGGCCATGGCCGAGGTGCAACTGCAGCA
GTCTGGGGCTGAACTGGTGAAGCCTGGGGCTTCAGTGAAGTTGTCCTGCA
AGGCTTCCGGCTACACCTTCACCAGCCACTGGATGCACTGGGTGAAGCAG
AGGGCTGGACAAGGCCTTGAGTGGATCGGAGAGTTTAATCCCAGCAACGG
CCGTACTAACTACAATGAGAAATTCAAGAGCAAGGCCACACTGACTGTAG
ACAAATCCTCCAGCACAGCCTACATGCAACTCAGCAGCCTGACATCTGAGG
ACTCTGCGGTCTATTACTGTGCCAGTCGGGACTATGATTACGACGGACGGTA
CTTTGACTACTGGGGCCAAGGGACCACGGTCACCGTCTCCTCAGGTGGCG
GTGGCTCGGGCGGTGGTGGGTCGGGTGGTGGCGGATCTGACATCGAGCTC
ACCCAGTCTCCAGCAATCATGTCTGCATCTCCAGGGGAGAAGGTCACTATG
ACCTGCAGTGCCAGCTCAAGTGTAACTTACATGTATTGGTACCAGCAGAAG
CCAGGATCCTCCCCCAGACTCCTGATTTATGACACATCCAACCTGGCTTCTG
GAGTCCCTGTTCGTTTCAGTGGCAGTGGGTCTGGGACCTCTTACTCTCTCA
CAATCAGCCGAATGGAGGCTGAAGATGCTGCCACTTATTACTGCCAGCAGT
GGAGTAGTCACATATTCACGTTCGGCTCGGGGACAGAACTCGAGATCAAAC
GGGCGGCCGCACTCGAGTCTAGAATGGACAAAGACTGCGAAATGAAGCGC
ACCACCCTGGATAGCCCTCTGGGCAAGCTGGAACTGTCTGGGTGCGAACA
GGGCCTGCACGAGATCAAGCTGCTGGGCAAAGGAACATCTGCCGCCGACG
CCGTGGAAGTGCCTGCCCCAGCCGCCGTGCTGGGCGGACCAGAGCCACTG
ATGCAGGCCACCGCCTGGCTCAACGCCTACTTTCACCAGCCTGAGGCCATC
GAGGAGTTCCCTGTGCCAGCCCTGCACCACCCAGTGTTCCAGCAGGAGAG
CTTTACCCGCCAGGTGCTGTGGAAACTGCTGAAAGTGGTGAAGTTCGGAG

AGGTCATCAGCTACCAGCAGCTGGCGGCCCTGGCGGGCAATCCCGCCGCC
ACCGCCGCCGTGAAAACCGCCCTGAGCGGAAATCCCGTGCCCATTCTGATC
CCCTGCCACCGGGTGGTGTCTAGCTCTGGCGCCGTGGGGGGCTACGAGGG
CGGGCTCGCCGTGAAAGAGTGGCTGCTGGCCCACGAGGGCCACAGACTG
GGCAAGCCTGGGCTGGGCGCTGAGCACGAATTTCGAGGAGGGCCCGAAC
AAAAACTCATCTCAGAAGAGGATCTGAATAGCGCCGTCGACCATCATCATC
ATCATCATTGA

9.1.3 scFv-αEpCAM-SNAP

ATGGAGACAGACACACTCCTGCTATGGGTACTGCTGCTCTGGGTTCCAGGT
TCCACTGGTGACGCGGCCCAGCCGGCCATGGCCCAGGTGCAGCTGGTGCA
GTCTGGGGCTGAGGTGAAGAAGCCTGGGTCCTCGGTGAGGGTCTCCTGCA
AGGCTTCTGGAGGCACCTTCAGCAGCTATGCTATCAGCTGGGTGCGACAGG
CCCCTGGACAAGGGCTTGAGTGGATGGGAGGGATCATCCCTATCTTTGGTA
CAGCAAACTACGCACAGAAGTTCCAGGGCAGAGTCACGATTACCGCGGAC
GAATCCACGAGCACAGCCTACATGGAGCTGAGCAGCCTGAGATCTGAGGA
CACGGCTGTGTATTACTGTGCAAGAGACCCGTTTCTTCACTATTGGGGCCA
AGGTACCCTGGTCACCGTCTCGAGTGGTGGAGGCGGTTCAGGCGGAGGTG
GCTCTGGCGGTGGCGGATCGGAAATTGAGCTCACTCAGTCTCCACTCTCCC
TGCCCGTCACCCCTGGAGAGCCGGCCTCCATCTCCTGCAGGTCTAGTCAGA
GCCTCCTGCATAGTAATGGATACAACTATTTGGATTGGTACCTGCAGAAGCC
AGGGCAGTCTCCACAGCTCCTGATCTATTTGGGTTCTAATCGGGCCTCCGG
GGTCCCTGACAGGTTCAGTGGCAGTGGATCAGGCACAGATTTTACACTGAA
AATCAGCAGAGTGGAGGCTGAGGATGTTGGGGTTTATTACTGCATGCAAGC
TCTACAAACTTTCACTTTCGGCCCTGGGACCAAGGTGGAGATCAAACGTGC
GGCCGCACTCGAGTCTAGAATGGACAAAGACTGCGAAATGAAGCGCACCA
CCCTGGATAGCCCTCTGGGCAAGCTGGAACTGTCTGGGTGCGAACAGGGC
CTGCACGAGATCAAGCTGCTGGGCAAAGGAACATCTGCCGCCGACGCCGT
GGAAGTGCCTGCCCCAGCCGCCGTGCTGGGCGGACCAGAGCCACTGATGC

AGGCCACCGCCTGGCTCAACGCCTACTTTCACCAGCCTGAGGCCATCGAG
GAGTTCCCTGTGCCAGCCCTGCACCACCCAGTGTTCCAGCAGGAGAGCTT
TACCCGCCAGGTGCTGTGGAAACTGCTGAAAGTGGTGAAGTTCGGAGAGG
TCATCAGCTACCAGCAGCTGGCGGCCCTGGCGGGCAATCCCGCCGCCACC
GCCGCCGTGAAAACCGCCCTGAGCGGAAATCCCGTGCCCATTCTGATCCCC
TGCCACCGGGTGGTGTCTAGCTCTGGCGCCGTGGGGGGCTACGAGGGCGG
GCTCGCCGTGAAAGAGTGGCTGCTGGCCCACGAGGGCCACAGACTGGGC
AAGCCTGGGCTGGGCGCTGAGCACGAATTTCGAGGAGGGCCCGAACAAA
AACTCATCTCAGAAGAGGATCTGAATAGCGCCGTCGACCATCATCATCATC
ATCATTGA

9.1.4 scFv-Herceptin-SNAP

ATGGAGACAGACACACTCCTGCTATGGGTACTGCTGCTCTGGGTTCCAGGT
TCCACTGGTGACGCGGCCCAGCCGGCCGCCACCATGGATTGGACTTGGAG
AGTGTTTTGCCTGCTGGCTGTCGCACCTGGGGCTCATAGTGAAGTGCAGCT
GGTCGAGAGTGGAGGAGGGCTGGTGCAGCCTGGCGGCAGCCTGAGGCTG
TCCTGCGCAGCCTCTGGCTTCAACATCAAGGACACCTACATCCACTGGGTG
CGGCAGGCCCCTGGCAAGGGCCTGGAGTGGGTGGCCAGGATCTATCCAAC
CAATGGCTACACACGGTATGCCGACAGCGTGAAGGGCCGGTTCACCATCA
GCGCCGACACCTCCAAGAACACAGCCTACCTCCAGATGAACAGCCTGAGG
GCCGAGGATACAGCCGTGTACTATTGCTCTCGCTGGGGAGGCGACGGCTTC
TACGCTATGGACTATTGGGGACAGGGCACCCTGGTGACCGTGAGCAGCGGT
GGAGGCGGTTCAGGCGGAGGTGGCAGCGGCGGTGGCGGGTCGGACATCC
AGATGACTCAGTCCCCTAGCTCCCTGAGTGCTTCAGTGGGCGACAGGGTCA
CTATTACCTGCCGCGCATCTCAGGATGTGAACACCGCAGTCGCCTGGTATCA
GCAGAAGCCTGGAAAAGCTCCAAAGCTGCTGATCTACAGCGCATCCTTCCT
GTATTCCGGCGTGCCCTCTCGGTTTTCTGGGAGTAGATCAGGAACTGACTT
CACACTGACTATTTCTAGTCTGCAGCCTGAGGATTTTGCCACCTACTATTGC
CAGCAGCACTACACCACACCCCCTACTTTCGGCCAGGGGACCAAAGTGGA

GATCAAGTCTAGAATGGACAAAGACTGCGAAATGAAGCGCACCACCCTGG
ATAGCCCTCTGGGCAAGCTGGAACTGTCTGGGTGCGAACAGGGCCTGCAC
GAGATCAAGCTGCTGGGCAAAGGAACATCTGCCGCCGACGCCGTGGAAGT
GCCTGCCCCAGCCGCCGTGCTGGGCGGACCAGAGCCACTGATGCAGGCCA
CCGCCTGGCTCAACGCCTACTTTCACCAGCCTGAGGCCATCGAGGAGTTCC
CTGTGCCAGCCCTGCACCACCCAGTGTTCCAGCAGGAGAGCTTTACCCGCC
AGGTGCTGTGGAAACTGCTGAAAGTGGTGAAGTTCGGAGAGGTCATCAGC
TACCAGCAGCTGGCGGCCCTGGCGGGCAATCCCGCCGCCACCGCCGCCGT
GAAAACCGCCCTGAGCGGAAATCCCGTGCCCATTCTGATCCCCTGCCACCG
GGTGGTGTCTAGCTCTGGCGCCGTGGGGGGCTACGAGGGCGGGCTCGCCG
TGAAAGAGTGGCTGCTGGCCCACGAGGGCCACAGACTGGGCAAGCCTGG
GCTGGGCGCTGAGCACGAATTTCGAGGAGGGCCCGAACAAAAACTCATCT
CAGAAGAGGATCTGAATAGCGCCGTCGACCATCATCATCATCATCATTGA

9.1.5 scFv-Sacit-SNAP

ATGGAGACAGACACACTCCTGCTATGGGTACTGCTGCTCTGGGTTCCAGGT
TCCACTGGTGACGCGGCCCAGCCGGCCCAGGTGCAGCTGCAGCAGTCCGG
CTCTGAGCTGAAGAAGCCCGGCGCCAGCGTGAAGGTGTCCTGCAAGGCCT
CTGGCTACACCTTCACAAACTATGGCATGAATTGGGTGAAGCAGGCACCTG
GACAGGGCCTGAAGTGGATGGGCTGGATCAACACCTACACAGGCGAGCCA
ACCTATACAGACGACTTCAAGGGCAGGTTCGCCTTTTCCCTGGACACCAGC
GTGTCCACAGCCTACCTGCAGATCAGCTCCCTGAAGGCCGACGATACCGCC
GTGTATTTCTGCGCAAGGGGAGGATTTGGCTCTAGCTACTGGTATTTCGACG
TGTGGGGACAGGGAAGCCTGGTGACAGTGTCCTCTGGAGGAGGAGGATCT
GGAGGAGGAGGAAGCGGAGGAGGAGGATCCGATATCCAGCTGACCCAGTC
TCCAAGCTCCCTGTCTGCCAGCGTGGGCGACCGGGTGAGCATCACCTGTAA
GGCAAGCCAGGACGTGAGCATCGCAGTGGCATGGTACCAGCAGAAGCCAG
GCAAGGCCCCTAAGCTGCTGATCTATTCCGCCTCTTACCGGTATACCGGCGT
GCCTGACAGATTCAGCGGCTCCGGCTCTGGCACAGACTTCACCCTGACAAT

CTCTAGCCTGCAGCCAGAGGATTTCGCCGTGTACTATTGTCAGCAGCACTA
CATCACCCCCCTGACATTTGGCGCCGGCACCAAGGTGGAGATCAAGTCTAG
AATGGACAAAGACTGCGAAATGAAGCGCACCACCCTGGATAGCCCTCTGG
GCAAGCTGGAACTGTCTGGGTGCGAACAGGGCCTGCACGAGATCAAGCTG
CTGGGCAAAGGAACATCTGCCGCCGACGCCGTGGAAGTGCCTGCCCCAGC
CGCCGTGCTGGGCGGACCAGAGCCACTGATGCAGGCCACCGCCTGGCTCA
ACGCCTACTTTCACCAGCCTGAGGCCATCGAGGAGTTCCCTGTGCCAGCCC
TGCACCACCCAGTGTTCCAGCAGGAGAGCTTTACCCGCCAGGTGCTGTGG
AAACTGCTGAAAGTGGTGAAGTTCGGAGAGGTCATCAGCTACCAGCAGCT
GGCGGCCCTGGCGGGCAATCCCGCCGCCACCGCCGCCGTGAAAACCGCCC
TGAGCGGAAATCCCGTGCCCATTCTGATCCCCTGCCACCGGGTGGTGTCTA
GCTCTGGCGCCGTGGGGGGCTACGAGGGCGGGCTCGCCGTGAAAGAGTGG
CTGCTGGCCCACGAGGGCCACAGACTGGGCAAGCCTGGGCTGGGCGCTGA
GCACGAATTTCGAGGAGGGCCCGAACAAAAACTCATCTCAGAAGAGGATC
TGAATAGCGCCGTCGACCATCATCATCATCATCATTGA

9.1.6 scFv-Erbitux-Zip2

ATGGAGACAGACACACTCCTGCTATGGGTACTGCTGCTCTGGGTTCCAGGT
TCCACTGGTGACGCGGCCCAGCCGGCCCAGGTGCAGCTGAAGCAGAGCG
GCCCCGGCCTGGTGCAGCCCAGCCAGAGCCTGAGCATCACCTGCACCGTG
AGCGGCTTCAGCCTGACCAACTACGGCGTGCACTGGGTGAGGCAGAGCCC
CGGCAAGGGCCTGGAGTGGCTGGGCGTGATCTGGAGCGGCGGCAACACC
GACTACAACACCCCCTTCACCAGCAGGCTGAGCATCAACAAGGACAACAG
CAAGAGCCAGGTGTTCTTCAAGATGAACAGCCTGCAGAGCAACGACACCG
CCATCTACTACTGCGCCAGGGCCCTGACCTACTACGACTACGAGTTCGCCT
ACTGGGGCCAGGGCACCCTGGTGACCGTGAGCGCCGGTGGAGGCGGTTCA
GGCGGAGGTGGCAGCGGCGGTGGCGGGTCGGACATCCTGCTGACCCAGA
GCCCCGTGATCCTGAGCGTGAGCCCCGGCGAGAGGGTGAGCTTCAGCTGC
AGGGCCAGCCAGAGCATCGGCACCAACATCCACTGGTATCAGCAGAGGAC

CAACGGCAGCCCCAGGCTGCTGATCAAGTACGCCAGCGAGAGCATCAGCG
GCATCCCCAGCAGGTTCAGCGGCAGCGGCAGCGGCACCGACTTCACCCTG
AGCATCAACAGCGTGGAGAGCGAGGACATCGCCGACTACTACTGCCAGCA
GAACAACAACTGGCCCACCACCTTCGGCGCCGGCACCAAGCTGGAGCTGA
AGGGGTCTTCTAGAGCGCGGAACGCGTATCTAAGAAAAAAAATAGCAAGA
CTCAAAAAAGATAATCTCCAGCTAGAAAGAGACGAACAGAACCTCGAGAA
GATCATTGCGAATTTACGTGACGAAATTGCAAGATTAGAGAACGAAGTGGC
GTCTCACGAACAGGCTGAGCACGAATTTCGAGGAGGGCCCGAACAAAAA
CTCATCTCAGAAGAGGATCTGAATAGCGCCGTCGACCATCATCATCATCATC
ATTGA

9.1.7 scFv-425-Zip2

ATGGAGACAGACACACTCCTGCTATGGGTACTGCTGCTCTGGGTTCCAGGT
TCCACTGGTGACGCGGCCCAGCCGGCCATGGCCGAGGTGCAACTGCAGCA
GTCTGGGGCTGAACTGGTGAAGCCTGGGGCTTCAGTGAAGTTGTCCTGCA
AGGCTTCCGGCTACACCTTCACCAGCCACTGGATGCACTGGGTGAAGCAG
AGGGCTGGACAAGGCCTTGAGTGGATCGGAGAGTTTAATCCCAGCAACGG
CCGTACTAACTACAATGAGAAATTCAAGAGCAAGGCCACACTGACTGTAG
ACAAATCCTCCAGCACAGCCTACATGCAACTCAGCAGCCTGACATCTGAGG
ACTCTGCGGTCTATTACTGTGCCAGTCGGGACTATGATTACGACGGACGGTA
CTTTGACTACTGGGGCCAAGGGACCACGGTCACCGTCTCCTCAGGTGGCG
GTGGCTCGGGCGGTGGTGGGTCGGGTGGTGGCGGATCTGACATCGAGCTC
ACCCAGTCTCCAGCAATCATGTCTGCATCTCCAGGGGAGAAGGTCACTATG
ACCTGCAGTGCCAGCTCAAGTGTAACTTACATGTATTGGTACCAGCAGAAG
CCAGGATCCTCCCCCAGACTCCTGATTTATGACACATCCAACCTGGCTTCTG
GAGTCCCTGTTCGTTTCAGTGGCAGTGGGTCTGGGACCTCTTACTCTCTCA
CAATCAGCCGAATGGAGGCTGAAGATGCTGCCACTTATTACTGCCAGCAGT
GGAGTAGTCACATATTCACGTTCGGCTCGGGGACAGAACTCGAGATCAAAC
GGGCGGCCGCACTCGAGTCTAGAGCGCGGAACGCGTATCTAAGAAAAAAA

ATAGCAAGACTCAAAAAAGATAATCTCCAGCTAGAAAGAGACGAACAGAA
CCTCGAGAAGATCATTGCGAATTTACGTGACGAAATTGCAAGATTAGAGAA
CGAAGTGGCGTCTCACGAACAGGCTGAGCACGAATTTCGAGGAGGGCCCG
AACAAAAACTCATCTCAGAAGAGGATCTGAATAGCGCCGTCGACCATCATC
ATCATCATCATTGA

9.1.8 scFv-αEpCAM-Zip2

ATGGAGACAGACACACTCCTGCTATGGGTACTGCTGCTCTGGGTTCCAGGT
TCCACTGGTGACGCGGCCCAGCCGGCCATGGCCCAGGTGCAGCTGGTGCA
GTCTGGGGCTGAGGTGAAGAAGCCTGGGTCCTCGGTGAGGGTCTCCTGCA
AGGCTTCTGGAGGCACCTTCAGCAGCTATGCTATCAGCTGGGTGCGACAGG
CCCCTGGACAAGGGCTTGAGTGGATGGGAGGGATCATCCCTATCTTTGGTA
CAGCAAACTACGCACAGAAGTTCCAGGGCAGAGTCACGATTACCGCGGAC
GAATCCACGAGCACAGCCTACATGGAGCTGAGCAGCCTGAGATCTGAGGA
CACGGCTGTGTATTACTGTGCAAGAGACCCGTTTCTTCACTATTGGGGCCA
AGGTACCCTGGTCACCGTCTCGAGTGGTGGAGGCGGTTCAGGCGGAGGTG
GCTCTGGCGGTGGCGGATCGGAAATTGAGCTCACTCAGTCTCCACTCTCCC
TGCCCGTCACCCCTGGAGAGCCGGCCTCCATCTCCTGCAGGTCTAGTCAGA
GCCTCCTGCATAGTAATGGATACAACTATTTGGATTGGTACCTGCAGAAGCC
AGGGCAGTCTCCACAGCTCCTGATCTATTTGGGTTCTAATCGGGCCTCCGG
GGTCCCTGACAGGTTCAGTGGCAGTGGATCAGGCACAGATTTTACACTGAA
AATCAGCAGAGTGGAGGCTGAGGATGTTGGGGTTTATTACTGCATGCAAGC
TCTACAAACTTTCACTTTCGGCCCTGGGACCAAGGTGGAGATCAAACGTGC
GGCCGCACTCGAGTCTAGAGCGCGGAACGCGTATCTAAGAAAAAAAATAG
CAAGACTCAAAAAAGATAATCTCCAGCTAGAAAGAGACGAACAGAACCTC
GAGAAGATCATTGCGAATTTACGTGACGAAATTGCAAGATTAGAGAACGAA
GTGGCGTCTCACGAACAGGCTGAGCACGAATTTCGAGGAGGGCCCGAACA
AAAACTCATCTCAGAAGAGGATCTGAATAGCGCCGTCGACCATCATCATCA
TCATCATTGA

9.1.9 scFv-Herceptin-Zip2

ATGGAGACAGACACACTCCTGCTATGGGTACTGCTGCTCTGGGTTCCAGGT
TCCACTGGTGACGCGGCCCAGCCGGCCGCCACCATGGATTGGACTTGGAG
AGTGTTTTGCCTGCTGGCTGTCGCACCTGGGGCTCATAGTGAAGTGCAGCT
GGTCGAGAGTGGAGGAGGGCTGGTGCAGCCTGGCGGCAGCCTGAGGCTG
TCCTGCGCAGCCTCTGGCTTCAACATCAAGGACACCTACATCCACTGGGTG
CGGCAGGCCCCTGGCAAGGGCCTGGAGTGGGTGGCCAGGATCTATCCAAC
CAATGGCTACACACGGTATGCCGACAGCGTGAAGGGCCGGTTCACCATCA
GCGCCGACACCTCCAAGAACACAGCCTACCTCCAGATGAACAGCCTGAGG
GCCGAGGATACAGCCGTGTACTATTGCTCTCGCTGGGGAGGCGACGGCTTC
TACGCTATGGACTATTGGGGACAGGGCACCCTGGTGACCGTGAGCAGCGGT
GGAGGCGGTTCAGGCGGAGGTGGCAGCGGCGGTGGCGGGTCGGACATCC
AGATGACTCAGTCCCCTAGCTCCCTGAGTGCTTCAGTGGGCGACAGGGTCA
CTATTACCTGCCGCGCATCTCAGGATGTGAACACCGCAGTCGCCTGGTATCA
GCAGAAGCCTGGAAAAGCTCCAAAGCTGCTGATCTACAGCGCATCCTTCCT
GTATTCCGGCGTGCCCTCTCGGTTTTCTGGGAGTAGATCAGGAACTGACTT
CACACTGACTATTTCTAGTCTGCAGCCTGAGGATTTTGCCACCTACTATTGC
CAGCAGCACTACACCACACCCCCTACTTTCGGCCAGGGGACCAAAGTGGA
GATCAAGTCTAGAGCGCGGAACGCGTATCTAAGAAAAAAAATAGCAAGAC
TCAAAAAAGATAATCTCCAGCTAGAAAGAGACGAACAGAACCTCGAGAAG
ATCATTGCGAATTTACGTGACGAAATTGCAAGATTAGAGAACGAAGTGGCG
TCTCACGAACAGGCTGAGCACGAATTTCGAGGAGGGCCCGAACAAAAACT
CATCTCAGAAGAGGATCTGAATAGCGCCGTCGACCATCATCATCATCATCAT
TGA

9.1.10 scFv-Sacit-Zip2

ATGGAGACAGACACACTCCTGCTATGGGTACTGCTGCTCTGGGTTCCAGGT
TCCACTGGTGACGCGGCCCAGCCGGCCCAGGTGCAGCTGCAGCAGTCCGG

CTCTGAGCTGAAGAAGCCCGGCGCCAGCGTGAAGGTGTCCTGCAAGGCCT
CTGGCTACACCTTCACAAACTATGGCATGAATTGGGTGAAGCAGGCACCTG
GACAGGGCCTGAAGTGGATGGGCTGGATCAACACCTACACAGGCGAGCCA
ACCTATACAGACGACTTCAAGGGCAGGTTCGCCTTTTCCCTGGACACCAGC
GTGTCCACAGCCTACCTGCAGATCAGCTCCCTGAAGGCCGACGATACCGCC
GTGTATTTCTGCGCAAGGGGAGGATTTGGCTCTAGCTACTGGTATTTCGACG
TGTGGGGACAGGGAAGCCTGGTGACAGTGTCCTCTGGAGGAGGAGGATCT
GGAGGAGGAGGAAGCGGAGGAGGAGGATCCGATATCCAGCTGACCCAGTC
TCCAAGCTCCCTGTCTGCCAGCGTGGGCGACCGGGTGAGCATCACCTGTAA
GGCAAGCCAGGACGTGAGCATCGCAGTGGCATGGTACCAGCAGAAGCCAG
GCAAGGCCCCTAAGCTGCTGATCTATTCCGCCTCTTACCGGTATACCGGCGT
GCCTGACAGATTCAGCGGCTCCGGCTCTGGCACAGACTTCACCCTGACAAT
CTCTAGCCTGCAGCCAGAGGATTTCGCCGTGTACTATTGTCAGCAGCACTA
CATCACCCCCCTGACATTTGGCGCCGGCACCAAGGTGGAGATCAAGTCTAG
AGCGCGGAACGCGTATCTAAGAAAAAAAATAGCAAGACTCAAAAAAGATA
ATCTCCAGCTAGAAAGAGACGAACAGAACCTCGAGAAGATCATTGCGAAT
TTACGTGACGAAATTGCAAGATTAGAGAACGAAGTGGCGTCTCACGAACA
GGCTGAGCACGAATTTCGAGGAGGGCCCGAACAAAAACTCATCTCAGAAG
AGGATCTGAATAGCGCCGTCGACCATCATCATCATCATCATTGA

9.1.11 Zip1-SNAP

ATGGAGACAGACACACTCCTGCTATGGGTACTGCTGCTCTGGGTTCCAGGT
TCCACTGGTGACGCGGCCCAGCCGGCCAATCTCGTAGCCCAACTAGAAAA
CGAGGTGGCCTCGCTTGAGAACGAGAATGAGACGTTGAAAAAAAAGAATT
TGCACAAGAAAGACCTAATAGCATATTTGGAGAAGGAAATAGCTAATTTAC
GGAAAAAGATTGAGGAGTCTAGAATGGACAAAGACTGCGAAATGAAGCGC
ACCACCCTGGATAGCCCTCTGGGCAAGCTGGAACTGTCTGGGTGCGAACA
GGGCCTGCACGAGATCAAGCTGCTGGGCAAAGGAACATCTGCCGCCGACG
CCGTGGAAGTGCCTGCCCCAGCCGCCGTGCTGGGCGGACCAGAGCCACTG

ATGCAGGCCACCGCCTGGCTCAACGCCTACTTTCACCAGCCTGAGGCCATC
GAGGAGTTCCCTGTGCCAGCCCTGCACCACCCAGTGTTCCAGCAGGAGAG
CTTTACCCGCCAGGTGCTGTGGAAACTGCTGAAAGTGGTGAAGTTCGGAG
AGGTCATCAGCTACCAGCAGCTGGCGGCCCTGGCGGGCAATCCCGCCGCC
ACCGCCGCCGTGAAAACCGCCCTGAGCGGAAATCCCGTGCCCATTCTGATC
CCCTGCCACCGGGTGGTGTCTAGCTCTGGCGCCGTGGGGGGCTACGAGGG
CGGGCTCGCCGTGAAAGAGTGGCTGCTGGCCCACGAGGGCCACAGACTG
GGCAAGCCTGGGCTGGGCGCTGAGCACGAATTTCGAGGAGGGCCCGAAC
AAAAACTCATCTCAGAAGAGGATCTGAATAGCGCCGTCGACCATCATCATC
ATCATCATTGA

9.1.12 Annexin V-SNAP

ATGGAGACAGACACACTCCTGCTATGGGTACTGCTGCTCTGGGTTCCAGGT
TCCACTGGTGACATGGCGGGTGGTTGTGGTCACGCACAGGTTCTCAGAGG
CACTGTGACTGACTTCCCTGGATTTGATGAGCGGGCTGATGCAGAAACTCT
TCGGAAGGCTATGAAAGGCTTGGGCACAGATGAGGAGAGCATCCTGACTC
TGTTGACATCCCGAAGTAATGCTCAGCGCCAGGAAATCTCTGCAGCTTTTA
AGACTCTGTTTGGCAGGGATCTTCTGGATGACCTGAAATCAGAACTAACTG
GAAAATTTGAAAAATTAATTGTGGCTCTGATGAAACCCTCTCGGCTTTATGA
TGCTTATGAACTGAAACATGCCTTGAAGGGAGCTGGAACAAATGAAAAAG
TACTGACAGAAATTATTGCTTCAAGGACACCTGAAGAACTGAGAGCCATCA
AACAAGTTTATGAAGAAGAATATGGCTCAAGCCTGGAAGATGACGTGGTG
GGGGACACTTCAGGGTACTACCAGCGGATGTTGGTGGTTCTCCTTCAGGCT
AACAGAGACCCTGATGCTGGAATTGATGAAGCTCAAGTTGAACAAGATGC
TCAGGCTTTATTTCAGGCTGGAGAACTTAAATGGGGGACAGATGAAGAAA
AGTTTATCACCATCTTTGGAACACGAAGTGTGTCTCATTTGAGAAAGGTGT
TTGACAAGTACATGACTATATCAGGATTTCAAATTGAGGAAACCATTGACCG
CGAGACTTCTGGCAATTTAGAGCAACTACTCCTTGCTGTTGTGAAATCTATT
CGAAGTATACCTGCCTACCTTGCAGAGACCCTCTATTATGCTATGAAGGGAG

CTGGGACAGATGATCATACCCTCATCAGAGTCATGGTTTCCAGGAGTGAGA
TTGATCTGTTTAACATCAGGAAGGAGTTTAGGAAGAATTTTGCCACCTCTCT
TTATTCCATGATTAAGGGAGATACATCTGGGGACTATAAGAAAGCTCTTCTG
CTGCTCTCTGGAGAAGATGACTCTAGAATGGACAAAGACTGCGAAATGAA
GCGCACCACCCTGGATAGCCCTCTGGGCAAGCTGGAACTGTCTGGGTGCG
AACAGGGCCTGCACGAGATCAAGCTGCTGGGCAAAGGAACATCTGCCGCC
GACGCCGTGGAAGTGCCTGCCCCAGCCGCCGTGCTGGGCGGACCAGAGCC
ACTGATGCAGGCCACCGCCTGGCTCAACGCCTACTTTCACCAGCCTGAGGC
CATCGAGGAGTTCCCTGTGCCAGCCCTGCACCACCCAGTGTTCCAGCAGG
AGAGCTTTACCCGCCAGGTGCTGTGGAAACTGCTGAAAGTGGTGAAGTTC
GGAGAGGTCATCAGCTACCAGCAGCTGGCGGCCCTGGCGGGCAATCCCGC
CGCCACCGCCGCCGTGAAAACCGCCCTGAGCGGAAATCCCGTGCCCATTC
TGATCCCCTGCCACCGGGTGGTGTCTAGCTCTGGCGCCGTGGGGGGCTACG
AGGGCGGGCTCGCCGTGAAAGAGTGGCTGCTGGCCCACGAGGGCCACAG
ACTGGGCAAGCCTGGGCTGGGCGCTGAGCACGAATTTCGAGGAGGGCCCG
AACAAAAACTCATCTCAGAAGAGGATCTGAATAGCGCCGTCGACCATCATC
ATCATCATCATTGA

9.2 Supplementary figures

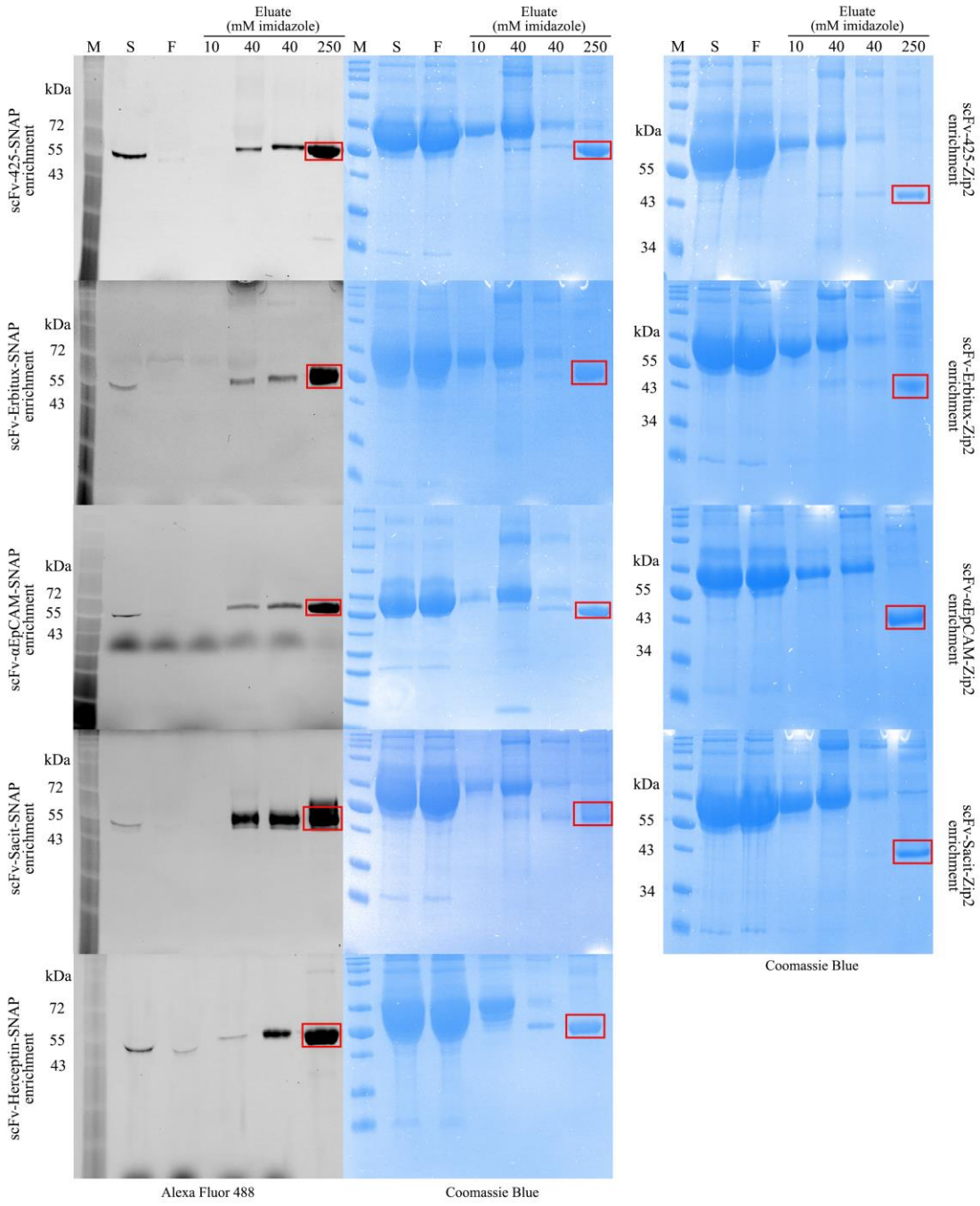

Supplementary Figure 1. SNAP-tag and Zip2 fusion proteins are enriched. The His-tagged proteins were enriched by nickel purification and confirmed by SDS-PAGE. While the SNAP-tag fusion proteins were confirmed by SNAP-Surface® Alexa Fluor® 488 followed by Coomassie blue staining, the Zip2 fusion proteins were confirmed by Coomassie blue staining (highlighted with red box). The signal was visualized with ChemiDoc XRS+ System. M: Blue prestained protein standard broad range (11-250 kDa). S: cell-free culture supernatant; F: flowthrough.

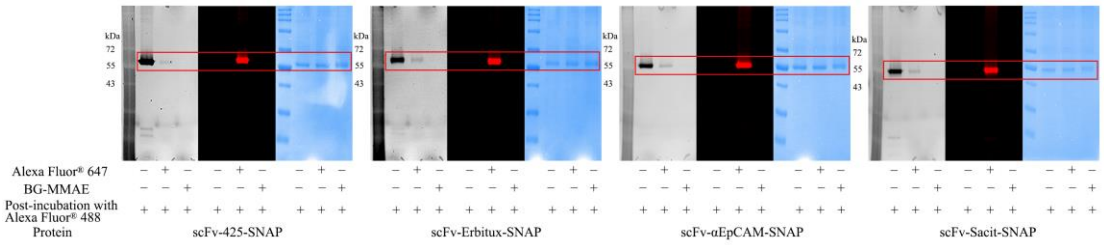

Supplementary Figure 2. High conjugation efficiency between SNAP-fusion proteins and BG-modified agents. SNAP-fusion proteins were conjugated with either SNAP-Surface® Alexa Fluor® 647 or BG-MMAE followed by post-incubation with SNAP-Surface® Alexa Fluor® 488. The fluorescence was visualized and corresponding Coomassie blue staining was shown

Abbreviation

mAb	Monoclonal antibody
FDA	Food and Drug Administration
scFv	Single-chain variable fragment
ADC	Antibody drug conjugate
DAR	Drug-to-antibody ratio
TF	Tissue factor
Trop2	Trophoblast cell-surface antigen 2
FRα	Folate receptor alpha
Nectin4	Nectin cell adhesion molecule 4
Her2	Human epidermal growth factor receptor 2
BCMA	B-cell maturation antigen
MMAE	Monomethyl auristatin E
MMAF	Monomethyl auristatin F
TNBC	Triple-negative breast cancer
UC	Urothelial cancer
DLBCL	Diffuse large B-cell lymphoma
HGBL	High-grade B-cell lymphoma
ALL	Acute lymphoblastic leukemia
AML	Acute myeloid leukemia
PD-1	Programmed death receptor-1
PD-L1	Programmed death-ligand 1
ASCT	Autologous stem cell transplant
Ig	Immunoglobulins
VH	Variable heavy region
CH	Constant heavy region
VL	Variable light region
CL	Constant light region
Fab	Fragment antigen-binding region

Fc	Fragment crystallizable region
IC_{50}	Half maximal inhibitory concentration
DXd	Deruxtecan
BG	Benzylguanine
ER	Estrogen receptor
PgR	Progesterone receptor
T-DM1	Ado-trastuzumab emtansine
PFS	Progression-free survival
OS	Overall survival
ORR	Objective response rate
T-DXd	Trastuzumab deruxtecan
SG	Sacituzumab govitecan
MIRV	Mirvetuximab soravtansine
bZip	basic leucine-zipper
CAR	Chimeric antigen receptor
EGFR	Epidermal growth factor receptor
EpCAM	Epithelial cell adhesion molecule
PCR	Polymerase chain reaction
SDS-PAGE	Sodium dodecyl-sulfate polyacrylamide gel electrophoresis
BSA	Bovine serum albumin
BG-MMAE	BG-GLA-PEG4-Val-Cit-PAB-MMAE
HPLC	High-performance liquid chromatography
PVDF	Polyvinylidene difluoride
PI	propidium iodide
CMV	Cytomegalovirus enhancer and promoter
IgK leader	Murine immunoglobulin kappa chain leader
GS	Glycine-serine

Acknowledgement

To begin with I am extremely grateful to meet all these kind and friendly people in Germany. Even we are from all over the world, we have shared so many wonderful moments during the last four years, which will be my lifelong treasure.

My sincere and hearty thanks and appreciations go firstly to my supervisor Prof. Dr. med. Ivo Meinhold-Heerlein who provided me the opportunity to go further in the researh feld. Along the same lines, I would like to express my big thanks to my advisor as well as my tutor Dr. Ahmad Fawzi Hussain who passed on knowledge, imparted lab skills and has always been there to help me. I would also love to thank Prof. Dr. rer. nat. Sandra B. Hake to be my co-supervisor, providing valuable advices and providing writing skills.

I am deeply indebted to all my colleagues and friends who are my spiritual pillar. My thanks go to Wenjie, Mohiuddin, Armin, Swantje and Kai who were always willing to help me in lab or in daily life. We shared both the office and lab; we learned new skills, discussed problems and found solutions; and we spent our free time out of the lab toghther. Also, my thanks go to Xuesong and Yuxi who made me feel at home. My special thanks go to Lian Jie who is always standing by me even we are miles apart. Her encouragement and positivity got me through the depressing times, and her help always keeps me motivated to my research and also life.

I feel so grateful to work and study in Justus-Liebig-University Gießen and Harbin medical university. Thank you for all the people there to achieve my medical dream.

Lastly and most importantly, my warm gratitude goes to my beloved families for supporting me with all their trust and faith in me. Thank you for being my backup force during the last thirty years and also for the rest of my life. I will never be tired of saying love you.

I could not have come so far without these families, friends and supervisors. Not only people I specifically mentioned here, but also all the kind people I have met. You all know what you mean to me.